University of the Witwatersrand

Masters of Science

Numerical Investigation into Sound Synthesis by Physical modeling.

Author:
Lethabo Borole

Supervisor:
Dr B. A. Jacobs

A thesis submitted in fulfilment of the requirements for the degree of Master of Science

in the

School of Computer Science and Applied Mathematics

August 2018

Declaration of Authorship

I, Lethabo Borole, declare that this thesis titled, 'Numerical Investigation into Sound Synthesis through Differential Equations' and the work presented in it are my own. I confirm that:

- This work was done wholly or mainly while in candidature for a research degree at this University.
- Where any part of this thesis has previously been submitted for a degree or any other qualification at this University or any other institution, this has been clearly stated.
- Where I have consulted the published work of others, this is always clearly attributed.
- Where I have quoted from the work of others, the source is always given. With the exception of such quotations, this thesis is entirely my own work.
- I have acknowledged all main sources of help.
- Where the thesis is based on work done by myself jointly with others, I have made clear exactly what was done by others and what I have contributed myself.

Witwatersrand University

Abstract

Faculty of Science
Computer Science and Applied Mathematics

Numerical Investigation in to Sound Synthesis by Physical Modeling.

by Lethabo Borole

A linear and a non-linear partial differential equation is used as a phenomenological model to describe the synthesis of a vibrating string. The models are numerically simulated using finite difference method and an exact solution of the linear partial differential equation is derived using a functional transformation method. The functional transformation method is based on the transformation to the frequency domain in time and in space by applying the Laplace transformation and the Finite Sine transformation. The string is excited through the initial conditions, initial displacement and an initial velocity, of the system. Another excitation mode that is considered is the force density, where the initial conditions are set to zero. The force density is added as a Source term to the partial differential equation and the initial excitation enters the system by the use of this term. To analyse the model different observation positions are considered, the observation points are the positions of the string where the vibrations are observed. The exact solution is used to verify the Finite difference approximation and a spectrogram analysis of the different excitation points is used to asses the methods. The finite difference method is then used to analysis the vibrations of the string. The nonlinear model include the effects of tension modulation, which is defined by the Kirchhoff-Carrier equation. The results are analysed using a quantitative analysis and a Fourier analysis.

Acknowledgements

I would like to thank my supervisor, Dr. Byron Jacobs for his endless patiences, for the time he has invested and the guidance he has provided. I am truly grateful for his support.

Contents

List of Figures

Chapter 1

Introduction

1.1 Introduction

Sound synthesis is a technique of generating sound using electronic hardware or software. Synthesis methods are commonly used to generate interesting and unique sounds that can not be produced acoustically, to modelling sounds of real instruments and to producing automation of systems and processes [18]. There are various methods that are used to synthesize sound. The most common methods used are additive synthesis, a technique that generates a sound by combining sinusoidal oscillators, subtractive synthesis, a technique where a filter is applied to a waveform and the filter alters the sound by partitioning the sound, digital waveguides method, a method where a partial differential equation is simplified to the wave equation, which has a closed form solution in terms of a forward and backwards travelling wave. The advantage of the waveguide method is that it has the ability to synthesize sound in real time since the method makes use of digital delay lines. A delay line is an audio effect which records and stores an input signal that can be played back after a period of time [18]. The sound synthesis method that this research will focus on is physical modelling.

Physical modelling is a sound synthesis technique, where mathematical model describe the physical mechanism that produces the sound [10, 23]. The physical description of the main vibrating structures of the musical instruments are represented by partial differential equations (PDEs) together with the system's initial conditions and boundary conditions. The partial differential equation is derived from the general laws of physics [9, 13]. The Phenomenological Model that will be considered is a string that is clamped at both ends and is initially plucked, struck or bowed these provide three sets of initial conditions. Physical modelling synthesis involves a physical description of the musical instrument as the starting point for algorithm design [18]. Sound synthesis by physical modelling requires two essential steps: the phenomenological description of a vibrating structure and the transformation into a discrete-time, discrete-space model for computer aided simulation [9]. The advantage of physical modelling is in the combination of highly flexible and physically correct models. The algorithm that is created when using signal synthesis, additive synthesis and subtractive synthesis, can be fast and provide real time versions for the simulation but the parameters loss their physical significance. Where as in physical modelling synthesis the parameters in the model represent real physical parameters of the sound production mechanism, which allow for a more natural simulation of the physical system but the method is often computationally expensive.

Sound has the general structure defined by an envelope where the envelope represents the varying levels of the sound wave over time. An envelope is contoured by four areas: the attack time, the decay time, the sustain level and the release time. The envelope is depicted in Figure 1.1. The attack phase is the time taken for amplitude to reach a maximum level and the decay phase begins as soon as the attack phase has reached its peak, then the signal level begins to decay until it reaches a sustained level. The sustain level is the period during the main sequence of the sounds duration before the sound enters the release period, where the release period is where the amplitude fades to zero over time.

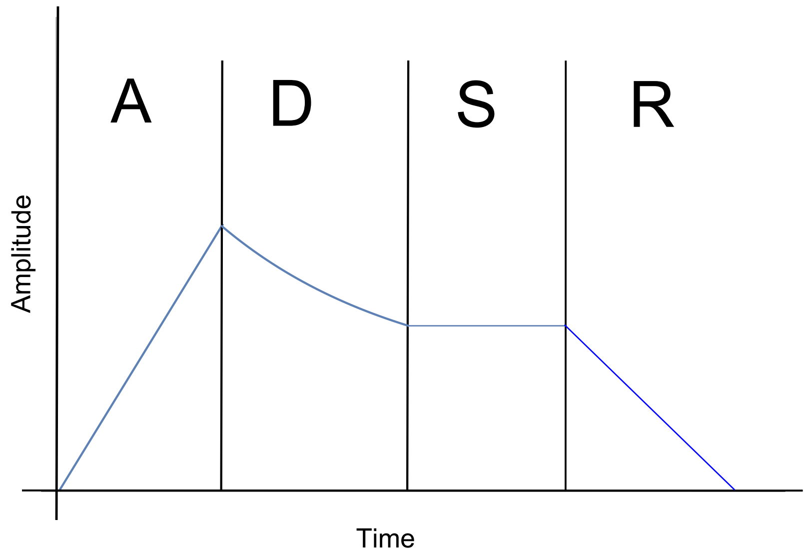

FIGURE 1.1: The region A: the attack time, the region D: decay time, region S: sustain level, region R: release time.

A review of the relevant literature is provided in Section 1.2. Chapter 2 provides a description of the methodology used throughout the research. The description of the linear model and its boundary conditions and initial conditions are given in Chapter 3. To solve the model numerically we consider a finite difference method, which is derived in Section 3.5 and to produce an exact solution of the model we apply the functional transform method (FTM), which is derived in Section 3.6. The nonlinear model physical model that includes the effects of tension modulation is described in Chapter 4. The nonlinear model is solve numerically using the Finite difference scheme and the derivation of the scheme is provided in Section 4.3. Chapter 5 presents the results of the linear and nonlinear model and Chapter 6 provides the conclusion of the research.

1.2 Literature review

Sound synthesis techniques are investigated by Rabenstein and Trautmann [9]. The authors describe several approaches to digital sound synthesis, in particular physical modelling methods. A discrete-time models, which are suitable for real time implementation is derived and the paper discusses four methods for the synthesis of musical sounds, namely; wavetable synthesis, spectral synthesis, and physical modelling. Wavetable synthesis is based on sampled waveform in the time domain, which are stored in the internal memory and can be played back on demand. The samples are stored in a table where the frequency can be generated by reading through the table. The quality of the output is dependent on the number of values stored in the table [18]. Spectral synthesis produces sound from the frequency domain models. The method is based on a common generic signal representation where the superposition of the basis function with time varying amplitude form the model. Physical modelling is based on models of the physical properties of the vibrating structures and the authors present four approaches to discretizing physical models; finite difference methods, modal synthesis, digital waveguides and transfer function models.

Erkut and Karjalainen [5] show that a one dimensional time domain method based on the finite difference (FDTD) and the digital waveguide method are equivalent for the homogeneous wave equation with frequency independent damping term. A comparison between the FDTD, which is constructed by a finite difference approximation of the wave equation in a one dimensional, and the waveguide method and the digital waveguide method, which is based on the travelling wave solution of the lossless wave equation where the total displacement is computed by adding the travelling wave solutions. This equivalence is also shown in the work done by Smith [6]. The digital waveguides method can be made effective by combining the arithmetic operations, that define the losses and dispersions in the model and by leaving out the large blocks of pure delays. A delay line is an audio effect which records and stores the input signals. The sound can then be played back at any time. Doing this is said to imply a trade of between the spatial accuracy and computational efficiency [6]. The 1D-FDTD achieves a better trade off between the spatial accuracy and the computational efficiency. However the efficiency is achieved by limiting the models accuracy [5].

Numerical methods are used when testing the validity of the physical model since an analytical solution can not be computed for all physical models. Chainge and Askenfelt [13] show how the finite difference numerical approach and the underlying physical model can be improved in order to simulate the motion of the piano strings with a high degree of realism. Obtaining a solution directly in the time domain allows us to listen to the computed waveform directly and judge the realism of the simulation. Finite difference methods are suited for solving hyperbolic equations in the time domain but the main limitation is in the rapidly increasing computing time. An advantage of using a finite difference method is that each physical quantity is directly available for all discrete points at each time step [13]. The author begins by presenting a model describing the transverse motion of a piano string in a plane perpendicular to the soundboard. The vibrations are governed by a PDE in which stiffness and damping terms are included. It has been shown that the stiffness term gives rise to a precursor which precedes the main pulses in the string waveform, especially in the lowest range of the instrument. The decay terms of the partials in the simulated tones will decrease with frequency since the two partial derivatives of odd order with respect to time in the equation simulate a frequency dependent decay rate.

Trautmann, Petrausch and Rabenstein [10] use a functional transformation method to solve the physical model that describes a two dimensional drum. The waveguide method and finite-difference methods are alternative ways of solving a PDE [13] but for systems of two or more dimensions in space both methods become computationally inefficient and when considering the waveguide method the parameters of the model loose physical meaning. Trautmann, Petrausch and Rabenstein [10] consider circular and rectangular membrane and note the difference in the changes in the wave propagation. Striking a drum with circular membrane of radius R in the centre, radius $= 0$, yields fewer vibrations than striking the drum at the radius $= \frac{2}{3}R$. A physics based multidimensional partial differential equation can be transformed into temporal and spatial frequency domain by use of the functional transformation method. The method is preformed by applying the Laplace transformation on the temporal domain of the partial differential equation and the Strum-Louville transformation on the spatial domain of the partial differential equation. The model has now been transformed in to an algebraic equation that can is solved analytically [10].

Trautmann and Rabenstien [14] present a discrete system for digital sound synthesis derived from the functional transformation method (FTM) of a physical model. The discretized is done because preserves the inherent physical stability of the continuous system and leads to a parallel arrangement of non-linear recursive systems without delay-free loops [14]. The delay-free loop is an audible effect that allows the sound or section of sound to be repeated. The system is stabilised by monitoring the instantaneous energy of the string vibrations and the vibrations energy is transferred to energy that deforms the material. The FTM is performed by using the Laplace transformation to transform the initial-boundary value problem in to a boundary value problem, ODE with boundary conditions, and by using the Sturm-Liouville transformation to transform the boundary value problem in to an algebraic equation [10, 14, 23]. The inverse Laplace transformation and the inverse Strum-Liouville transformation, which is computed numerically by a parallel arrangement of recursive discrete systems[10], yield a solution of the model.

The mapping between ordinary differential equations' (ODE) coefficients and the control parameters with physical meaning such as pitch, pitch bend, decay rate and attack time [1]. A system of first order ODEs can be used to generate both decaying and sustained oscillation, which can then be synthesised in to sound. The sprectrum of the sound that is generated can be enriched by applying nonlinear terms to the system. The advantage in using a complex variable is that it provides information about the phase and the envelope at each time instant simultaneously. The numerically integration of the dynamic system is preformed using Runge-Kutta-Ferlberg method. Since the system provided in the paper can be solved analytically the exact maximum amplitude can be reached and the attack time in known [1]. The dynamical system is able to accept external input such as; stochastic or impulsive signals that are physically or synthetically produced.

The application of the equation for frequency modulation described Chowning [7] allows the production of complex spectra with great simplicity to control the spectral components and their evolution in time. The method is limited since when changing the techniques of synthesis it becomes difficult to control the temporal evolution of the frequency components of the spectrum. It is then describes that the instantaneous frequency of a carrier wave is varied according to a modulating wave such that the rate at which the carrier varies is the frequency modulating wave [7]. The amount of carrier waves varies around its average and its peak frequency deviation is proportional to the amplitude of the modulating wave. The technique of frequency modulation synthesis provided a simple temporal control over the bandwidth of the spectra. The technique is simpler than additive or subtractive synthesis techniques that provide similar spectra [7].

The nonlinear model of a musical instrument is formulated by considering tension modulation. The tension of a string modulates as the sting displaces. The nonlinear model was investigated by Avanzini, Marogna and bank [19]. The authors describe the tension modulation in a string and a membrane by the Kirchhoff-Carrier approach, where the tension modulation is dependent on the total variation in the displacement of the string. The authors show that the tension variation is linearly proportional to the energy of the system [19]. Mohamad, Dixon and Harte [12] describe a technique that estimates the magnetic pickup points and plucking point location along the string of an electric guitar. The estimated values are calculated by minimising the difference between the magnitude of the spectrum of the recorded tone and that of an electric guitar model that is based on an ideal string. An electric guitar produces sound using magnetic pickups to capture the vibrations of its string and convert it into electrical signals. The magnetic pickup senses the velocity of the string, thus the authors use a time derivative of the ideal string model to model the the electric guitar string. The error is minimised by calculating the mean error between the magnitude of the spectrum of the observed data and the electric guitar model. Which corresponds to the estimated plucking position and pickup points.

1.3 Research Question

The research aims to numerically investigate sound synthesis using a linear differential equation and a nonlinear partial differential equation. The partial differential equations are used as a phenomenological model to describe the synthesis of a vibrating string. The linear model is numerically simulated using finite difference method and functional transformation method is used to find an exact solution. The nonlinear partial differential equation describes a phenomenological model where tension modulation is included in the description of the vibrating string and the nonlinear model is simulated using the Finite difference method. A string has a number of excitation modes, namely; striking, plucking and bowing the string, which are defined as initial conditions of the system. Another excitation mode that is consider is a force density, where the initial conditions are set to zero. The force density is added as a source term to the partial differential equation and the initial excitation enters the system by the use of this term.

Chapter 2

Methodology

2.1 Introduction

The phenomenological model will be numerically simulated using finite difference methods, digital waveguides and functional transformation methods. The chapter provides an explanation of each of these methods and how they have been used in literature.

2.2 Finite Difference Approximation

Finite difference approximation is the most direct way to discretize a partial derivatives with respect to time and space [9]. The objective is to transform the derivatives that appear in the differential equation in to finite differences approximations of the derivatives. The finite difference approximations are obtained by introducing a time step Δt and a spatial step Δx. We can compute $u(x,t)$ for discrete positions $x_i = i\Delta x$ at discrete time $t_n = n\Delta t$. The notation can then become

$$u(x,t) \rightarrow u(x_i, t_n), \tag{2.1}$$

The spatial domain of a continuous system is restricted by a grid constructed of finite sets of points where the numerical values an be computed. The derivatives in the model are approximated by differences between the values at nearby grid points [18]. Central differences are used to approximate the first-order and second-order temporal partial derivatives and are given by:

$$\frac{\partial u}{\partial t} = \frac{u\left(x_i, t_{n+1}\right) - u\left(x_i, t_{n-1}\right)}{2\Delta t} + \mathcal{O}(\Delta t^2), \tag{2.2}$$

$$\frac{\partial^2 u}{\partial t^2} = \frac{u\left(x_i, t_{n+1}\right) - 2u\left(x_i, t_n\right) + u\left(x_i, t_{n-1}\right)}{\Delta t^2} + \mathcal{O}(\Delta t^2). \tag{2.3}$$

Central differences are also used to approximate the first-order and second-order spatial partial derivatives and are given by:

$$\frac{du}{dx} = \frac{u\left(x_{i+1}, t_n\right) - u\left(x_{i-1}, t_n\right)}{2\Delta x} + \mathcal{O}(\Delta x^2), \tag{2.4}$$

$$\frac{\partial^2 u}{\partial x^2} = \frac{u\left(x_{i+1}, t_n\right) - 2u\left(x_i, t_n\right) + u\left(x_{i-1}, t_n\right)}{\Delta x^2} + \mathcal{O}(\Delta x^2), \tag{2.5}$$

Finite difference methods are a common way to solve partial differential equations but this result in computationally inefficient algorithms especially for models with two or more spatial dimensions [10] and the method can be numerical unstable [18].

2.3 Numerical Integration

The trapezoidal rule is numerical method that is used to approximate the solution to an integral. The method approximates a function by using the area of a trapezoid under the function, where the function, $f(x)$, is continuous on the interval $[x_0, x_N]$ [37]. The Trapezoidal method is given by,

$$\begin{aligned}\int_{x_0}^{x_N} f(x)dx &= \frac{\Delta x}{2}\left[f(x_0) + f(x_1)\right] + \cdots + \frac{\Delta x}{2}\left[f(x_{N-1}) + f(x_N)\right] \\ &= \frac{\Delta x}{2}\left[f(x_0) + 2\sum_{k=1}^{N-1} f(x_k) + f(x_N)\right]\end{aligned} \tag{2.6}$$

where $\Delta x = \dfrac{x_N - x_0}{N}$ since the interval has been subdivided in to n equal length intervals. The interval value are computed by letting $x_{j+1} = x_j + \Delta x$ for $j = 0, 1, 2.., N-1$.

2.4 Functional Transformation Method

The functional transformation method (FTM) provides a method for the solution of multidimensional systems [23] and describes a discrete model from its multidimensional transfer function description. The method is based on the transformation to the frequency domain in time and in space. The Laplace transformation is used to transform the model in to the temporal frequency domain. The Laplace transformation with respects to time, is given by

$$\mathcal{L}\left\{u(x,t)\right\} = \Upsilon(x,s) = \int_0^\infty u(x,t)e^{-st}dt \tag{2.7}$$

where $s = i\omega + \sigma$ is a complex-valued frequency variable. The Laplace transformation is applied to obtain a boundary value problem with spatial derivatives only, ODE with boundary conditions, and turns the initial conditions of the differential equation in to additive terms [9, 16, 23]. The transfer with respects to spatial domain will convert a boundary value problem into an algebraical equation [23]. The spatial domain is transformed using the Finite Sine transformation.

$$\mathcal{S}\left\{u(x,t)\right\} = U(n,t) = \int_0^L u(x,t)\sin\left(\frac{n\pi x}{L}\right)dx, \tag{2.8}$$

where the transformation Kernel is $\sin\left(\frac{n\pi x}{L}\right)$. The Finite Sine transformation to transform the model in to the spatial frequency domain. The PDE has been transferred into an algebraic equation. The resulting multidimensional transfer function in the frequency domain is equivalent to the intial partial differential equation [9]. An analytical solution in the temporal and spatial domain can be obtained by applying the inverse transformations. The inverse Laplace transform is given by,

$$u(x,t) = \mathcal{L}^{-1}\left\{\Upsilon(x,s)\right\} = \frac{1}{2\pi i}\lim_{T\to\infty}\int_{\gamma-iT}^{\gamma+iT} e^{st}\Upsilon(x,s)ds, \tag{2.9}$$

and the inverse Sine transform is given by

$$u(x,t) = \mathcal{S}^{-1}\left\{U(n,t)\right\} = \sum_{n=1}^{\infty}\sin(\frac{n\pi x}{L})U(n,t). \tag{2.10}$$

Figure 2.1 depicts the general process of the Functional Transformation method.

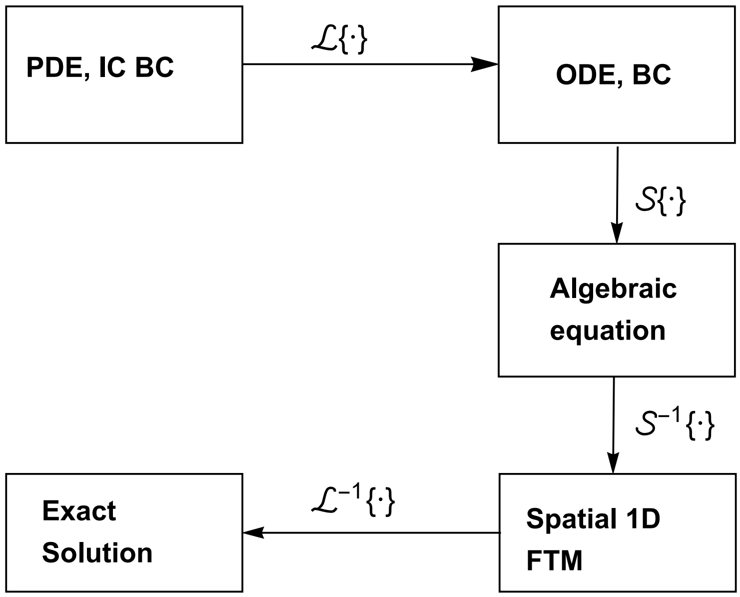

FIGURE 2.1: The process of FTM to solve an initial-boundary value problem. $\mathcal{L}\{\cdot\}$ denotes the Laplace transform, $\mathcal{S}\{\cdot\}$ denotes the Finite Sine transformation, $\mathcal{L}^{-1}\{\cdot\}$ denotes the inverse Laplace transform and $\mathcal{S}^{-1}\{\cdot\}$ denotes the inverse Finite Sine transformation.

Chapter 3

Synthesis of the Linear Model through Physical Modeling

3.1 Introduction

The model that is presented describes the transverse motion of a guitar string in a plane perpendicular to the soundboard, where t represents the temporal domain and x represents the spatial domain. We consider a vibrating string of length L, cross section area A and the moment of inertia I. The string material is characterized by the density, ρ, and its Young's modulus, E. A tension, T, is applied to the string and a frequency independent decay variable, α and a frequency dependent decay variable, β. The decay variable are constants that were derived experimentally [13]. Table 3.1 provides a description and the SI units of the variables used in the mathematical model.

TABLE 3.1: The parameters used in the linear mathematical model, with each variables description and SI units.

parameter	Description	SI units
α	Frequency independent decay rate	$kg(m.s)^{-1}$
β	Frequency dependent decay variable	$kg.m.s^{-1}$
L	Length of the string	m
E	Young's modulus	Pa
T	Tension applied to the string	$kg.m.s^{-2}$
A	Cross section area	m^2
I	The second moment of inertia	m^4
ρ	Density of the string	$kg.m^{-3}$

3.1.1 Model Assumptions

The following assumptions will be made to help describe the model.

- The temporal and spatial dependence of the force density term are separated since the term is assumed to not propagate along the string [13].
- The excitation term is limited in time and distributed over certain width.
- The strings on the instruments are hinged at both ends.

3.2 Mathematical Model

Using parameters defined above, the space coordinate, x, and the time coordinate, t, the simplest vibration model results from un-damped longitudinal wave can be written as,

$$\rho A \frac{\partial^2 u}{\partial t^2} - T \frac{\partial^2 u}{\partial x^2} = 0, \tag{3.1}$$

where T is the tension applied to the string. The fourth order spatial derivative accounts for the effects of the bending stiffness, which is proportional to the Young's modulus of the string,

$$EI \frac{\partial^4 u}{\partial x^4} + \rho A \frac{\partial^2 u}{\partial t^2} - T \frac{\partial^2 u}{\partial x^2} = 0. \tag{3.2}$$

The model includes the damping that takes place in the string and that is considered by adding the decay variables, α and β. The term α introduces a frequency independent damping and the term β introduces frequency dependent losses [9]. Thus the vibrations of the string are governed by

$$\rho A \frac{\partial^2 u}{\partial t^2} + EI \frac{\partial^4 u}{\partial x^4} - T \frac{\partial^2 u}{\partial x^2} + \alpha \frac{\partial u}{\partial t} + \beta \frac{\partial^3 u}{\partial t \partial x^2} = f\left(x, x_0, t\right). \tag{3.3}$$

The model does not include the mechanisms which give rise to two different decay times in the tone. The force density term in equation (3.3) represents the external force through which the excitation conditions may be imposed.

3.3 Boundary Conditions

The deflection of a string is determined by both the model equation and boundary conditions at the ends of the string. The string in the system is clamped at the ends, $x = 0$ and $x = L$. The deflection, defined by equation (3.4), and the skewness, defined by equation (3.5), at the end points are zero [9],

$$u\left(0, t\right) = 0, \qquad u\left(L, t\right) = 0, \tag{3.4}$$

$$\frac{\partial^2 u}{\partial x^2}\left(0, t\right) = 0, \qquad \frac{\partial^2 u}{\partial x^2}\left(L, t\right) = 0. \tag{3.5}$$

3.4 Initial Conditions

The types of excitation modes for a string instrument are by plucking or striking the string. These excitation can be expressed mathematical as initial conditions of the system or can be introduced in the form of a force density term.

Since the highest time derivative in equation (3.3) is two, we need two initial conditions for the PDE to be well-posed.

$$u(x, 0) = h(x), \tag{3.6}$$

$$\frac{\partial u}{\partial t}\left(x, 0\right) = p(x), \tag{3.7}$$

where equation (3.6) is the initial displacement, equation (3.7) is the initial velocity. When the excitation of the system is represented by the initial conditions, the force density is set to zero, $f(x, x_0, t) = 0$. When the excitation of the system is represented as the force density, $f(x, x_0, t)$, in equation (3.3) then

$$u(x, 0) = 0, \tag{3.8}$$

$$\frac{\partial u}{\partial t}(x, 0) = 0. \tag{3.9}$$

The force density term $f(x, x_0, t)$ is limited in time and distributed over a certain width [13]. The spatial and temporal dependence are seperated and the force density term is defined by

$$f(x, x_0, t) = f_H(t)g(x, x_0). \tag{3.10}$$

For a struck string, the motion starts at $t = 0$ as the hammer with velocity V_{H0} in the region centered around x_0. The dimensionless spatial term $g(x, x_0)$ accounts for the width of the apparatus striking the string. The force density $f_H(t)$ is related to the time history of the force, $F_H(t)$, exerted on the string. When the string is struck the force, $F_H(t)$, is the result of a non-linear interaction process [9, 13]. It is assumed that $F_H(t)$ is given by the power law,

$$F_H(t) = K|\nu(t) - u(x_0, t)|^p, \tag{3.11}$$

where the displacement $\nu(t)$ of the apparatus striking the string and where the stiffness parameter K is derived from experimental data [13]. The stiffness parameter, p, is derived experimentally to be $2 < p < 5$ [26]. When the force density is implemented the initial displacement and initial velocity are zero.

3.5 Derivation of Finite Difference Approximation

In this section the model, Equation (3.3), will be discretize using finite difference approximation. This is achieved using central difference approximation of the derivatives, with respects to time and space.

$$u(x,t) \approx u_i^n \tag{3.12}$$

$$f(x,x_0,t) \approx f_i^n \tag{3.13}$$

$$\frac{\partial^3 u}{\partial t \partial x^2} \approx \frac{u_{i+1}^{n+1} - 2u_i^{n+1} + u_{i-1}^{n+1} - u_{i+1}^{n-1} + 2u_i^{n-1} - u_{i-1}^{n-1}}{2\Delta t \Delta x^2} \tag{3.14}$$

$$\frac{\partial^4 u}{\partial x^4} \approx \frac{u_{i+2}^n - 4u_{i+1}^n + 6u_i^n - 4u_{i-1}^n + u_{i-2}^n}{\Delta x^4} \tag{3.15}$$

$$\frac{\partial^2 u}{\partial t^2} \approx \frac{u_i^{n+1} - 2u_i^n + u_i^{n-1}}{\Delta t^2} \tag{3.16}$$

$$\frac{\partial^2 u}{\partial x^2} \approx \frac{u_{i+1}^n - 2u_i^n + u_{i-1}^n}{\Delta x^2} \tag{3.17}$$

$$\frac{\partial u}{\partial t} \approx \frac{u_i^{n+1} - u_i^{n-1}}{2\Delta t} \tag{3.18}$$

The above approximations are substituted in place of the derivatives.

$$\begin{aligned} F_i^n &= EI\frac{u_{i+2}^n - 4u_{i+1}^n + 6u_i^n - 4u_{i-1}^n + u_{i-2}^n}{\Delta x^4} + \rho A\frac{u_i^{n+1} - 2u_i^n + u_i^{n-1}}{\Delta t^2} - T\frac{u_{i+1}^n - 2u_i^n + u_{i-1}^n}{\Delta x^2} \\ &+ \alpha\frac{u_i^{n+1} - u_i^{n-1}}{2\Delta t} + \beta\frac{u_{i+1}^{n+1} - 2u_i^{n+1} + u_{i-1}^{n+1} - u_{i+1}^{n-1} + 2u_i^{n-1} - u_{i-1}^{n-1}}{2\Delta t \Delta x^2} \end{aligned} \tag{3.19}$$

Let $\lambda_1 = \frac{EI}{\Delta x^4}$, $\lambda_2 = \frac{\rho A}{\Delta t^2}$, $\lambda_3 = -\frac{T}{\Delta x^2}$, $\lambda_4 = \frac{\alpha}{2\Delta t}$, $\lambda_5 = \frac{\beta}{2\Delta t \Delta x^2}$ and rearrange equation (3.19).

$$\begin{aligned} F_i^n &= \lambda_5 u_{i+1}^{n+1} + (-2\lambda_5 + \lambda_4 + \lambda_2)\, u_i^{n+1} + (\lambda_5)\, u_{i-1}^{n+1} + \lambda_1 u_{i+2}^n + (-4\lambda_1 + \lambda_3)\, u_{i+1}^n - \lambda_5 u_{i-1}^{n-1} \\ &+ (6\lambda_1 - 2\lambda_2 - 2\lambda_3)\, u_i^n + (-4\lambda_1 + \lambda_3)\, u_{i-1}^n + \lambda_1 u_{i-2}^n - \lambda_5 u_{i+1}^{n-1} + (\lambda_2 - \lambda_4 + 2\lambda_5)\, u_i^{n-1} \end{aligned} \tag{3.20}$$

Equation (3.20) can be written in the form

$$A_1 u^{n+1} + A_2 u^n + A_3 u^{n-1} = F_i^n. \tag{3.21}$$

The first iteration of the scheme is calculated by,

$$B_1 u^1 + A_2 u^0 = F_i^0, \tag{3.22}$$

where, $B_1 = A_1 + A_3$. To simplify the matrices we let $\Lambda_1 = -2\lambda_5 + \lambda_4 + \lambda_2$, $\Lambda_2 = 6\lambda_1 - 2\lambda_2 - 2\lambda_3$ and $\Lambda_3 = 2\lambda_5 - \lambda_4 + \lambda_2$ and $\Lambda_5 = -4\lambda_1 + \lambda_3$. Thus, A_1 is given by:

$$\begin{bmatrix} \Lambda_1 & 0 & 0 & \dots & \dots & 0 \\ \lambda_5 & \Lambda_1 & \lambda_5 & 0 & \dots & 0 \\ 0 & \lambda_5 & \Lambda_1 & \lambda_5 & 0 & \vdots \\ \vdots & 0 & \ddots & \ddots & \ddots & \vdots \\ \vdots & \vdots & \dots & \lambda_5 & \ddots & \lambda_5 \\ 0 & \dots & \dots & \dots & 0 & \Lambda_1 \end{bmatrix}$$

A_2 is given by:

$$\begin{bmatrix} \Lambda_2 & 0 & 0 & \dots & \dots & \dots & 0 \\ \Lambda_5 & \Lambda_2 & \Lambda_5 & \lambda_1 & 0 & \dots & 0 \\ \lambda_1 & \Lambda_5 & \Lambda_2 & \Lambda_5 & \lambda_1 & \dots & \vdots \\ 0 & \lambda_1 & \ddots & \ddots & \ddots & \ddots & 0 \\ \vdots & \vdots & \ddots & \ddots & \ddots & \ddots & \lambda_1 \\ \vdots & 0 & \ddots & \lambda_1 & \Lambda_5 & \ddots & \Lambda_5 \\ 0 & \dots & \dots & \dots & \dots & 0 & \Lambda_2 \end{bmatrix}$$

and A_3 is given by:

$$\begin{bmatrix} \Lambda_3 & 0 & 0 & \dots & \dots & \dots & 0 \\ -\lambda_5 & \Lambda_3 & -\lambda_5 & 0 & \dots & \dots & 0 \\ 0 & -\lambda_5 & \Lambda_3 & -\lambda_5 & 0 & \dots & \vdots \\ \vdots & 0 & \ddots & \ddots & \ddots & \ddots & \vdots \\ \vdots & \vdots & \ddots & \ddots & \ddots & \ddots & 0 \\ \vdots & \vdots & \dots & 0 & -\lambda_5 & \ddots & -\lambda_5 \\ 0 & \dots & \dots & \dots & \dots & 0 & \Lambda_3 \end{bmatrix}$$

The boundary conditions are given in section 3.3 and are discretized using central difference approximation. Equation (3.4) and equation (3.5) are discretized as equation (3.23) and equation (3.24), respectively.

$$u_0^n = 0 \qquad\qquad u_L^n = 0 \tag{3.23}$$

$$u_{-1}^n = -u_1^n \qquad\qquad u_{L+1}^n = -u_{L-1}^n \tag{3.24}$$

The initial conditions ar edefined in section 3.4. First consider the system with an initial displacement, thus $f(x,t) = 0$ and $p(x) = 0$.

$$u_i^0 = h(x) \tag{3.25}$$

$$u_i^{-1} = u_i^1 \tag{3.26}$$

Then the system is considered with initial velocity , thus $f(x,t) = 0$ and $h(x) = 0$.

$$u_i^0 = 0 \tag{3.27}$$

$$u_i^{-1} = u_i^1 + 2\Delta t p(x) \tag{3.28}$$

The system is considered with initial velocity and displacement, thus $f(x,t) = 0$.

$$u_i^0 = h(x) \tag{3.29}$$

$$u_i^{-1} = u_i^1 + 2\Delta t p(x) \tag{3.30}$$

Then the system is considered with a force density,f, thus $p(x) = 0$ and $h(x) = 0$. The force density is separated in to temporal and spacial dependence

3.5.1 Consistency

The finite difference scheme, $\bar{Q}(u)$, is consistent with the PDE, $Q(u)$, if for any smooth function $u(x,t)$, $|Q(u) - \bar{Q}(u)| \to 0$ as $\Delta t, \Delta x \to 0$. In order to show the consistency of the scheme, let

$$u_{i+j}^{n+k} = u(x + j\Delta x, t + k\Delta t), \qquad j,k \in \mathbb{Z} \tag{3.31}$$

Substituting Equation (3.31) in to Equation (3.20) and taking the Taylor series expansion about the grid points $x = i\Delta x$ and $t = n\Delta t$ gives,

$$u\left(x,t\right) = u(x,t) + \Delta x u_x + \frac{1}{2}\Delta x^2 u_{xx} + \frac{1}{3!}\Delta x^3 u_{xxx} + \frac{1}{4!}\Delta x^4 u_{xxxx} + \mathcal{O}(\Delta x^5) \tag{3.32}$$

$$u\left(x+\Delta x,t\right) = u(x,t) + \Delta x u_x + \frac{1}{2}\Delta x^2 u_{xx} + \frac{1}{3!}\Delta x^3 u_{xxx} + \frac{1}{4!}\Delta x^4 u_{xxxx} + \mathcal{O}(\Delta x^5) \tag{3.33}$$

$$u\left(x+2\Delta x,t\right) = u(x,t) + 2\Delta x u_x + \frac{1}{2}4\Delta x^2 u_{xx} + \frac{1}{3!}8\Delta x^3 u_{xxx} + \frac{1}{4!}16\Delta x^4 u_{xxxx} + \mathcal{O}(\Delta x^5) \tag{3.34}$$

$$u\left(x-2\Delta x,t\right) = u(x,t) - 2\Delta x u_x + \frac{4}{2}\Delta x^2 u_{xx} - \frac{8}{3!}\Delta x^3 u_{xxx} + \frac{16}{4!}\Delta x^4 u_{xxxx} + \mathcal{O}(\Delta x^5) \tag{3.35}$$

$$u\left(x,t+\Delta t\right) = u(x,t) + \Delta t u_t + \frac{1}{2}\Delta t^2 u_{tt} + \frac{1}{3!}\Delta t^3 u_{ttt} + \frac{1}{4!}\Delta x^4 u_{xxxx} + \mathcal{O}(\Delta x^5) \tag{3.36}$$

$$u\left(x,t-\Delta t\right) = u(x,t) - \Delta t u_t + \frac{1}{2}\Delta t^2 u_{tt} - \frac{1}{3!}\Delta t^3 u_{ttt} + \frac{1}{4!}\Delta t^4 u_{tttt} + \mathcal{O}(\Delta t^5) + \mathcal{O}(\Delta x^5) \tag{3.37}$$

$$\begin{aligned} u\left(x+\Delta x,t+\Delta t\right) &= u(x,t) + \Delta t u_t + \Delta x u_x + \frac{1}{2}\left[\Delta t^2 u_{tt} + \Delta x^2 u_{xx} + 2\Delta x\Delta t u_{tx}\right] \\ &+ \frac{1}{3!}\left[\Delta t^3 u_{ttt} + \Delta x^3 u_{xxx} + 3\Delta x^2\Delta t u_{txx} + 3\Delta x^2\Delta t u_{txx}\right] \\ &+ \frac{1}{4!}\left[\Delta t^4 u_{tttt} + 3\Delta x^3\Delta t u_{xxxt} + 6\Delta x^2\Delta t^2 u_{ttxx} + 3\Delta x\Delta t^3 u_{tttx} + \Delta x^4 u_{xxxx}\right] \\ &+ \mathcal{O}(\Delta t^5) + \mathcal{O}(\Delta x^5) \end{aligned} \tag{3.38}$$

$$\begin{aligned} u\left(x-\Delta x,t+\Delta t\right) &= u(x,t) + \Delta t u_t - \Delta x u_x + \frac{1}{2}\left[\Delta t^2 u_{tt} + \Delta x^2 u_{xx} - 2\Delta x\Delta t u_{tx}\right] \\ &+ \frac{1}{3!}\left[\Delta t^3 u_{ttt} - \Delta x^3 u_{xxx} + 3\Delta x^2\Delta t u_{txx} - 3\Delta x^2\Delta t u_{txx}\right] \\ &+ \frac{1}{4!}\left[\Delta t^4 u_{tttt} - 3\Delta x^3\Delta t u_{xxxt} + 6\Delta x^2\Delta t^2 u_{ttxx} - 3\Delta x\Delta t^3 u_{tttx} + \Delta x^4 u_{xxxx}\right] \\ &+ \mathcal{O}(\Delta t^5) + \mathcal{O}(\Delta x^5) \end{aligned} \tag{3.39}$$

$$
\begin{aligned}
u\left(x-\Delta x, t-\Delta t\right) &= u(x,t) - \Delta t u_t - \Delta x u_x + \frac{1}{2}\left[\Delta t^2 u_{tt} + \Delta x^2 u_{xx} + 2\Delta x \Delta t u_{tx}\right] \\
&+ \frac{1}{3!}\left[-\Delta t^3 u_{ttt} - \Delta x^3 u_{xxx} - 3\Delta x^2 \Delta t u_{txx} - 3\Delta x^2 \Delta t u_{txx}\right] \\
&+ \frac{1}{4!}\left[\Delta t^4 u_{tttt} + 3\Delta x^3 \Delta t u_{xxxt} + 6\Delta x^2 \Delta t^2 u_{ttxx} + 3\Delta x \Delta t^3 u_{tttx} + \Delta x^4 u_{xxxx}\right] \\
&+ \mathcal{O}(\Delta t^5) + \mathcal{O}(\Delta x^5)
\end{aligned} \tag{3.40}
$$

$$
\begin{aligned}
u\left(x+\Delta x, t-\Delta t\right) &= u(x,t) - \Delta t u_t + \Delta x u_x + \frac{1}{2}\left[\Delta t^2 u_{tt} + \Delta x^2 u_{xx} - 2\Delta x \Delta t u_{tx}\right] \\
&+ \frac{1}{3!}\left[-\Delta t^3 u_{ttt} + \Delta x^3 u_{xxx} - 3\Delta x^2 \Delta t u_{txx} - 3\Delta x^2 \Delta t u_{txx}\right] \\
&+ \frac{1}{4!}\left[\Delta t^4 u_{tttt} - 3\Delta x^3 \Delta t u_{xxxt} + 6\Delta x^2 \Delta t^2 u_{ttxx} - 3\Delta x \Delta t^3 u_{tttx} + \Delta x^4 u_{xxxx}\right] \\
&+ \mathcal{O}(\Delta t^5) + \mathcal{O}(\Delta x^5)
\end{aligned} \tag{3.41}
$$

Substituting the above Taylor Series expansions in to equation (3.20) gives that as Δt and Δx tends to zero, the scheme equates to equation (3.3). Thus, $|Q(u) - \bar{Q}(u)| \to 0$ as $\Delta t, \Delta x \to 0$, showing that the scheme, equation (3.20), is consistent for the PDE, equation (3.3).

3.5.2 Stability Analysis

Recall that the CTCS scheme is given by equation (3.20). Consider the stability of the homogeneous scheme,

$$
\begin{aligned}
&\lambda_1 u_{i+1}^n + \left(-4\lambda_1 + \lambda_3\right) u_i^n + \left(6\lambda_1 - 2\lambda_2 + 2\lambda_3\right) u_i^n + u_{i-1}^n \left(-4\lambda_1 + \lambda_3\right) + \lambda_1 u_{i-2}^n \\
&+ \left(\lambda_2 + \lambda_4 - 2\lambda_5\right) u_i^{n+1} + \left(\lambda_2 - \lambda_4 + 2\lambda_5\right) u_i^{n-1} + \lambda_5 u_{i+1}^{n+1} + \lambda_5 u_{i-1}^{n+1} - \lambda_5 u_{i+1}^{n-1} \\
&+ \lambda_5 u_{i-1}^{n-1} = 0
\end{aligned} \tag{3.42}
$$

The stability of a numerical scheme is closely related to the numerical error of the scheme and the Von Neumann analysis is based on the Fourier decomposition of the numerical error [30]. A numerical scheme is said to be stable the numerical error is said not to grow faster then than exponential. The definition for stability allows the error to grow by it is limited. A Von Neumann stability is Preformed by substituting Equation (3.43) in to Equation (3.42).

$$
u\left(n, i\right) = \zeta^n e^{I\omega\Delta x i}, \tag{3.43}
$$

where, $I = \sqrt{-1}$ and w is the wave number. To simplify we let $\gamma_1 = -4\lambda_1 + \lambda_3$, $\gamma_2 = (6\lambda_1 - 2\lambda_2 + 2\lambda_3)$, $\gamma_3 = (\lambda_2 + \lambda_4 - 2\lambda_5)$, $\gamma_4 = (\lambda_2 - \lambda_4 + 2\lambda_5)$ and $\theta = I\Delta x\omega$. By substituting the above and Equation (3.43) in to Equation (3.42)

$$\begin{aligned} &\lambda_1 \zeta^n e^{I\omega\Delta x(i+1)} + \gamma_1 \zeta^n e^{I\omega\Delta xi} + \gamma_2 \zeta^n e^{I\omega\Delta xi} + \gamma_1 \zeta^n e^{I\omega\Delta x(i-1)} + \lambda_1 \zeta^n e^{I\omega\Delta x(i-2)} \\ &+ \gamma_3 \zeta^{n+1} e^{I\omega\Delta xi} + \gamma_4 \zeta^{n-1} e^{I\omega\Delta xi} + \lambda_5 \zeta^{n+1} e^{I\omega\Delta x(i+1)} + \lambda_5 \zeta^{n+1} e^{I\omega\Delta x(i-1)} \\ &- \lambda_5 \zeta^{n-1} e^{I\omega\Delta x(i+1)} + \lambda_5 u \zeta^{n-1} e^{I\omega\Delta x(i-1)} = 0 \end{aligned} \tag{3.44}$$

$\zeta^{n-1} e^{I\omega\Delta xi} \neq 0$, giving the quadratic equation,

$$\begin{aligned} &\zeta^2 \left[\lambda_5 \left(e^{\theta} + e^{-\theta}\right) + \gamma_3\right] + \zeta \left[\lambda_1 \left(e^{2\theta} + e^{-2\theta}\right) + \gamma_1 \left(e^{\theta} + e^{-\theta}\right) + \gamma_2\right] \\ &- \lambda_5 \left(e^{\theta} + e^{-\theta}\right) + \gamma_4 = 0. \end{aligned} \tag{3.45}$$

Recall Euler's formula,

$$\cos(\theta) = \frac{e^{\theta} + e^{-\theta}}{2}, \tag{3.46}$$

and substitute it in to Equation 3.45.

$$\begin{aligned} &\zeta^2 \left[2\lambda_5 \cos(\theta) + \gamma_3\right] + \zeta \left[2\lambda_1 \cos(2\theta) + 2\gamma_1 \cos(\theta) + \gamma_2\right] \\ &- 2\lambda_5 \cos(\theta) + \gamma_4 = 0. \end{aligned} \tag{3.47}$$

The quadratic formula is used to solve the quadratic equation, giving

$$\zeta = \frac{-\left(2\lambda_1 \cos(2\theta) + 2\gamma_1 \cos(\theta) + \gamma_2\right) \pm \sqrt{\left(2\lambda_1 \cos(2\theta) + 2\gamma_1 \cos(\theta) + \gamma_2\right)^2 - 4\kappa}}{2\left(2\lambda_5 \cos(\theta) + \gamma_3\right)}, \tag{3.48}$$

where, $\kappa = (2\lambda_5 \cos(\theta) + \gamma_3)(-2\lambda_5 \cos(\theta))$. By applying the boundedness of the Cosine function, $|\cos(\theta)| \leq 1$, and substituting in $\gamma_1 = -4\lambda_1 + \lambda_3$, $\gamma_2 = (6\lambda_1 - 2\lambda_2 + 2\lambda_3)$, $\gamma_3 = (\lambda_2 + \lambda_4 - 2\lambda_5)$ and $\gamma_4 = (\lambda_2 - \lambda_4 + 2\lambda_5)$, gives that

$$\zeta = \frac{-\left(4\lambda_3 - 2\lambda_2\right) \pm \sqrt{\left(4\lambda_3 - 2\lambda_2\right)^2 - 4\left((\lambda_2)^2 - (\lambda_4)^2\right)}}{2\left(\lambda_2 + \lambda_4\right)}. \tag{3.49}$$

The scheme is said to be stable if $|\zeta| \leq 1$, thus

$$\left| \frac{-\left(4\lambda_3 - 2\lambda_2\right) \pm \sqrt{\left(4\lambda_3 - 2\lambda_2\right)^2 - 4\left((\lambda_2)^2 - (\lambda_4)^2\right)}}{2\left(\lambda_2 + \lambda_4\right)} \right| \leq 1 \tag{3.50}$$

$$\left| \frac{\left(2\frac{T}{\Delta x^2} + \frac{\rho A}{\Delta t^2}\right) \pm \sqrt{\left(4\frac{T^2}{\Delta x^4} + 4\frac{T\rho A}{\Delta x^2 \Delta t^2} + \frac{\alpha^2}{\Delta t^2}\right)}}{\left(\frac{\rho A}{\Delta t^2} + \frac{\alpha}{\Delta t}\right)} \right| \leq 1 \tag{3.51}$$

Since T, ρ and A are given values, the stability of the scheme is dependent on the choice of Δt and Δx. The choice of α can effect the stability of the scheme and since it is chosen experimentally it is important to take in to account the effect the parameter has on the stability.

The stability of a homogeneous scheme along with the convergence of the scheme is significant to prove the convergence for a non-homogeneous scheme [30]. Thus the numerical scheme is conditionally stable and convergent.

3.6 Functional Transformation Method

In this section the functional transformation method is applied to the model, Equation (3.3). We begin by applying the Finite Sine transformation (FST) on the spacial terms and that is followed by applying the Laplace transformation (LT) on the temporal domain. Finite sine transformation (FST) is given by

$$S\left\{u(x,t)\right\} = \frac{2}{L}\int_0^L \sin\left(\frac{n\pi x}{L}\right) u(x,t)dx = U(n,t). \tag{3.52}$$

Now the Finite Sine transformation is applied to $\dfrac{\partial^2 u(x,t)}{\partial t^2}$ and $\dfrac{\partial u(x,t)}{\partial t}$.

$$S\left\{\frac{\partial^2 u(x,t)}{\partial t^2}\right\} = \frac{\partial^2 U(n,t)}{\partial t^2}, \tag{3.53}$$

$$S\left\{\frac{\partial u(x,t)}{\partial t}\right\} = \frac{\partial U(n,t)}{\partial t}, \tag{3.54}$$

$$S\left\{F_H(t)g(x,x_0)\right\} = F(n,t) = F_H(t)G(n,x_0). \tag{3.55}$$

Applying the Finite sine transformation to $\dfrac{\partial^2 u(x,t)}{\partial x^2}$ gives,

$$S\left\{\frac{\partial^2 u(x,t)}{\partial x^2}\right\} = \frac{2}{L}\int_0^L \sin\left(\frac{n\pi x}{L}\right)\frac{\partial^2 u(x,t)}{\partial x^2}dx. \tag{3.56}$$

Preforming integration by parts obtains,

$$\frac{2}{L}\int_0^L \sin\left(\frac{n\pi x}{L}\right)\frac{\partial^2 u(x,t)}{\partial x^2}dx = \frac{2}{L}\sin(\frac{n\pi x}{L})\frac{\partial u}{\partial x}\bigg|_0^L - \frac{2n\pi}{L^2}\int_0^L \cos(\frac{n\pi x}{L})\frac{\partial u}{\partial x}dx. \tag{3.57}$$

We substitute $\sin(0) = 0$ at $x = 0$ and $\sin(n\pi) = 0$ at $x = L$. Integration by parts is applied to the right hand side of equation (3.58). We substitute equation (3.52) in to equation (3.59). Thus,

$$\frac{2}{L}\int_0^L \sin\left(\frac{n\pi x}{L}\right)\frac{\partial^2 u(x,t)}{\partial x^2}dx = -\frac{2n\pi}{L^2}\int_0^L \frac{\partial u}{\partial x}\cos(\frac{n\pi x}{L})dx, \tag{3.58}$$

$$= -\frac{2n\pi}{L^2}\left[\cos(\frac{n\pi x}{L})u(x,t)\bigg|_0^L + \frac{n\pi}{L}\int_0^L \sin(\frac{n\pi x}{L})u(x,t)dx\right], \tag{3.59}$$

$$= \frac{2n\pi}{L^2}\left(u(0,t) + (-1)^{n+1}u(L,t)\right) - \left(\frac{n\pi}{L}\right)^2 U(n,t). \tag{3.60}$$

From the boundary conditions we know that $u(0,t) = 0$ and $u(L,t) = 0$. The boundary conditions are substituted to get that

$$\frac{2}{L}\int_0^L \sin\left(\frac{n\pi x}{L}\right)\frac{\partial^2 u(x,t)}{\partial x^2}dx = -\left(\frac{n\pi}{L}\right)^2 U(n,t). \tag{3.61}$$

We apply the Finite sine transformation to $\dfrac{\partial^4 u(x,t)}{\partial t^4}$.

$$S\left\{\frac{\partial^4 u(x,t)}{\partial x^4}\right\} = \frac{2}{L}\int_0^L \sin\left(\frac{n\pi x}{L}\right)\frac{\partial^4 u(x,t)}{\partial x^4}dx. \tag{3.62}$$

Preforming integration by parts obtains,

$$\frac{2}{L}\int_0^L \sin\left(\frac{n\pi x}{L}\right)\frac{\partial^4 u(x,t)}{\partial x^4}dx = \frac{2}{L}\sin(\frac{n\pi x}{L})\frac{\partial^3 u}{\partial x^3}\bigg|_0^L - \frac{2n\pi}{L^2}\int_0^L \cos(\frac{n\pi x}{L})\frac{\partial^3 u}{\partial x^3}dx. \tag{3.63}$$

We substitute $\sin(0) = 0$ at $x = 0$ and $\sin(n\pi) = 0$ at $x = L$. Integration by parts is applied to the right hand side of equation (3.64) to get equation (3.65). Thus,

$$\frac{2}{L}\int_0^L \sin\left(\frac{n\pi x}{L}\right)\frac{\partial^4 u(x,t)}{\partial x^4}dx = -\frac{2n\pi}{L^2}\int_0^L \frac{\partial^3 u}{\partial x^3}\cos(\frac{n\pi x}{L})dx, \tag{3.64}$$

$$= -\frac{2n\pi}{L^2}\left[\cos(\frac{n\pi x}{L})\frac{\partial^2 u}{\partial x^2}\bigg|_0^L + \frac{n\pi}{L}\int_0^L \sin(\frac{n\pi x}{L})\frac{\partial^2 u}{\partial x^2}dx\right], \tag{3.65}$$

$$= \frac{2n\pi}{L^2}\left(\frac{\partial^2 u(0,t)}{\partial x^2} + (-1)^{n+1}\frac{\partial^2 u(L,t)}{\partial x^2}\right),$$
$$- \frac{n^2\pi^2}{L^2}\frac{2}{L}\int_0^L \sin(\frac{n\pi x}{L})\frac{\partial^2 u}{\partial x^2}dx. \tag{3.66}$$

From the boundary conditions we know that $\dfrac{\partial^2 u(0,t)}{\partial x^2} = 0$ and $\dfrac{\partial^2 u(L,t)}{\partial x^2} = 0$. The right hand side of Equation (3.67) is similar to the left hand side of Equation (3.60) and we can substitute the right hand side of the equation,

$$\frac{2}{L}\int_0^L \sin\left(\frac{n\pi x}{L}\right)\frac{\partial^4 u(x,t)}{\partial x^4}dx = -\left(\frac{n\pi}{L}\right)^2\int_0^L \frac{2}{L}\sin(\frac{n\pi x}{L})\frac{\partial^2 u}{\partial x^2}dx, \tag{3.67}$$

$$= -\left(\frac{n\pi}{L}\right)^2\left[\frac{2n\pi}{L^2}\left(u(0,t) + (-1)^{n+1}u(L,t)\right) - \left(\frac{n\pi}{L}\right)^2 U(n,t)\right], \tag{3.68}$$

$$= \left(\frac{n\pi}{L}\right)^2\left(\frac{n\pi}{L}\right)^2 U(n,t). \tag{3.69}$$

Applying the Finite Sine transformation results in Equation (3.70),

$$F_H(t)G(n,x_0) = \left(\frac{n\pi EI}{L}\right)^4 U(n,t) + \rho A\frac{\partial^2 U(n,t)}{\partial t^2} + \left(\frac{n\pi T}{L}\right)^2 U(n,t) \\ +\alpha\frac{\partial U(n,t)}{\partial t} - \beta\left(\frac{n\pi}{L}\right)^2\frac{\partial U(n,t)}{\partial t}. \tag{3.70}$$

Apply the Laplace transformation to the time derivatives in Equation (3.70) and $U(n,t)$:

$$\mathcal{L}\left\{\frac{\partial^2 U(n,t)}{\partial t^2}\right\} = s^2\Upsilon(n,s) - sU(n,0) - \frac{\partial U(n,0)}{\partial t}, \tag{3.71}$$

$$\mathcal{L}\left\{\frac{\partial U(n,t)}{\partial t}\right\} = s\Upsilon(n,s) - U(n,0), \tag{3.72}$$

$$\mathcal{L}\left\{U(n,t)\right\} = \Upsilon(n,s), \tag{3.73}$$

$$\mathcal{L}\left\{F(n,t)\right\} = \Psi(n,s) = \psi(s)G(n,x_0). \tag{3.74}$$

Substitute Equations (3.71), (3.72), (3.73) and (3.74) in to Equation (3.70),

$$\Psi(s)G(n,x_0) = EI\left(\frac{n\pi}{L}\right)^4\Upsilon(n,s) + \rho A\left(s^2\Upsilon(n,s) - sU(n,0) - \frac{\partial U(n,0)}{\partial t}\right) + T\left(\frac{n\pi}{L}\right)^2\Upsilon(n,s) \\ +\alpha\left(s\Upsilon(n,s) - U(n,0)\right) - \beta\left(\frac{n\pi}{L}\right)^2\left(\Upsilon(n,s)s - U(n,0)\right). \tag{3.75}$$

Equation (3.76) is Equation (3.3) after applying the Finite Sine transformation and Laplace transformation,

$$\Upsilon(n,s) = \frac{\psi(s)G(n,x_0) + U(n,0)\left[\rho As - \beta\left(\frac{n\pi}{L}\right)^2 + \alpha\right] + \rho A\frac{\partial U(n,0)}{\partial t}}{\left[EI\left(\frac{n\pi}{L}\right)^4 + \rho As^2 + \left(\rho A\frac{n\pi}{L}\right)^2 - \beta\left(\frac{n\pi}{L}\right)^2 s + \alpha s\right]}. \tag{3.76}$$

The Laplace transformation is preformed on the initial conditions defined in Section 3.4. When an initial velocity and initial displacement are applied to excite the model, the force density is equal to zero, $\psi(s)G(n,x_0) = 0$. Thus, in this case Equation 3.76 becomes,

$$\Upsilon(n,s) = \frac{U(n,0)\left[\rho As - \beta\left(\frac{n\pi}{L}\right)^2 + \alpha\right] + \rho A\frac{\partial U(n,0)}{\partial t}}{\left[EI\left(\frac{n\pi}{L}\right)^4 + \rho As^2 + \left(\rho A\frac{n\pi}{L}\right)^2 - \beta\left(\frac{n\pi}{L}\right)^2 s + \alpha s\right]}. \tag{3.77}$$

The Inverse Laplace and inverse Finite Sine transform, defined by Equation (2.9) and Equation (2.10) respectively, are preformed using inbuilt functions on *mathematica*. The solution of the model is given by $u(x,t)$ and Equation (3.78) provides the first two terms of the solution.

The proposed method is found to be computationally intractable. The method is adapted by solving the differential equation, Equation (3.70), with the systems initial conditions. The inverse Finite Sine transformation is applied to the solution, which will result in an equation in the space and time domains. This equation describes the displacement of the string.

$$
\begin{aligned}
u(x,t) = 0.34788\Bigg(& - exp\left(t\left(-\frac{\alpha}{2A\rho}+\frac{\pi^2\beta}{2A\rho}-\frac{\sqrt{\alpha^2-2\pi^2\alpha\beta+\pi^4\beta^2-4AEI\pi^4\rho-4A\pi^2T\rho}}{2A\rho}\right)\right)\alpha \\
& + exp\left(t\left(-\frac{\alpha}{2A\rho}+\frac{\pi^2\beta}{2A\rho}+\frac{\sqrt{\alpha^2-2\pi^2\alpha\beta+\pi^4\beta^2-4AEI\pi^4\rho-4A\pi^2T\rho}}{2A\rho}\right)\right)\alpha \\
& + exp\left(t\left(-\frac{\alpha}{2A\rho}+\frac{\pi^2\beta}{2A\rho}-\frac{\sqrt{\alpha^2-2\pi^2\alpha\beta+\pi^4\beta^2-4AEI\pi^4\rho-4A\pi^2T\rho}}{2A\rho}\right)\right)\pi^2\beta \\
& - exp\left(t\left(-\frac{\alpha}{2A\rho}+\frac{\pi^2\beta}{2A\rho}+\frac{\sqrt{\alpha^2-2\pi^2\alpha\beta+\pi^4\beta^2-4AEI\pi^4\rho-4A\pi^2T\rho}}{2A\rho}\right)\right)\pi^2\beta \\
& + exp\left(t\left(-\frac{\alpha}{2A\rho}+\frac{\pi^2\beta}{2A\rho}-\frac{\sqrt{\alpha^2-2\pi^2\alpha\beta+\pi^4\beta^2-4AEI\pi^4\rho-4A\pi^2T\rho}}{2A\rho}\right)\right)\sqrt{\alpha^2-2\pi^2\alpha\beta+\pi^4\beta^2-4AEI\pi^4\rho-4A\pi^2T\rho} \\
& + exp\left(t\left(-\frac{\alpha}{2A\rho}+\frac{\pi^2\beta}{2A\rho}+\frac{\sqrt{\alpha^2-2\pi^2\alpha\beta+\pi^4\beta^2-4AEI\pi^4\rho-4A\pi^2T\rho}}{2A\rho}\right)\right)\sqrt{\alpha^2-2\pi^2\alpha\beta+\pi^4\beta^2-4AEI\pi^4\rho-4A\pi^2T\rho} \\
& \sin(\pi x)\Bigg) \div \sqrt{\alpha^2-2\pi^2\alpha\beta+\pi^4\beta^2-4AEI\pi^4\rho-4A\pi^2T\rho} \\
+ 0.16543\Bigg(& - exp\left(t\left(-\frac{\alpha}{2A\rho}+\frac{2\pi^2\beta}{A\rho}-\frac{\sqrt{\alpha^2-8\pi^2\alpha\beta+16\pi^4\beta-64AEI\pi^4\rho-16\pi^2T\rho}}{2A\rho}\right)\right)\alpha \\
& + exp\left(t\left(-\frac{\alpha}{2A\rho}+\frac{\pi^2\beta}{2A\rho}+\frac{\sqrt{\alpha^2-8\pi^2\alpha\beta+16\pi^4\beta-64AEI\pi^4\rho-16\pi^2T\rho}}{2A\rho}\right)\right)\alpha \\
& + exp\left(t\left(-\frac{\alpha}{2A\rho}+\frac{\pi^2\beta}{2A\rho}-\frac{\sqrt{\alpha^2-8\pi^2\alpha\beta+16\pi^4\beta-64AEI\pi^4\rho-16\pi^2T\rho}}{2A\rho}\right)\right)\pi^2\beta \\
& - exp\left(t\left(-\frac{\alpha}{2A\rho}+\frac{\pi^2\beta}{2A\rho}+\frac{\sqrt{\alpha^2-8\pi^2\alpha\beta+16\pi^4\beta-64AEI\pi^4\rho-16\pi^2T\rho}}{2A\rho}\right)\right)\pi^2\beta \\
& + exp\left(t\left(-\frac{\alpha}{2A\rho}+\frac{\pi^2\beta}{2A\rho}-\frac{\sqrt{\alpha^2-8\pi^2\alpha\beta+16\pi^4\beta-64AEI\pi^4\rho-16\pi^2T\rho}}{2A\rho}\right)\right)\sqrt{\alpha^2-8\pi^2\alpha\beta+16\pi^4\beta-64AEI\pi^4\rho-16\pi^2T\rho} \\
& + exp\left(t\left(-\frac{\alpha}{2A\rho}+\frac{\pi^2\beta}{2A\rho}+\frac{\sqrt{\alpha^2-8\pi^2\alpha\beta+16\pi^4\beta-64AEI\pi^4\rho-16\pi^2T\rho}}{2A\rho}\right)\right)\sqrt{\alpha^2-8\pi^2\alpha\beta+16\pi^4\beta-64AEI\pi^4\rho-16\pi^2T\rho} \\
& \sin(\pi x)\Bigg) \div \sqrt{\alpha^2-8\pi^2\alpha\beta+16\pi^4\beta-64AEI\pi^4\rho-16\pi^2T\rho} \\
& + \ldots
\end{aligned}
\tag{3.78}
$$

Chapter 4

Synthesis of the Nonlinear Model through Physical Modeling.

4.1 Introduction

The nonlinear model describes the transverse motion of a guitar string in a plane perpendicular to the soundboard, where t represents the temporal domain and x represents the spatial domain. The vibration of a string with length L at rest, cross section area A and the moment of inertia I. The string material is characterized by the density, ρ, and its Young's modulus, E. The frequency independent decay variable and a frequency dependent decay variable are defined by α and β, respectively. The Tension in the system is now defined by a function of displacement, $u(x,t)$. Table 3.1 provides a description and the SI units of the variables used in the mathematical model. The table is provided in Section 3.

4.2 Nonlinear Mathematical Model

Recall from Chapter 3, using parameters defined above, the space coordinate, x, and the time coordinate, t, that the simplest vibration model results from the un-damped longitudinal wave can be written as

$$\rho A \frac{\partial^2 u}{\partial t^2} - T \frac{\partial^2 u}{\partial x^2} = 0. \tag{4.1}$$

The fourth order spatial derivative accounts for the effects of the bending stiffness, which is proportional to the Young's modulus of the string,

$$EI\frac{\partial^4 u}{\partial x^4} + \rho A\frac{\partial^2 u}{\partial t^2} - T(u)\frac{\partial^2 u}{\partial x^2} = 0, \tag{4.2}$$

where $T(u)$ is the tension applied to the string. The tension is dependent on the displacement, $u(x,t)$. This term a nonlinearity to the equation which accounts for the tension modulation. The model includes the damping that takes place in the string and that is considered by adding the decay variables, α and β. The term α introduces a frequency independent damping and the term β introduces frequency dependent losses [9]. The vibrations of the string can be governed by

$$\rho A\frac{\partial^2 u}{\partial t^2} + EI\frac{\partial^4 u}{\partial x^4} - T(u)\frac{\partial^2 u}{\partial x^2} + \alpha\frac{\partial u}{\partial t} + \beta\frac{\partial^3 u}{\partial t \partial x^2} = f\left(x, x_0, t\right). \tag{4.3}$$

The tension modulation of a string is described by the Kirchhoff-Carrier equation and according to the Kirchhoff-Carrier equation, spatially uniform tension of the string at large displacements is approximated by the function $T(u)$ [18] is assumed to have the form,

$$T(u) = T_0 + T_N(u), \tag{4.4}$$

where T_0 is the tension at rest and T_N depends on the displacement $u(x,t)$ [4]. The tension is dependent on the change in the displacement of the string. When the string is displaced the tension of the string modulates. The length of the string expands in the The function T_N is defined as,

$$T_N(u) = EA\frac{L(u) - L}{L} = \frac{1}{2}\frac{EA}{L}\int_0^L \left(\frac{\partial u}{\partial x}\right)^2 dx. \tag{4.5}$$

The function, $T_N(u)$ where the integral represents the increase of the string length at large displacements, $L(u)$, with respect to the length at rest, L. The extension of the length of the string, $L(u)$, is dependent on the displacement $u(x,t)$ [4]. It is assumed that the tension modulation only depends on the total variation of the extended length, $L(u)$, thus, the tension of the string is defined as [18],

$$T(u) = T_0 + \frac{1}{2}\frac{EA}{L}\int_0^L \left(\frac{\partial u}{\partial x}\right)^2 dx, \tag{4.6}$$

where, $EA >> T_0$, which holds for musical instruments [4, 18].

4.3 Finite Difference Approximation

In this section the nonlinear model, equation (4.3), will be discretize using finite difference approximation. This is achieved using central difference approximation of the derivatives, with respects to time and space.
Obtaining an exact solution solution for the nonlinear PDE is difficult and cannot be done using the FTM since the Transformation are linear operators. In chapter 3 the linear model validates the FD method as a suitable numerical scheme and can be applied to the nonlinear model.

$$u(x,t) \approx u_i^n \tag{4.7}$$

$$f(x,t) \approx f_i^n \tag{4.8}$$

$$\frac{\partial^3 u}{\partial t \partial x^2} \approx \frac{u_{i+1}^{n+1} - 2u_i^{n+1} + u_{i-1}^{n+1} - u_{i+1}^{n-1} + 2u_i^{n-1} - u_{i-1}^{n-1}}{2\Delta t \Delta x^2} \tag{4.9}$$

$$\frac{\partial^4 u}{\partial x^4} \approx \frac{u_{i+2}^n - 4u_{i+1}^n + 6u_i^n - 4u_{i-1}^n + u_{i-2}^n}{\Delta x^4} \tag{4.10}$$

$$\frac{\partial^2 u}{\partial t^2} \approx \frac{u_i^{n+1} - 2u_i^n + u_i^{n-1}}{\Delta t^2} \tag{4.11}$$

$$\frac{\partial^2 u}{\partial x^2} \approx \frac{u_{i+1}^n - 2u_i^n + u_{i-1}^n}{\Delta x^2} \tag{4.12}$$

$$\frac{\partial u}{\partial t} \approx \frac{u_i^{n+1} - u_i^{n-1}}{2\Delta t} \tag{4.13}$$

$$\frac{\partial u}{\partial x} \approx \frac{u_{i+1}^n - u_{i-1}^n}{2\Delta x} \tag{4.14}$$

The tension modulation is given by

$$T(u) = T_0 + \frac{1}{2}\frac{EA}{L}\int_0^L \left(\frac{\partial u}{\partial x}\right)^2 dx, \tag{4.15}$$

and the Trapezoidal rule, defined in Chapter 2, is used to approximate the integral in that tension modulation. That approximation is given by

$$\int_0^{L_0} \left(\frac{\partial u}{\partial x}\right)^2 dx \approx \frac{\Delta x}{2}\left[\left(\frac{u_1^n - u_{-1}^n}{2\Delta x}\right)^2 + 2\sum_{i=1}^{N-1}\left(\frac{u_{i+1}^n - u_{i-1}^n}{2\Delta x}\right)^2 + \left(\frac{u_{N+1}^n - u_{N-1}^n}{2\Delta x}\right)^2\right]. \tag{4.16}$$

The above approximations are substituted in place of the derivatives and the integral,

$$\begin{aligned} F_i^n &= EI\frac{u_{i+2}^n - 4u_{i+1}^n + 6u_i^n - 4u_{i-1}^n + u_{i-2}^n}{\Delta x^4} + \rho A\frac{u_i^{n+1} - 2u_i^n + u_i^{n-1}}{\Delta t^2} - T_0\frac{u_{i+1}^n - 2u_i^n + u_{i-1}^n}{\Delta x^2} \\ &- \frac{\Delta x}{4}\frac{EA}{L_0}\left[\left(\frac{u_1^n - u_{-1}^n}{2\Delta x}\right)^2 + 2\sum_{i=1}^{N-1}\left(\frac{u_{i+1}^n - u_{i-1}^n}{2\Delta x}\right)^2 + \left(\frac{u_{N+1}^n - u_{N-1}^n}{2\Delta x}\right)^2\right]\frac{u_{i+1}^n - 2u_i^n + u_{i-1}^n}{\Delta x^2} \\ &+ \alpha\frac{u_i^{n+1} - u_i^{n-1}}{2\Delta t} + \beta\frac{u_{i+1}^{n+1} - 2u_i^{n+1} + u_{i-1}^{n+1} - u_{i+1}^{n-1} + 2u_i^{n-1} - u_{i-1}^{n-1}}{2\Delta t\Delta x^2}. \end{aligned} \tag{4.17}$$

To simplify we let $\lambda_1 = \frac{EI}{\Delta x^4}$, $\lambda_2 = \frac{\rho A}{\Delta t^2}$, $\lambda_3 = -\frac{T_0}{\Delta x^2}$, $\lambda_4 = \frac{\alpha}{2\Delta t}$, $\lambda_5 = \frac{\beta}{2\Delta t\Delta x^2}$, $\lambda_6 = -\frac{\Delta x EA}{4L}$ and

$$T^n = \left[\left(\frac{u_1^n - u_{-1}^n}{2\Delta x}\right)^2 + 2\sum_{i=1}^{N-1}\left(\frac{u_{i+1}^n - u_{i-1}^n}{2\Delta x}\right)^2 + \left(\frac{u_{N+1}^n - u_{N-1}^n}{2\Delta x}\right)^2\right], \tag{4.18}$$

and rearrange Equation (4.17) and we get that,

$$\begin{aligned} F_i^n &= \lambda_6 T^n\left(u_{i+1}^n - 2u_i^n + u_{i-1}^n\right) + (-2\lambda_5 + \lambda_4 + \lambda_2)\,u_i^{n+1} + (\lambda_5)\,u_{i-1}^{n+1} \\ &+ \lambda_1 u_{i+2}^n + (-4\lambda_1 + \lambda_3)\,u_{i+1}^n - \lambda_5 u_{i-1}^{n-1} + (6\lambda_1 - 2\lambda_2 - 2\lambda_3)\,u_i^n \\ &+ (-4\lambda_1 + \lambda_3)\,u_{i-1}^n + \lambda_1 u_{i-2}^n - \lambda_5 u_{i+1}^{n-1} + (\lambda_2 - \lambda_4 + 2\lambda_5)\,u_i^{n-1}. \end{aligned} \tag{4.19}$$

Equation (4.19) can be written in the form

$$A_1 u^{n+1} + A_2 u^n + A_3 u^{n-1} + A_4 T^n u^n = F_i^n. \tag{4.20}$$

The first iteration of the scheme is calculated by,

$$B_1 u^1 + A_2 u^0 + A_4 T^0 u^0 = F_i^0, \tag{4.21}$$

where, $B_1 = A_1 + A_3$. To simplify the matrices we let $\Lambda_1 = -2\lambda_5 + \lambda_4 + \lambda_2$, $\Lambda_2 = 6\lambda_1 - 2\lambda_2 - 2\lambda_3$ and $\Lambda_3 = 2\lambda_5 - \lambda_4 + \lambda_2$ and $\Lambda_5 = -4\lambda_1 + \lambda_3$. A_1 is given by:

$$\begin{bmatrix} \Lambda_1 & 0 & 0 & \dots & \dots & 0 \\ \lambda_5 & \Lambda_1 & \lambda_5 & 0 & \dots & 0 \\ 0 & \lambda_5 & \Lambda_1 & \lambda_5 & 0 & \vdots \\ \vdots & 0 & \ddots & \ddots & \ddots & \vdots \\ \vdots & \vdots & \dots & \lambda_5 & \ddots & \lambda_5 \\ 0 & \dots & \dots & \dots & 0 & \Lambda_1 \end{bmatrix}$$

A_2 is given by:

$$\begin{bmatrix} \Lambda_2 & 0 & 0 & \dots & \dots & \dots & 0 \\ \Lambda_5 & \Lambda_2 & \Lambda_5 & \lambda_1 & 0 & \dots & 0 \\ \lambda_1 & \Lambda_5 & \Lambda_2 & \Lambda_5 & \lambda_1 & \dots & \vdots \\ 0 & \lambda_1 & \ddots & \ddots & \ddots & \ddots & 0 \\ \vdots & \vdots & \ddots & \ddots & \ddots & \ddots & \lambda_1 \\ \vdots & 0 & \ddots & \lambda_1 & \Lambda_5 & \ddots & \Lambda_5 \\ 0 & \dots & \dots & \dots & \dots & 0 & \Lambda_2 \end{bmatrix}$$

A_3 is given by:

$$\begin{bmatrix} \Lambda_3 & 0 & 0 & \dots & \dots & \dots & 0 \\ -\lambda_5 & \Lambda_3 & -\lambda_5 & 0 & \dots & \dots & 0 \\ 0 & -\lambda_5 & \Lambda_3 & -\lambda_5 & 0 & \dots & \vdots \\ \vdots & 0 & \ddots & \ddots & \ddots & \ddots & \vdots \\ \vdots & \vdots & \ddots & \ddots & \ddots & \ddots & 0 \\ \vdots & \vdots & \dots & 0 & -\lambda_5 & \ddots & -\lambda_5 \\ 0 & \dots & \dots & \dots & \dots & 0 & \Lambda_3 \end{bmatrix}$$

and A_4 is given by:

$$\begin{bmatrix} -2\lambda_6 & 0 & 0 & \dots & \dots & 0 \\ \lambda_6 & -2\lambda_6 & \lambda_6 & 0 & \dots & 0 \\ 0 & \lambda_6 & -2\lambda_6 & \lambda_6 & 0 & \vdots \\ \vdots & 0 & \ddots & \ddots & \ddots & \vdots \\ \vdots & \vdots & \dots & \lambda_6 & \ddots & \lambda_6 \\ 0 & \dots & \dots & \dots & 0 & -2\lambda_6 \end{bmatrix}$$

The boundary conditions are given in section 3.3 and are discretized using central difference approximation. Equation (3.4) and equation (3.5) are discretized as equation (4.22) and equation (4.23), respectively.

$$u_0^n = 0 \qquad u_L^n = 0 \tag{4.22}$$

$$u_{-1}^n = -u_1^n \qquad u_{L+1}^n = -u_{L-1}^n \tag{4.23}$$

The initial conditions ar edefined in section 3.4. First consider the system with an initial displacement, thus $f(x,t) = 0$ and $p(x) = 0$.

$$u_i^0 = h(x) \tag{4.24}$$

$$u_i^{-1} = u_i^1 \tag{4.25}$$

Then the system is considered with initial velocity , thus $f(x,t) = 0$ and $h(x) = 0$.

$$u_i^0 = 0 \tag{4.26}$$

$$u_i^{-1} = u_i^1 + 2\Delta t p(x) \tag{4.27}$$

The system is considered with initial velocity and displacement, thus $f(x,t) = 0$.

$$u_i^0 = h(x) \tag{4.28}$$

$$u_i^{-1} = u_i^1 + 2\Delta t p(x) \tag{4.29}$$

Then the system is considered with a force density, thus $p(x) = 0$ and $h(x) = 0$.

4.3.1 Stability Analysis

The traditional stability analysis based on the Von Neumann's stability analysis is not amenable to the nonlinear equation and can only be conducted on linearised forms of the nonlinear equation, in which case the nonlinear model behaves as the linear model provided in Chapter 3 and hence the stability analysis done in Chapter 3 is a lower bound of stability for the nonlinear model. The stability condition of the linear model is a necessary condition for stability.

4.4 Tension Modulation

Recall tension modulation is defined as

$$T_N = \frac{1}{2}\frac{EA}{L_0}\int_0^{L_0}\left(\frac{\partial u}{\partial x}\right)^2 dx \tag{4.30}$$

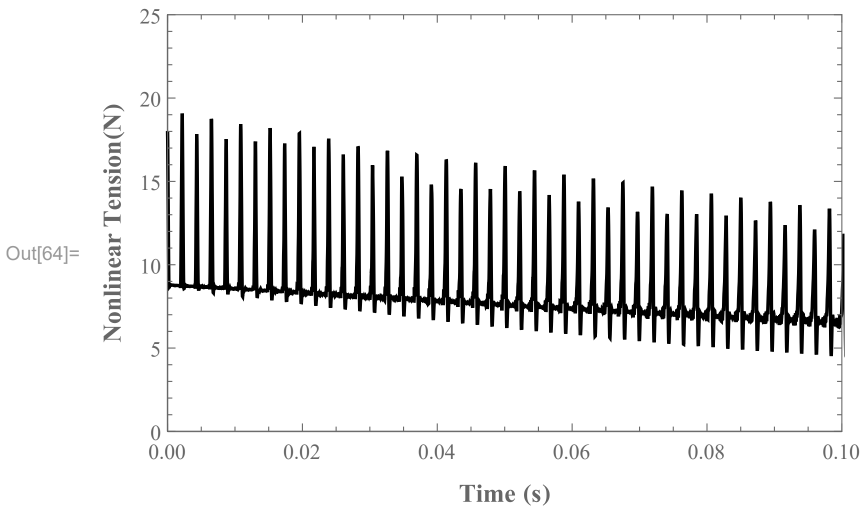

FIGURE 4.1: Tension modulation over time. 0.1 seconds of the simulation.

The tension modulation decrease over time since it is dependent on the total variation of the displacement. The model have a diffusive behaviour and the damping is also driven by the frequency dependent term and frequency independent term. Hence as the string vibrates the tension modulation will decrease. Figure 4.1 represents the tension modulation over time. The dark line represents the average tension modulation.

The tension modulation is at largest at the beginning of the simulation where the displacement variation will be at its largest, hence we expect the tension modulation to be most present at beginning of the sound and the tension then will decrease to the the initial tension of the string at rest.

Chapter 5

Results

In this chapter the vibrations of the model, under the three different initial conditions, defined in section 3.4, will be analysed at three different observation points. The model is discretised using a finite difference method, CTCS which is provided in Section 3.5, then the solution is computed on *Mathematica*. The model is also solved using Functional transformation method, LT/FST method provided in Section 3.6, where the inverse transforms are computed on *Mathematica*. For the purpose of this research only the audible frequency range, from the lowest frequency $20Hz$ to the largest frequency $20000Hz$, is being considered. The restriction of the audible frequency informs us of the choice of the frequency resolution and this then dictates the number of spatial points.

5.1 Implementation of the model.

The partial differential equation, equation 3.3, is used to create the sound of a guitar string that is infinitesimally plucked represented by an initial displacement, infinitesimally struck represented by an initial velocity, a combined initial displacement and initial velocity and a force density which is the most general way of imposing the physical force on the string. These excitation modes are defined in section 3.4. The string is $1m$ long, with cross section area $0.1963mm^2$ and the moment of inertia $0.00307mm^4$. The strings material is characterized by the density, $7800kgm^3$, its Young's modulus, $190GPa$ and the tension applied to the string is $350N$. The decay variables, α and β, are chosen experimentally. Three excitation points are considered and these points are observed at three different positions along the string. The excitation positions and observation positions are points close to the bridge of the guitar. The first position is the closest point to the bridge of the guitar, $\frac{1}{10}$ of the length of the string from the bridge. The second point is $\frac{1}{5}$ of the length of the string from the bridge and the third point is $\frac{3}{10}$ of the length of the string from the bridge.

The FTM, derived in section 3.6, is applied to the model. This method provides an exact solution when considered at infinite modes. For the purpose of this research we consider ten modes to reduce the computational time. While the FTM provides an exact solution it is computationally intractable to compute infinite modes. Ten modes are a poor approximation of infinity and can causes inconsistencies between the result of the FDM and those of the FTM. Since the FTM is computationally intractable a new transformation method was developed to produce an exact solution. This method involves applying the Finite Sine Transformation method and solving the system of ODE. This method produces an exact solution and the method is computationally efficient.
The model is also discretized using finite difference method, central space-central time, derived in section 3.5. The number of spatial steps along the string are set to N, where the step size in space are defined as Δx and the step size in time are defined as Δt.

5.2 Qualitative Comparison

In this section spectrograms of the resultant vibrations on the string are provided. Recall that the model is considered with three initial conditions and at varying observation points. A spectrogram is the visual representation of the spectrum of the frequencies. It illustrates how the frequencies varies in time. The spectrograms provided are of the model considered with different excitation states. Through the spectrograms provided in Section 5.2.1, Section 5.2.2 and Section 5.2.3 it is observed that the finite difference scheme approximates the exact solution derived from the FTM and the adapted FTM. We can then use the Finite Difference scheme to analyse the model further and in Appendix B the full Fourier analysis of the more efficient method is provided. The force density results are only analysis using the Finite difference scheme.

5.2.1 Spectrograms produced by the linear model with Initial Displacement and Initial Velocity

Figure 5.1 and Figure 5.2 illustrate the spectrum of the linear model provided in Section 3 where the model is excited with an initial displacement and initial velocity. The initial displacement and initial velocity are defined in Section 3.4 and are given as

$$
\begin{aligned}
&u(x,0) = h(x),\\
&\frac{\partial u}{\partial t}(x,0) = p(x)\\
&f(x_0,x,t) = 0.
\end{aligned}
$$

Figure 5.1 is spectrum provided by the Finite difference approximation scheme. The horizontal darker bands that appear in the lower frequencies show that a higher concentration of energy is observed at the pick up position. In the higher frequencies a lower concentration of energy is observed and the higher frequencies are not dominate in the sound, this is further illustrated in Appendix **??**. This is depicted by the faint colour in the spectrogram. From the spectrogram we can observe the behaviour of the frequency dependent damping term that appears in the model. Over time we can see the decay of frequency, the frequency over time vanishes. The higher frequencies decay faster due the fact that the higher frequencies are not as strong as the lower frequencies.

Figure 5.2 has a similar behaviour as seen as in Figure 5.3 and 5.1 except the FTM does not correctly capture the frequencies that contribute to the sound. The spectrogram appears darker, with more frequencies being present. Where as the adapted method, Figure 5.3, shows distinct dark bands where the energy is concentrated. This is similar to what is observed in Figure 5.1. The general sound and behaviour of the sound is observable in exact solution and can verify the results of the FDM. The frequency dependent decay variable is visible in the high frequencies first as there is less energy in the high frequencies. Thus the sound will dissipate in six seconds. The energy produced by the initial displacement is larger then that produced by the initial velocity.

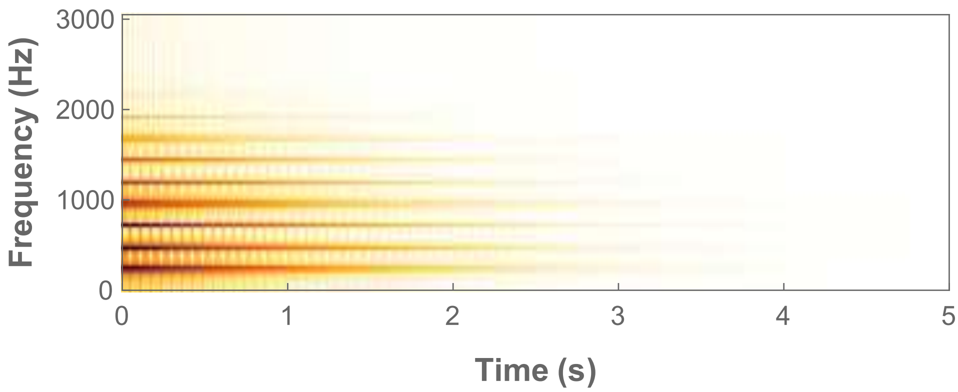

FIGURE 5.1: Spectrogram produced by the finite difference approximation scheme of the model.

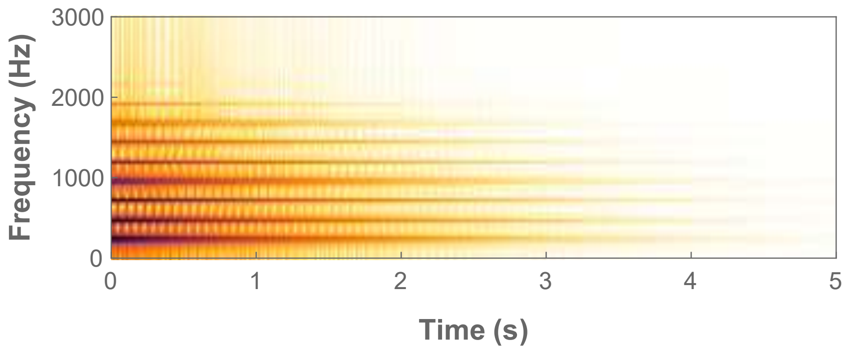

FIGURE 5.2: Spectrogram produced by the transformation method of the model.

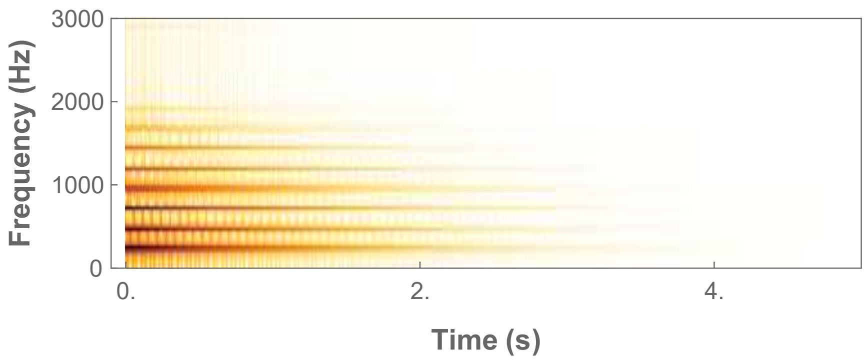

FIGURE 5.3: Spectrogram produced by the adapted Transformation method.

5.2.2 Spectrograms produced by the linear model with Initial Displacement

Figure 5.4 and Figure 5.5 illustrate the spectrum of the linear model provided in Section 3, where the model is excited with an initial displacement. The initial displacement is defined in Section 3.4 and is given as

$$
\begin{aligned}
&u(x,0) = h(x),\\
&\frac{\partial u}{\partial t}(x,0) = 0\\
&f(x_0,x,t) = 0.
\end{aligned}
$$

Figure 5.4 is spectrum provided by the Finite difference approximation scheme. We observed that the horizontal darker bands that appear in the lower frequencies show that a higher concentration of energy is observed. In the higher frequencies a lower concentration is observed and the higher frequencies do not dominate the sound. This is depicted by the faint colour in the spectrogram. The higher frequencies decay faster due to the fact that the higher frequencies have lower energy than the lower frequencies.
Figure 5.6 is the spectrogram of the exact solution produced by the adapted transformation method. When considering this spectrogram in comparison with that of Figure 5.4 we can see that the frequency profiles are similar and the model behaviour is seen in both, with the frequency dependent decay affecting the higher frequencies first since they are not as strong as the low frequency.

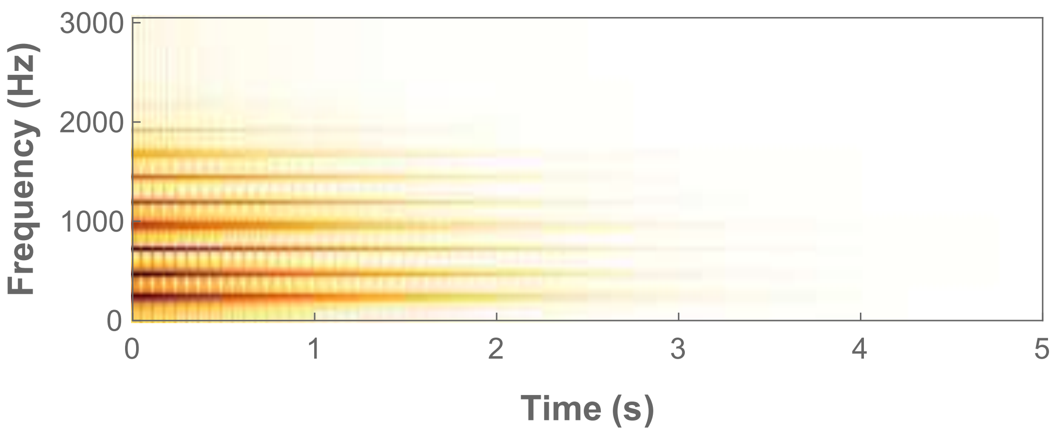

FIGURE 5.4: Spectrogram of the finite difference scheme.

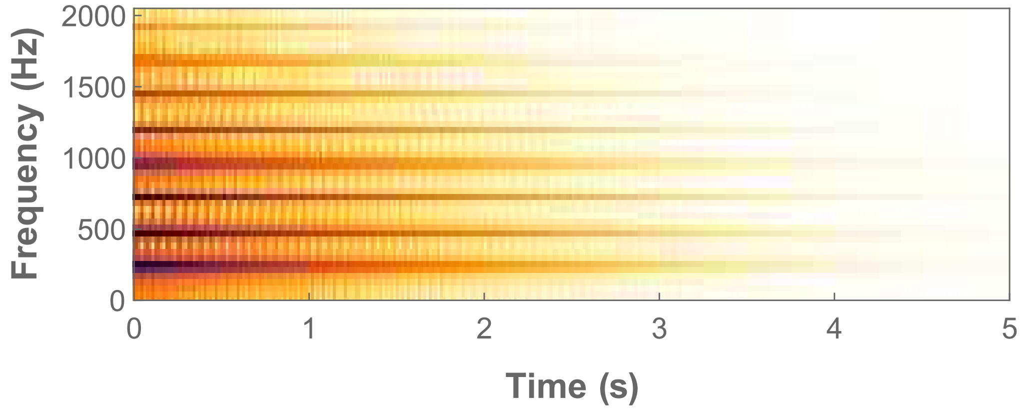

FIGURE 5.5: Spectrogram of the the FTM.

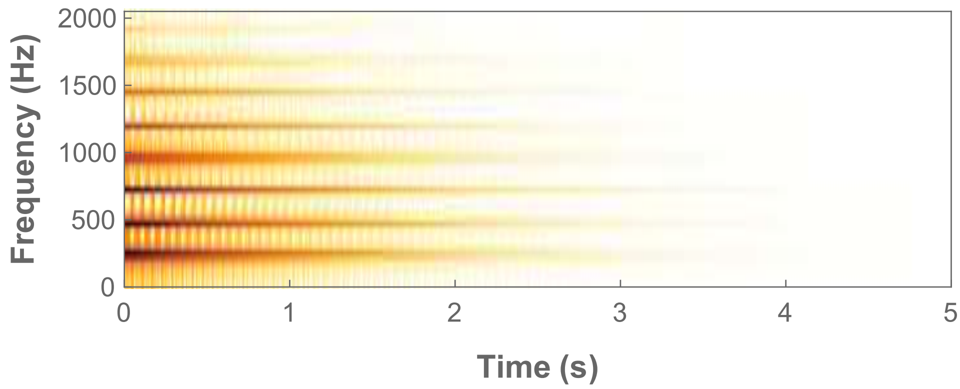

FIGURE 5.6: Spectrogram of the adapted functional transformation method.

5.2.3 Spectrograms produces by the linear model with Initial Velocity

Figure 5.4 and Figure 5.5 illustrate the spectrum of the linear model provided in Section 3 where the model is excited with an initial velocity. The initial velocity is defined in Section 3.4 and is given as

$$
\begin{aligned}
&u(x,0) = 0, \\
&\frac{\partial u}{\partial t}(x,0) = p(x), \\
&f(x_0,x,t) = 0.
\end{aligned}
$$

Figure 5.7 is the Finite difference spectrogram, Figure 5.8 is the FTM spectrogram and Figure 5.9 is the adapted transformation method spectrogram. The Figures have a thin bands which illustrates that the energy produced by applying an initial velocity is low even in the low frequencies. The initial velocity produces low frequencies with low energy. Their are no high frequencies present thus the sound will be a low pitch sound. Since the frequencies have less energy we see the effects of the frequency dependent decay term within less then one second of the simulation and the sound dissipates in two seconds.

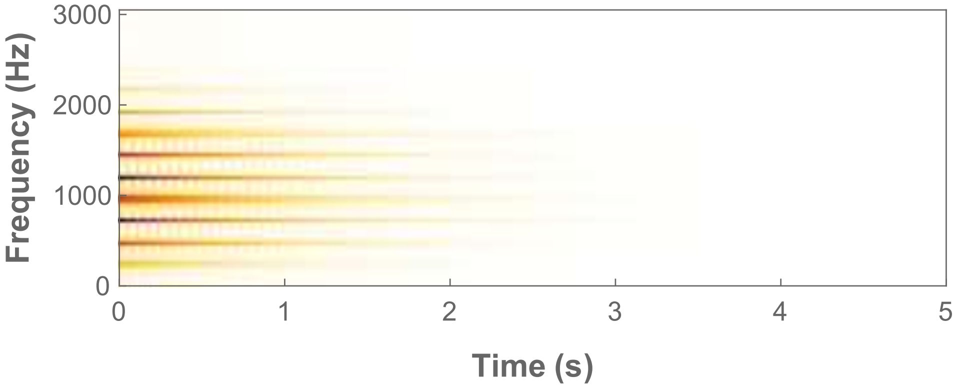

FIGURE 5.7: Spectrogram of the finite difference method.

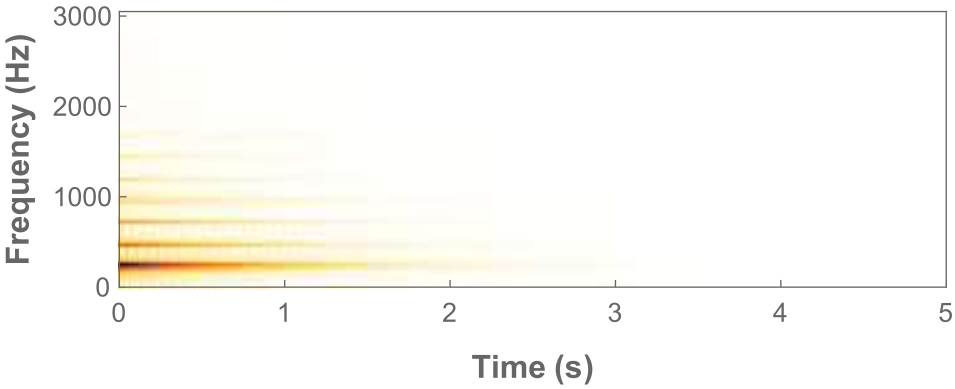

FIGURE 5.8: Spectrogram of the Transformation method.

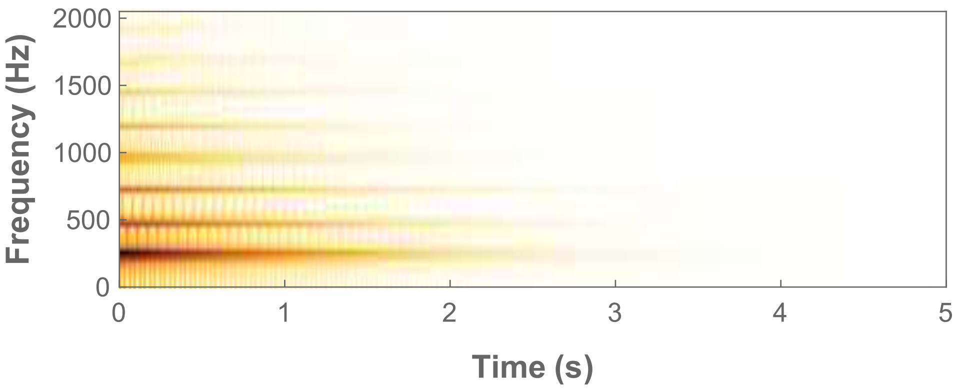

FIGURE 5.9: Spectrogram of the the adapted functional transformation method.

5.2.4 Spectrograms produced by the linear model with a Force Density.

The previous sections show that the FDM is an appropriate method to approximate the behaviour of a vibrating string. The FTM has less detail in the high frequencies which is a result of the method being computed for ten modes. Figure 5.10 illustrate the spectrum of the linear model provided in section 3, where the model is excited with a force density. The force density is defined in Section 3.4 and is given as

$$
\begin{aligned}
&u(x,0) = 0, \\
&\frac{\partial u}{\partial t}(x,0) = 0, \\
&f(x_0,x,t) = F(t)g(x_0,x).
\end{aligned}
$$

Figure 5.10 is the spectrogram produced by the finite difference scheme. Once again the Frequency dependent decay variables is observed. The higher frequencies have low energies and thus they are seen to decay at the faster rate then the low frequencies. There are distinct bands, in the lower frequency where the higher concentration is observed. The faint bands illustrating that the frequencies do not have high energy values and it is see that these bands decays sooner than the darker band. The frequency dependent decay term is the reason for this.

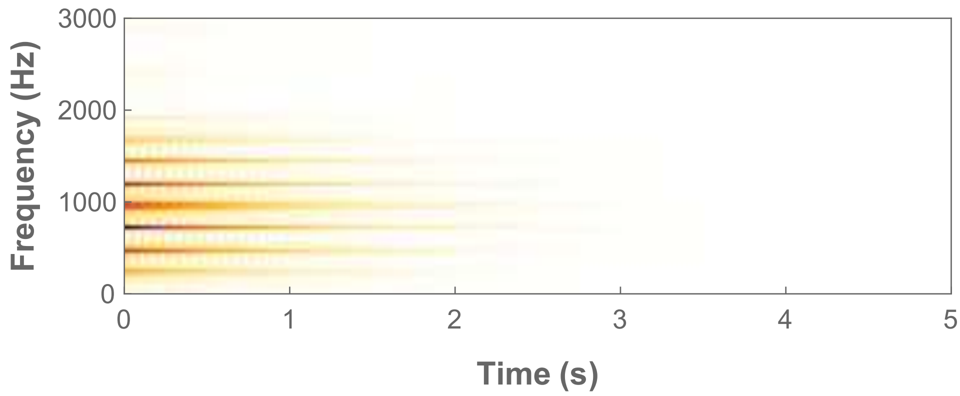

FIGURE 5.10: Spectrogram of the finite difference method.

5.2.5 Interpretation of linear model Spectrograms

From these results we can see the behaviour of the sounds over time. The vibrations of a string with all the initial condition configurations produce low frequencies sounds. The effects of the frequency dependent term is visible in all the methods. The effects vary depending on how much energy the frequencies have. In the case of the initial velocity the frequencies have low energy and thus decay sooner than those produced by the other initial conditions. The initial displacement produces the strongest spectrogram and the frequencies take the longest to decay over time. The initial velocity has a weak spectrogram which decays the fastest. The full range of spectrograms produced at the difference excitation positions and seen at the difference observation points is illustrated in Appendix A. The initial displacement and velocity spectrogram is similar to the initial displacement spectrogram, which is confirmed by the relatively weak initial velocity spectrogram. The sound generated is predominately constructed by the plucking of the string rather than the strumming of the string. The spectrum produced by the finite difference approximation scheme and the adapted transformation method is a fuller production of the sound than that of the exact solution since only a few modes in the FTM where considered. This was done to decrease the computational time of the method. The results of the FDM can be verified by the adapted transformation method. The force density spectrograms describe a behaviour similar to the struck string since the spectrogram illustrates a similar behaviour to the spectrogram of the initial velocity. The spectrogram is darker and thicker than the initial velocity spectrogram. This implies that the force density produces larger energy.

5.3 Fourier Analysis on the linear model

A Fourier Analysis is conducted on the resultant time series of the model, Equation (3.3), with the initial condition. The method transfers the time series into the frequency domain and decomposes it in to sinusoids that are harmonics of the fundamental frequency of the model. Thus, the Fourier analysis allows us to analyse the model in the frequency domain. The Fourier analysis provides the fundamental frequency of the vibrations of the string and the amplitudes of the given harmonic frequencies can be identified. This allows us to investigate the amplitudes of the frequencies and how the set up of the energies effects the sound produced by the string. To analyse the model a Fourier series of the data that is observed at a given position is extracted. The Fourier transform is implemented using *Mathematica* Fourier's function. Three different observation positions, points where the vibrations are observed, are investigated. The method allows us to see the different harmonic frequencies that are registered at an observation point and the energies of those frequencies at those points. A guitar is excited near the bridge of the guitar thus the observation points and excitation points are defined as a distance from the bridge of the guitar.

5.3.1 Fourier Transform of the linear model with an Initial displacement

The figures below are resulting from the Fourier analysis of the PDE, Equation (3.3), with an initial displacement applied to the string. The initial displacement is defined in Section 3.4 and is given as

$$\begin{aligned} &u(x,0) = h(x), \\ &\frac{\partial u}{\partial t}(x,0) = 0, \\ &f(x_0, x, t) = 0. \end{aligned}$$

Figure 5.11, 5.12 and 5.13 represents the frequencies observed at three different pick up positions on the string. Each figure illustrates the amplitudes that are produced by applying the initial displacement at different excitation positions. At the first observation point, Figure 5.11, the sounds produced have high frequency detail that results in bright sounds that very as you excite the string further from the bridge of the guitar. The high frequencies in the sound be come weaker and the fundamental frequency becomes stronger making the sound fuller as the excitation point moves away from the bridge. The energies produced by the first excitation position has low frequencies that have higher energy than the energy in the high frequencies but the higher frequencies have a strong presence in the sound, producing a bright and full sound. The second excitation point produces a sound that has weaker high frequencies than the sound produced at the first position meaning that the sound that is produced at this point is darker. The sound is still one of the brighter sounds since the high frequencies have a significant effect on the sound. The third excitation point produces the darkest of the three sounds

but the sound has high frequency detail that means that the sound is bright.
At the second observation position, Figure 5.12, the fundamental frequencies are strong and the high frequencies are in the same amplitude range as seem in Figure 5.11, the first point of observation. This result in the sounds having weaker high frequencies, as a result the sound is darker at this observation point. As the excitation point moves further from the bridge of the guitar the fundamental frequency has more energy and the high frequencies become weaker. The sounds become fuller and darker.

At the observation position furthest from the bridge of the guitar, Figure 5.13, the fundamental frequency have there highest energy and the high frequency range remains the same. At all the observation points it can be seen that the high frequencies have low energies and that the high energies are dominantly in the low frequencies. The first excitation point produces higher energy at all of the harmonic frequencies except at the fundamental frequencies where the energies are the highest in all the observation points for each of the excitation positions. It is seen that at the observation point furthest from the bridge of the guitar the energies of the fundamental frequencies are at there highest and thus the loudest sound is produced at this observation point. It is also seen that as the point of observation moves further from the bridge of the guitar, the change in energy from the low frequencies to the high frequencies becomes more dramatic where the lower frequencies are at there overall highest and the high frequencies stay in the same energy range.

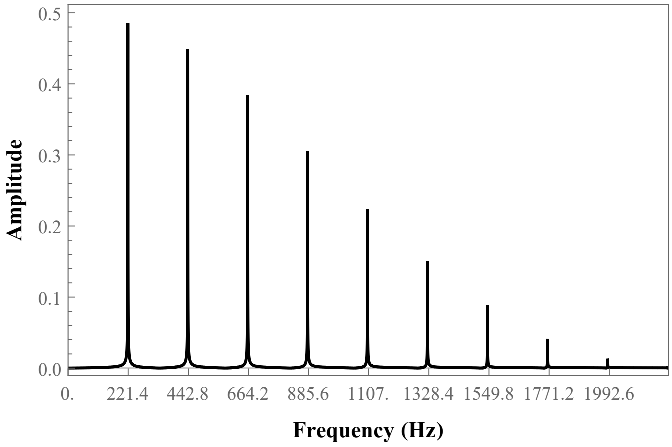

(A) Excitation 1

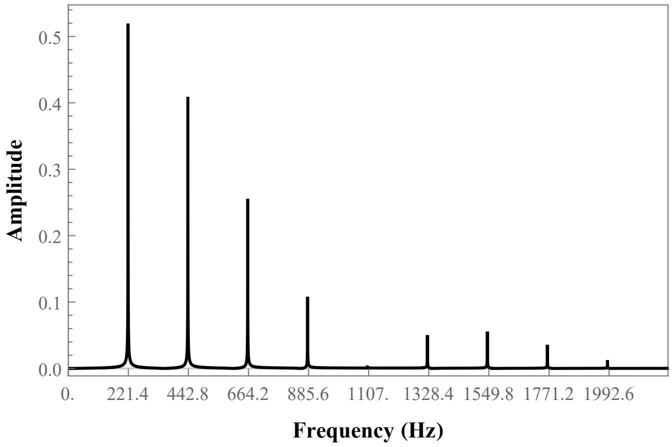

(B) Excitation 2

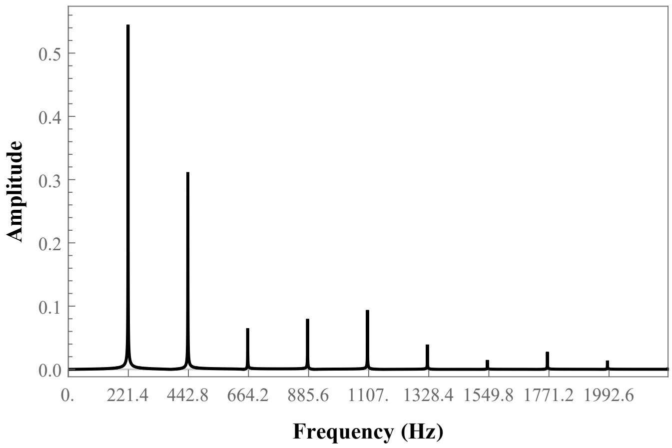

(C) Excitation 3

FIGURE 5.11: The Fourier analysis of the Finite Difference scheme at first observation positions where the model is excited by an initial velocity and initial displacement.

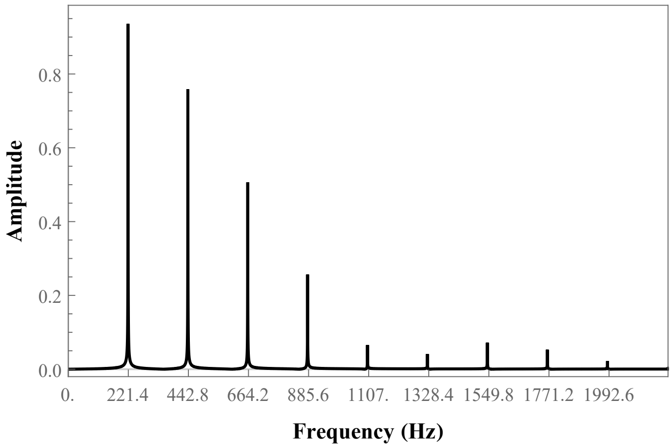

(A) Excitation 1

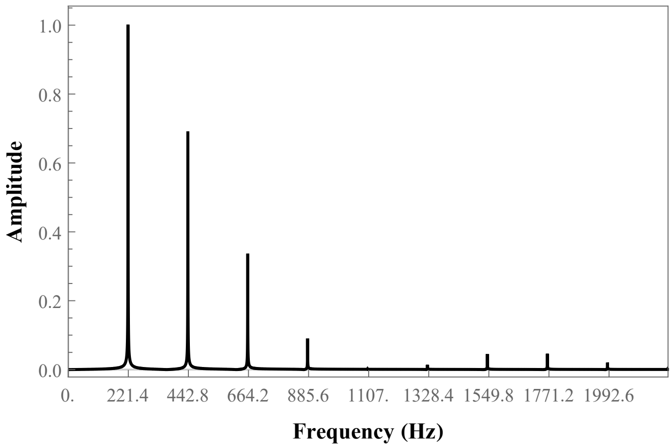

(B) Excitation 2

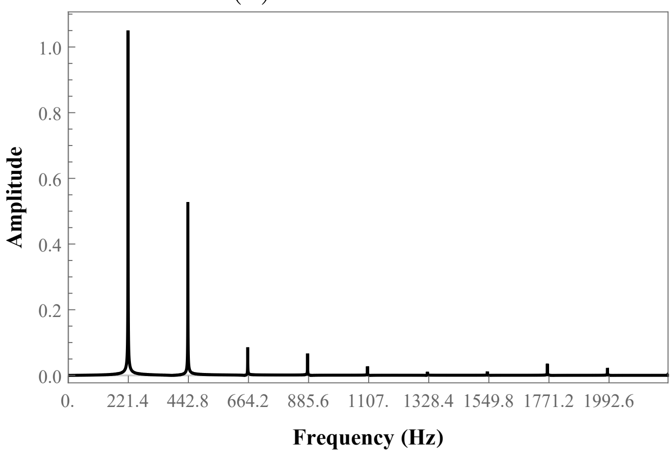

(C) Excitation 3

FIGURE 5.12: The Fourier analysis of the Finite Difference scheme at second observation positions where the model is excited by an initial velocity and initial displacement.

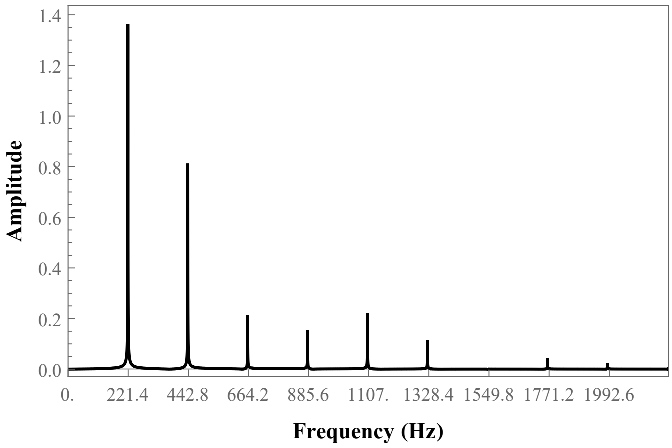

(A) Excitation 1

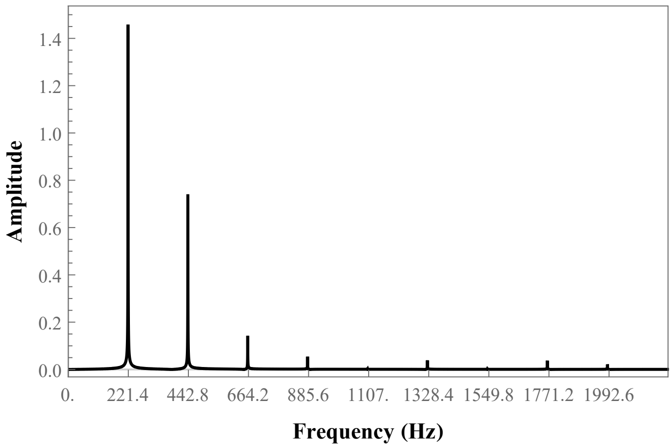

(B) Excitation 2

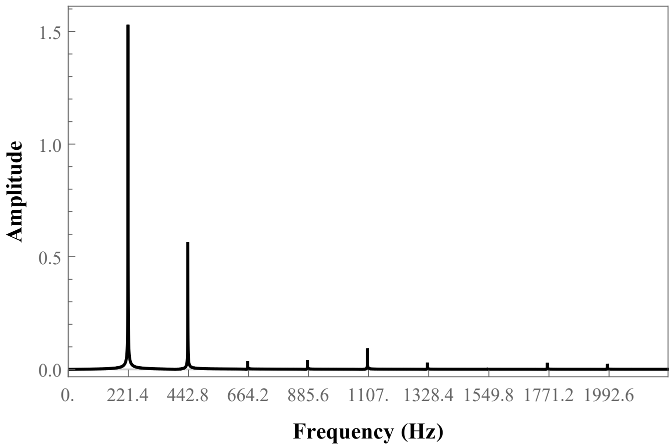

(C) Excitation 3

FIGURE 5.13: The Fourier analysis of the Finite Difference scheme at third observation positions where the model is excited by an initial velocity and initial displacement.

5.3.2 Fourier transform of the linear model with an Initial velocity

The figures below are the resulting Fourier analysis graphs of the PDE, Equation (3.3), with an initial velocity applied to the string. The initial velocity is defined in Section 3.4 and is given as

$$\begin{aligned}
&u(x,0) = 0,\\
&\frac{\partial u}{\partial t}(x,0) = p(x),\\
&f(x_0,x,t) = 0.
\end{aligned}$$

Figure 5.14 represents the frequencies registered at the first observation point. The sounds have low amplitudes in comparison to the sounds at in Section 5.3.1. The sound produced at the first excitation position is of a medium pitch since the highest amplitudes are in the middle of the frequency range but the sound is still dominant in the low frequencies. The second excitation position has two amplitude peaks and the peak with the highest energy is in the low frequencies range and the high frequency range has lower energies thus the sound is low pitch sound. The third excitation position has three peaks where the highest energy is in the low frequency and the energies in the peaks decrease with the lowest in the high frequencies.

Figure 5.15 represents the behaviour registered at the second pick up position. The low frequencies have the higher energies and the high frequency sounds will decay before the low frequency sounds. The sound will be dominantly low pitch.

Figure 5.16 represents the behaviour at the third pick up position. These sounds resonate in the low frequencies and this pick up point has the highest energies of all three pick up points. The first excitation position has the lowest energies of the three excitation positions and the third excitation position has the highest energies. As you move away from the bridge of the guitar the energies increase thus the sound becomes louder and the lower frequencies become more dominant, thus the pitch is lowest at the third observation point.

The results of the initial velocity have low energy in comparison to those produced in Section 5.3.1 thus the sounds are soft. The sounds produced in Section 5.3.1 are darker sounds that take a long time to decay.

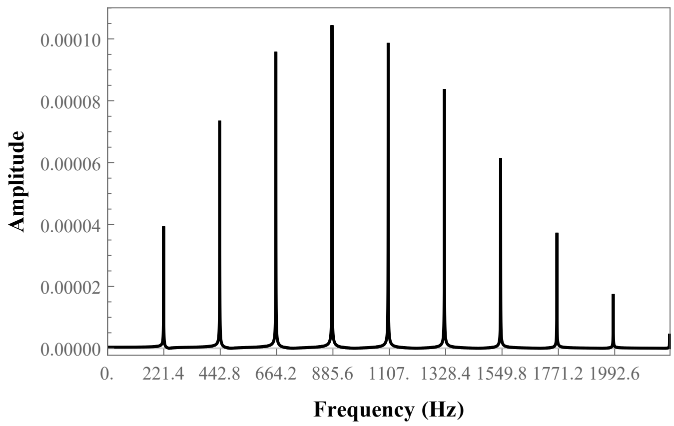

(A) Excitation 1

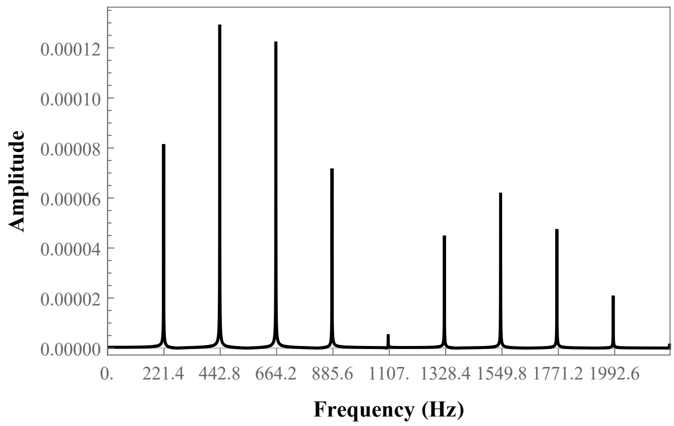

(B) Excitation 2

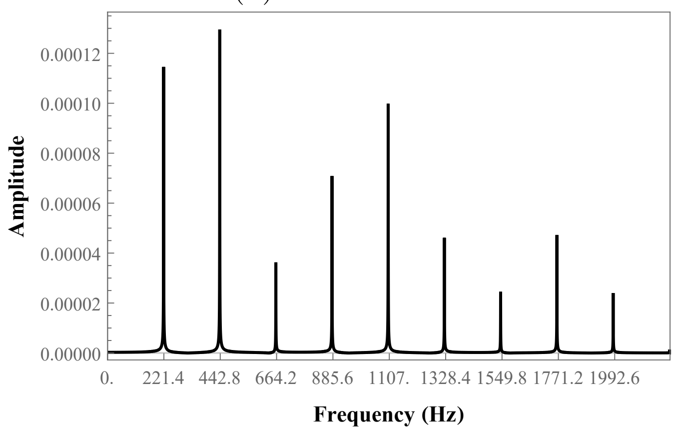

(C) Excitation 3

FIGURE 5.14: The Fourier analysis of the Finite Difference scheme at first observation positions where the model is excited by an initial velocity.

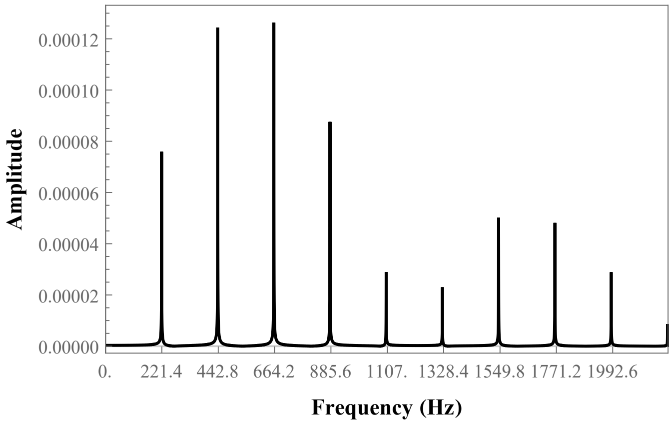

(A) Excitation 1

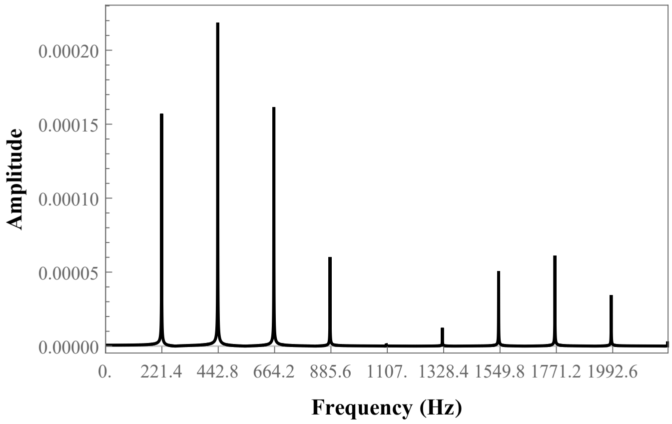

(B) Excitation 2

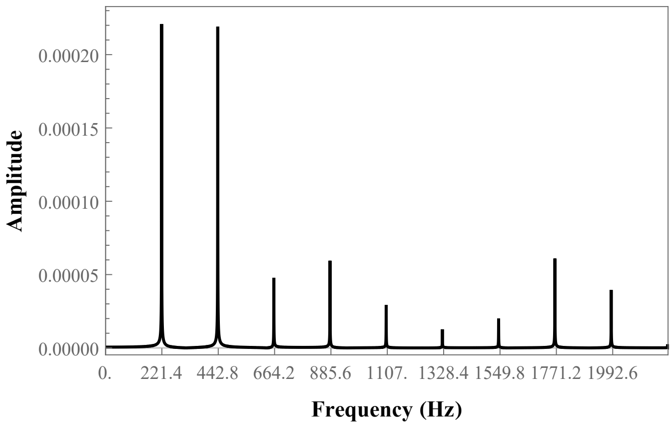

(C) Excitation 3

FIGURE 5.15: The Fourier analysis of the Finite Difference scheme at second observation positions where the model is excited by an initial velocity.

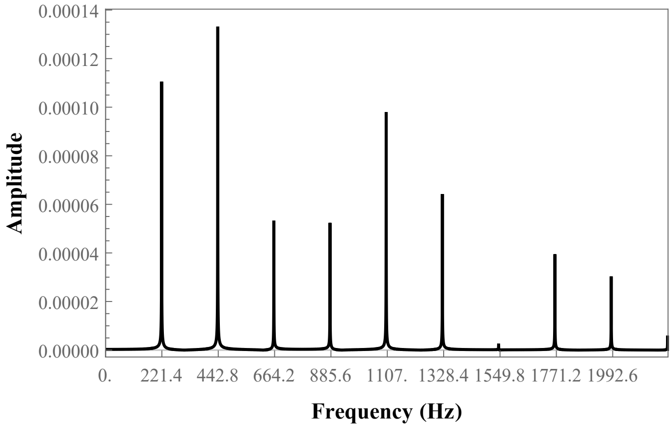

(A) Excitation 1

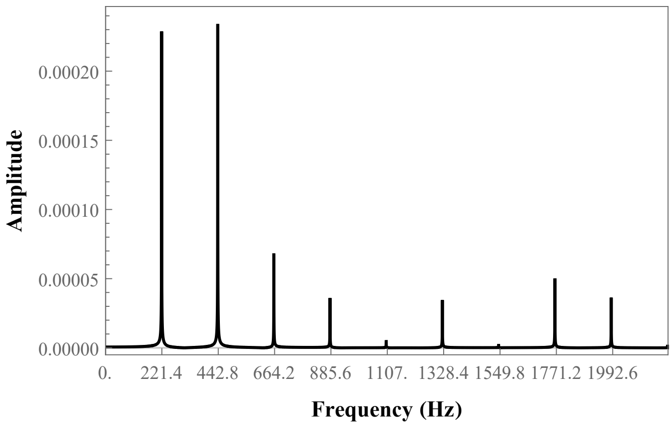

(B) Excitation 2

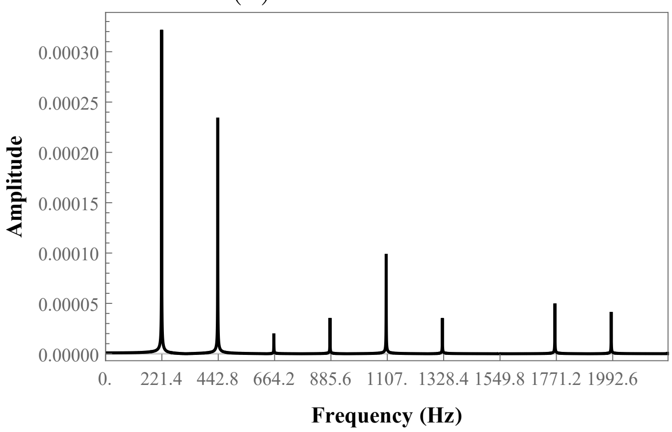

(C) Excitation 3

FIGURE 5.16: The Fourier analysis of the Finite Difference scheme at third observation positions where the model is excited by an initial velocity.

5.3.3 Fourier transform of the linear model with an Initial displacement and initial velocity

Consider Equation (3.3) with initial conditions defined in Section 3.4. The figures below are the resulting Fourier analysis graphs of the PDE, Equation (3.3), with an initial displacement and initial velocity applied to the string. The initial condition is defined in Section 3.4 and is given as

$$\begin{aligned} &u(x,0) = h(x),\\ &\frac{\partial u}{\partial t}(x,0) = p(x),\\ &f(x_0,x,t) = 0. \end{aligned}$$

In Section 5.3.3 the spectrograms of the initial displacement and the spectrogram of the initial displacement and initial velocity suggested that the sounds produced at these excitation produces similar sounds. The Fourier Analysis confirms that the amplitudes of the initial displacement are significantly larger then those produced by the initial velocity and the effects of the initial displacement dominate the excitation. As the excitation position moves further from the bridge of the guitar the sound becomes darker as the high frequency detail reduces and the amplitude of the fundamental frequency increases. As the observation position moves further from the bridge of the guitar the high frequencies stay in the same amplitude range and the amplitudes of the low frequencies increase. Thus the sound loses high frequency detail and the sound at the third observed point excited at the third position is the darkest sound produced.

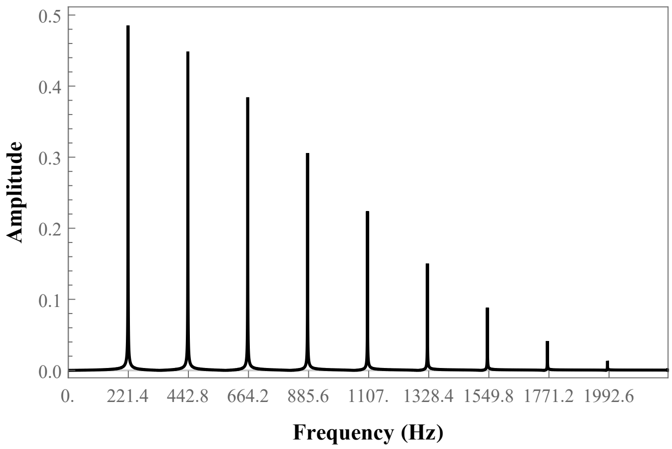

(A) Excitation 1

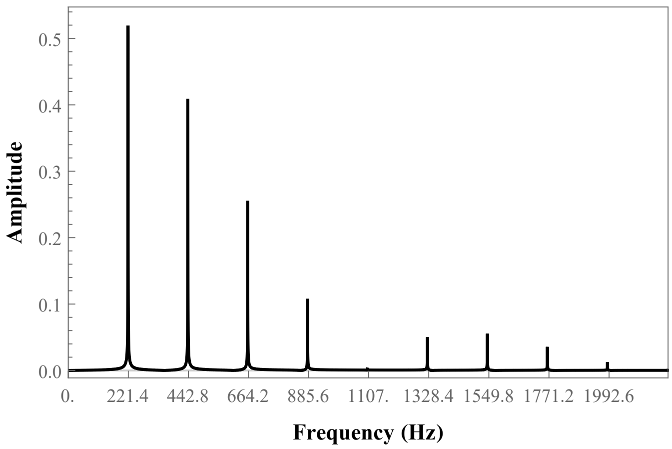

(B) Excitation 2

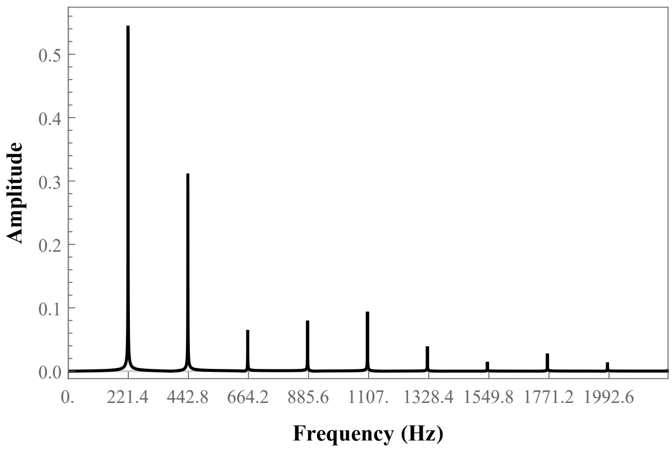

(C) Excitation 3

FIGURE 5.17: The Fourier analysis of the Finite Difference scheme at first observation positions where the model is excited by an initial velocity and initial displacement.

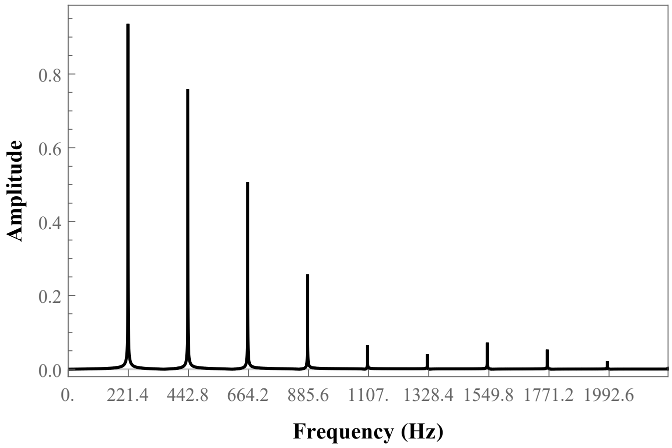

(A) Excitation 1

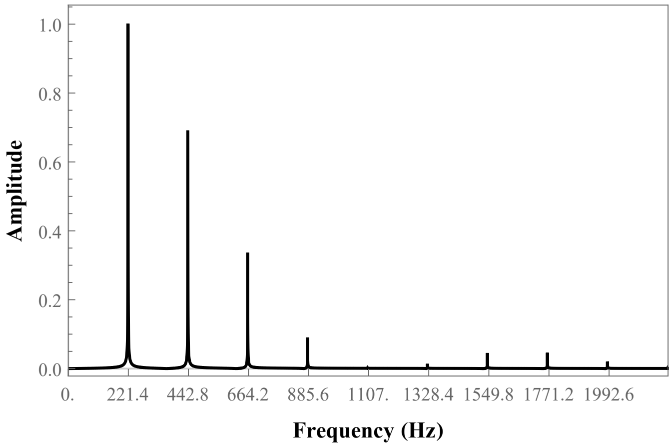

(B) Excitation 2

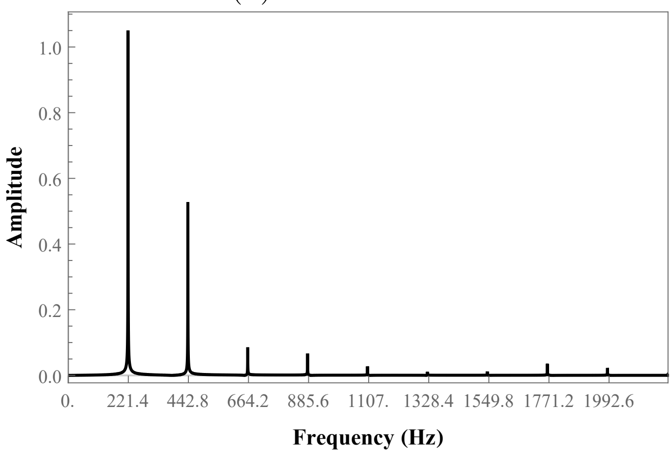

(C) Excitation 3

FIGURE 5.18: The Fourier analysis of the Finite Difference scheme at second observation positions where the model is excited by an initial velocity and initial displacement.

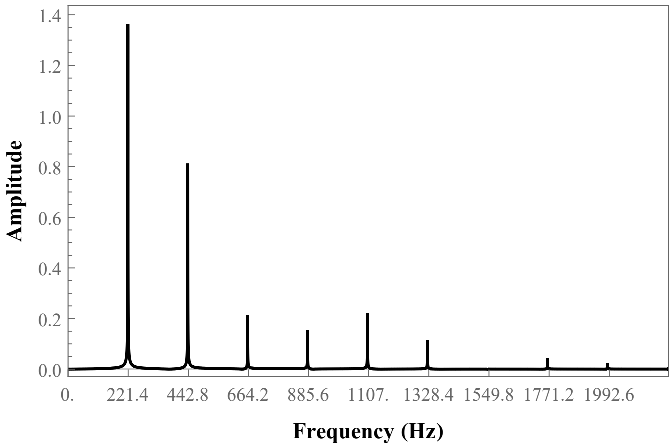

(A) Excitation 1

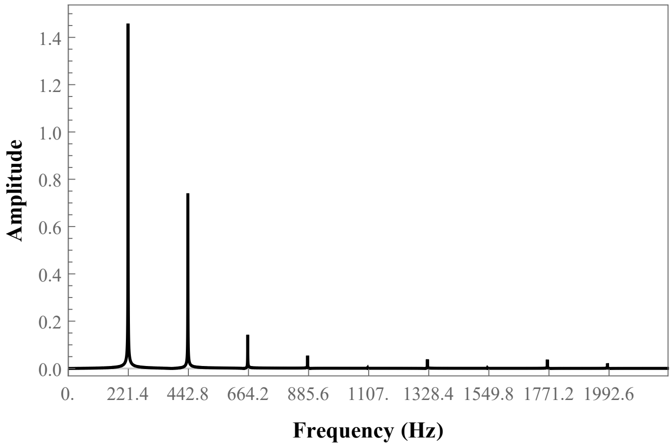

(B) Excitation 2

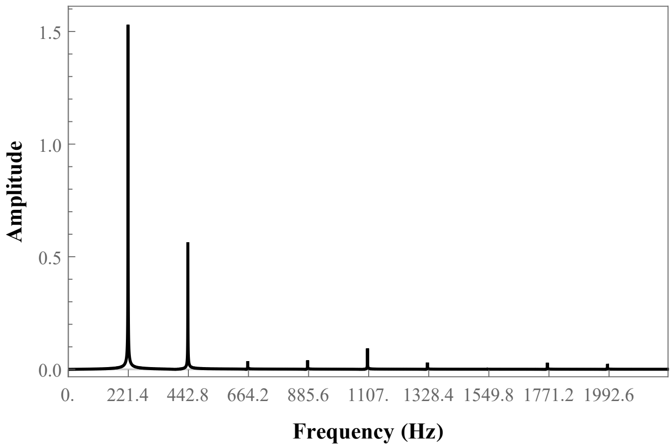

(C) Excitation 3

FIGURE 5.19: The Fourier analysis of the Finite Difference scheme at third observation positions where the model is excited by an initial velocity and initial displacement.

5.3.4 Fourier transform of the linear model with a Force density

In this section a force density term, defined in Section 3.4, is used to excite the system. The Force density is defined in Section 3.4 and is given as

$$
\begin{aligned}
&u(x,0) = 0,\\
&\frac{\partial u}{\partial t}(x,0) = 0\\
&f(x_0,x,t) = F(t)g(x_0,x).
\end{aligned}
$$

Figure 5.20, 5.21 and 5.22 represents the frequencies observed at three different observation positions on the string. Each figure illustrates the amplitudes that are produced by applying a force density at different positions to excite the string.
In Figure 5.20 the sound produced by the first excitation position has a smooth transition in frequencies and is a low energy sound. The sound that is generated is a bright sound with high frequency detail and since the high frequencies have the relatively high energy in comparison to the low frequencies the sound is thin and bright. The sound is high pitched and harsh. The sound produced by the second excitation position has two distinct envelopes, the first envelope is over the low frequencies, which has the higher energies and the second envelope which is over the high frequencies has a lower energies. The sound is bight and has more energy then the first sound. The low frequency and the high frequency have a larger difference and thus the sound is darker than the first excitation point sound. The sound at the third excitation is a bright and thin sound since the harmonic frequencies have relatively large energies.
In Figure 5.21 the sounds at all the excitation positions have its highest energies in the lower frequencies and the high frequencies have low energies. The sound produced by exciting the sting at the first observation point has the lowest energies thus the sound here is darker than the sound at the other two excitation positions. As the string is excited further away from the bridge of the guitar the energies of the low frequencies increase.

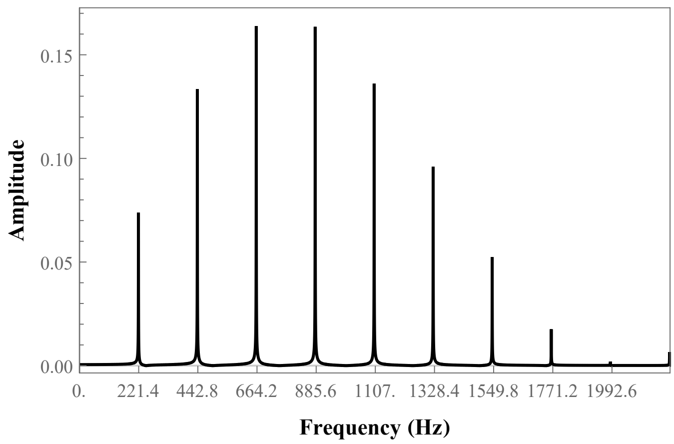

(A) Excitation 1

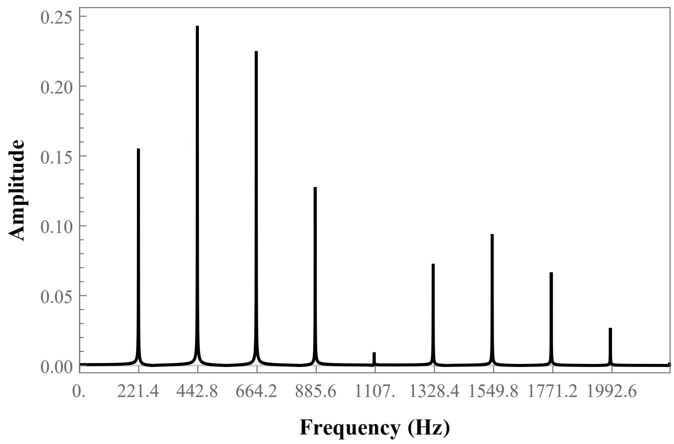

(B) Excitation 2

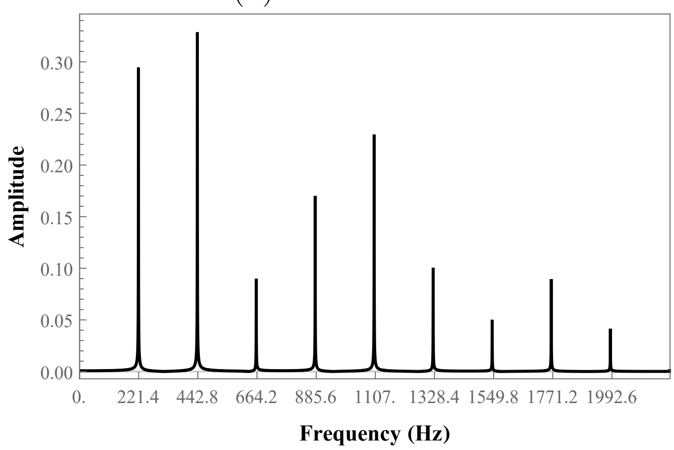

(C) Excitation 3

FIGURE 5.20: The Fourier analysis of the Finite Difference scheme at first observation positions where the model is excited by a force density.

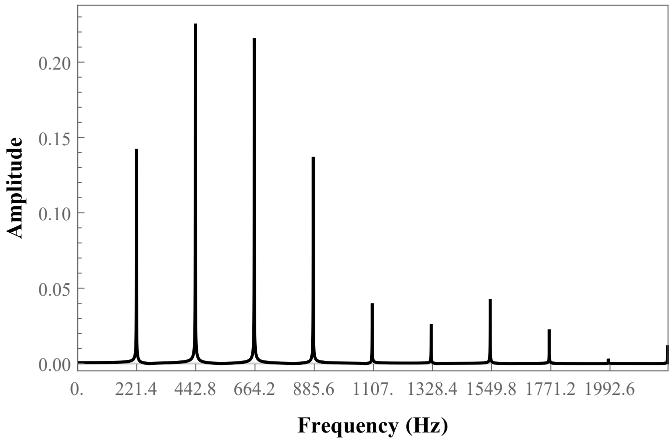

(A) Excitation 1

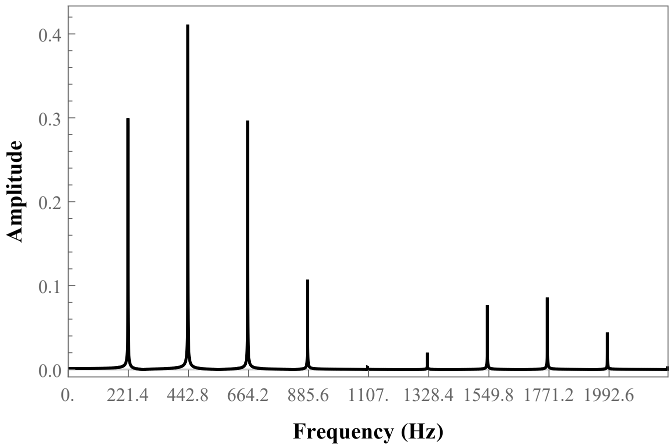

(B) Excitation 2

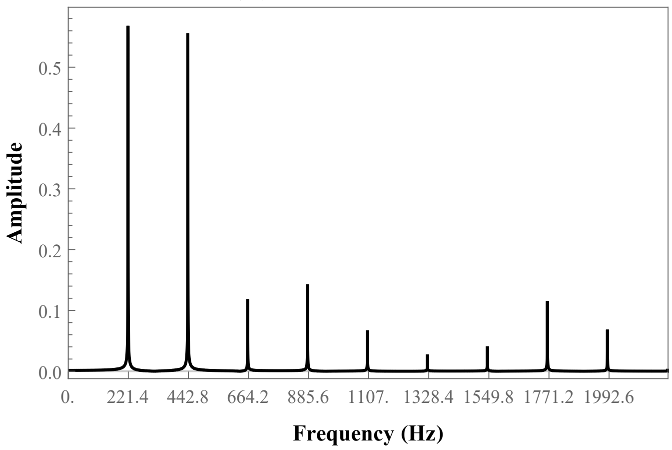

(C) Excitation 3

FIGURE 5.21: The Fourier analysis of the Finite Difference scheme at second observation positions where the model is excited by a force density.

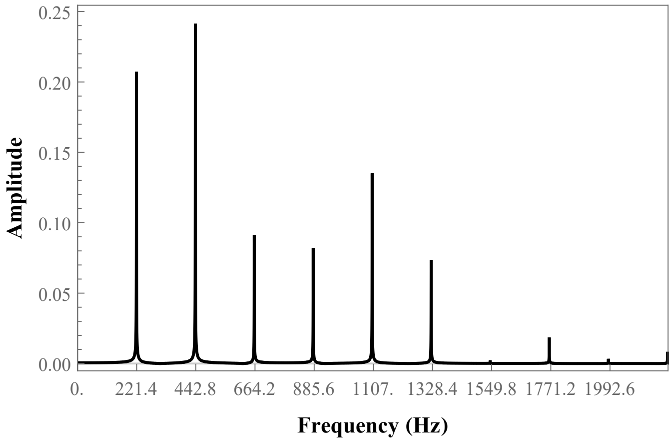

(A) Excitation 1

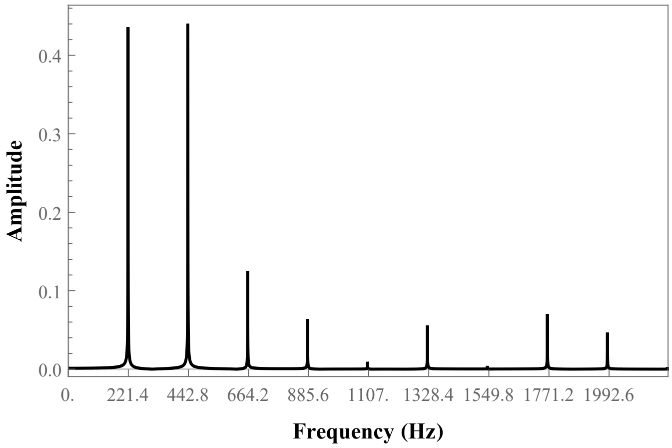

(B) Excitation 2

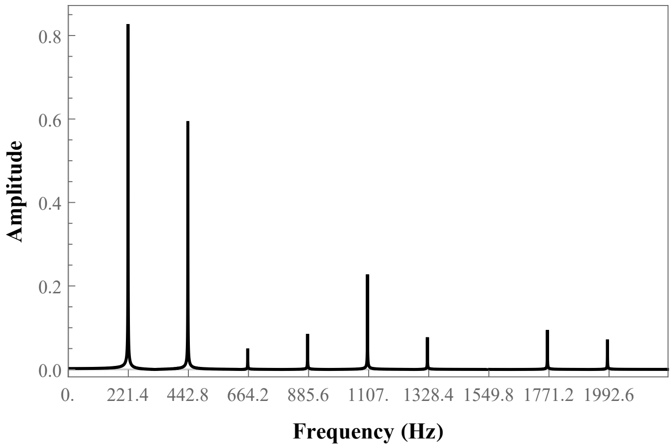

(C) Excitation 3

FIGURE 5.22: The Fourier analysis of the Finite Difference scheme at third observation positions where the model is excited by a force density.

In Figure 5.22 the sound at all the excitation positions has an energies highest in the low frequencies and very low energies in the high frequencies. The first excitation position has the lowest energies. The second excitation point and the third excitation point has the highest energies at the fundamental frequency and there is a dramatic change in the energies observed at the lowest frequencies and at the higher frequencies. Thus the sound generated at this excitation point is dark and still have detail in the high frequencies.

5.4 Discussion on the linear model

From the above results we see that the sound of the guitar is dependent on the point of observation and the excitation position. The effects of the excitation point are viewed at each point of observation. As the observation point moves further from the bridge of the guitar the sound becomes darker and rounder since the low frequencies increase in energy, making the high frequencies less significant in the sound. As the excitation point moves away from the bridge the fundamental frequency becomes stronger and that results in the sound becoming fuller and darker. The high frequencies become less prominent. This implies that the sound that is heard at the third observation point and is excited at the furthers excitation point will have the least presence of high frequency sounds. The sound is dark and full in comparison to the sounds at the first two observation points. The sound that is heard at the first observation point, the closest to the bridge of the guitar, and excited at the first excitation point is a bright sound with high frequency detail.

The initial displacement frequency analysis is similar to the initial displacement and initial velocity. This behaviour is seen in the spectrogram analysis and the Fourier analysis further confirms that the initial displacement takes preference over the initial velocity which is seen to have an infinitesimal effect on the results. The relatively low amplitudes produced by the initial velocity are insignificant in comparison to the amplitudes produced by the initial displacement. The frequency analysis of the force density results have a similar behaviour to those of the initial velocity implying that the force density describes a string being initially struck. This further confirms the spectrogram analysis. The amplitudes of the force density results are relatively large compared to the amplitudes produced by the initial velocity, meaning the sound produced will have more detail and better describe the act of striking a string.

Appendix A provides the spectrogram at each point of excitation for all of the examined observation points. We see that as the observation point moves further from the bridge of the guitar the spectrum have less detail in the high frequencies.

The sound strongly resonates in the low frequencies. It can be seen that all the sounds observes at the first point are bright since the high frequencies have the most detail at this point for their respective excitation point. The first excitation point generates the spectrograms with the most high frequency detail at all the observation points, with the first point of observation having the brightest sound. As the excitation point moves further from the bridge the sound darkens since the high frequencies become weaker. The darkest sounds are created when the string is excited at the third excitation point and where the sounds low frequency intensity increases as you move the point of observation further form the bridge of the guitar, this results in a dark and full sound. Appendix B provides the Fourier analysis of the adapted functional transformation method. From this the results produced by the FDM are verified since the method provides an exact solution. The solution produced by the method does not simulate infinite modes but the sounds produced are similar. However the initial velocity results are inconsistent.

5.5 Nonlinear Spectrograms

The spectrograms provided in this section illustrate the tension modulation over time. The change in frequency is caused by the tension modulation. This will result in a sound that changes pitch over time. The change in pitch is dominant in the beginning of the sound.

A spectrogram is the visual representation of the spectrum of the frequencies. It illustrates how the frequencies varies in time. The spectrograms provided are of the model considered with different excitation states. These spectrograms are of sounds produced at the four initial conditions, where Figure 5.23 is excited by an initial displacement, Figure 5.24 is excited by an initial velocity, Figure 5.25 is excited by an initial displacement and velocity, and Figure 5.26 is excited by a force density. The string is excited at the excitation point closest to the bridge of the guitar and observed at the first observation point. Thus these spectrograms will correspond to bright sounds.

The behaviour of the model is preserved, the frequency dependent decay is seen first in the high frequencies since they have the least energy. The high frequencies are seen to gradually decay over time and the tension modulation decreases over time. The vertical lines become lighter over time, this is expected since the tension modulation is dependent on the displacement and the displacement decreases over time due to the diffusive nature of the vibrating string.

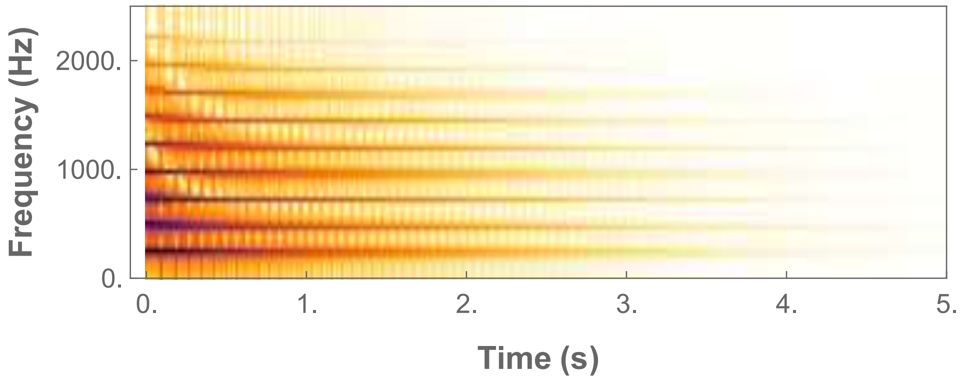

FIGURE 5.23: Finite difference method with an applied initial displacement and initial velocity. The string is excited at first position and Observed at first observation position.

In the spectrogram, Figure 5.23, we see a dense cluster of frequency change, this is where the effect of the tension modulation is at its largest since the total variation in the displacement is largest after the string has been excited and as the string dampens the tension modulation decreases and the intensity seen in the spectrogram decreases.

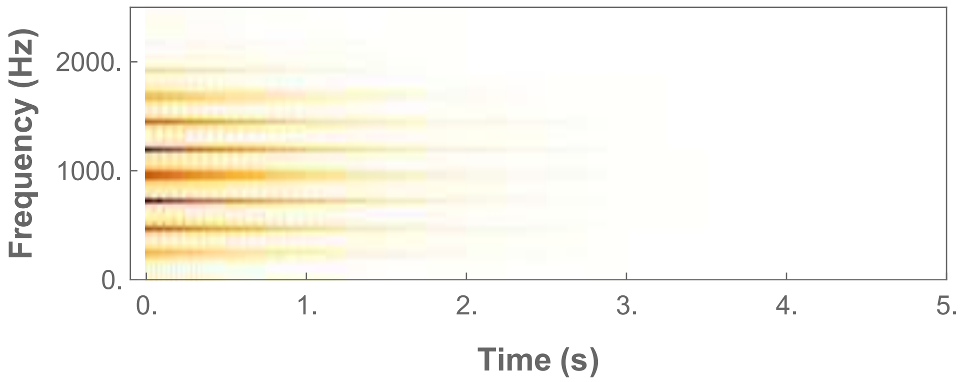

FIGURE 5.24: Finite difference method with an applied initial velocity. The string is excited at first position and Observed at first observation position.

The spectrogram in Figure 5.24 does not appear to have any effects caused by tension modulation. The initial velocity does not produce large displacements and as a result the tension modulation is infinitesimal. The results of the nonlinear model excited with an initial velocity will are similar to those of the linear model.

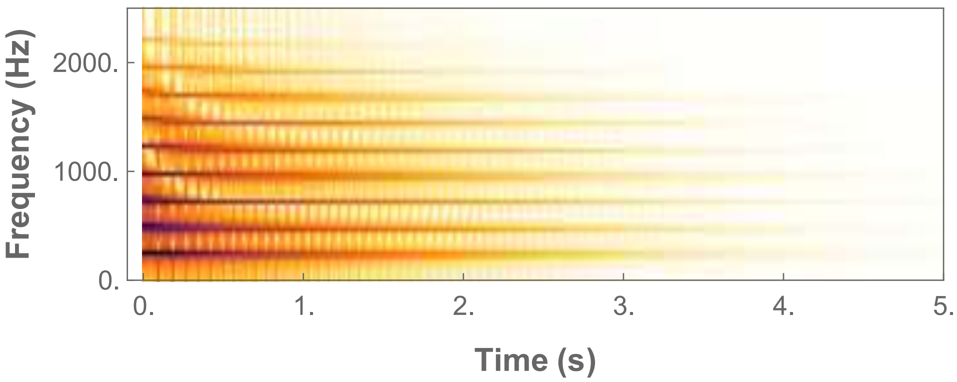

FIGURE 5.25: Finite difference method with an applied initial displacement. The string is excited at first position and Observed at first observation position.

Figure 5.25 is similar to Figure 5.23 this is due to the weak initial velocity spectrogram. The initial displacement dominates the effects of the initial velocity and the sound is prominently constructed by the initial displacement.

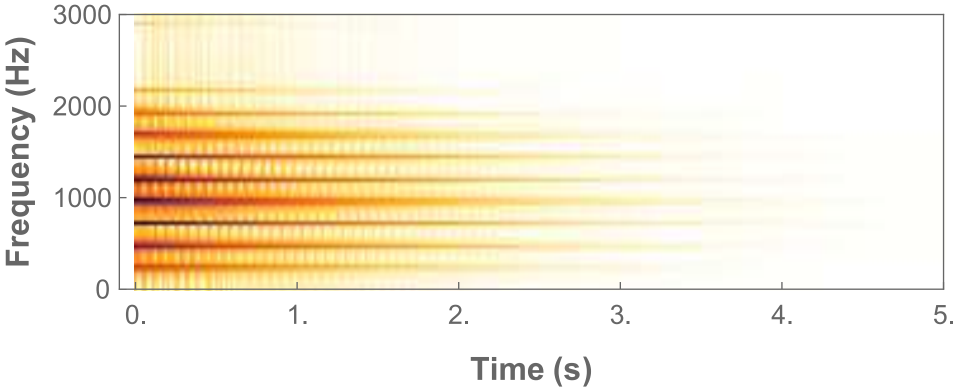

FIGURE 5.26: Finite difference method with an applied force density. The string is excited at first position and Observed at first observation position.

In the spectrogram, Figure 5.26, we see that the force density behaves in a similar way as the initial velocity spectrogram. The force density has a darker spectrogram meaning the energy in the spectrogram is larger and the force density provides a better simulation of a struck string. The tension modulation is more prominent in the beginning of the spectrogram where a cluster of vertical lines can be seen. As the time increases the change in frequency is seen to decay and the spectrogram lightens. The tension modulation decreases over time and the vibrations of the string dampen.

5.6 Fourier Analysis on the nonlinear model

In this Section the results of the nonlinear model are analysed using a Fourier Analysis. Three different observation positions, points where the vibrations are observed, are investigated. The method allows us to see the different harmonic frequencies that are registered at an observation point and the energies of those frequencies at those points. A guitar is excited near the bridge of the guitar thus the observation points and excitation points are defined as a distance from the bridge of the guitar. The Fourier transform is implemented using *Mathematica* Fourier's function.

5.6.1 Fourier of the nonlinear model with an Initial Displacement

The figures below are the resulting Fourier analysis graphs of the nonlinear PDE, Equation (4.3), with an initial displacement applied to the string. The initial displacement is defined in Section 3.4 and is given as

$$\begin{aligned} &u(x,0) = h(x), \\ &\frac{\partial u}{\partial t}(x,0) = 0, \\ &f(x_0,x,t) = 0. \end{aligned}$$

In Figure 5.27a the tension modulation causes a change in frequency. The fundamental frequency resembles that seen in the linear case. The harmonic frequencies shift and the amplitudes decrease as the frequency increases. The tension modulation is prominent in the high frequency range and will effect the high frequency detail in the sound. In Figure 5.27b the amplitudes of the high frequency range are small and the change in frequency is still visible. The fundamental frequency has a higher amplitude resulting in a darker sound since the high frequencies are weak. In Figure 5.27c the fundamental frequency amplitude has increased and the sound has less high frequency detail. The change in frequency is small. At the second observation point, Figure 5.28, the high frequencies have relatively small amplitudes and the sound at this observation point have strong fundamental frequency with low amplitude high frequencies. The sound at the first excitation point, Figure 5.28a has a visible change in frequency in the harmonic frequencies but as the excitation point moves away from the bridge of the guitar the effects of the tension modulation are less. The tension is still modulating in those sounds and the full spectrum behaviour can be seen in the spectrogram in Appendix C. At the third observation position, Figure 5.29, the fundamental frequencies are at the highest. The nonlinear model generates sounds that are darker than the sounds generated by the linear model. It can been seen that the nonlinear model has lower energy in the high frequencies. The tension modulation has the effect of reducing the energy in the high frequencies and shifting the harmonic frequencies.

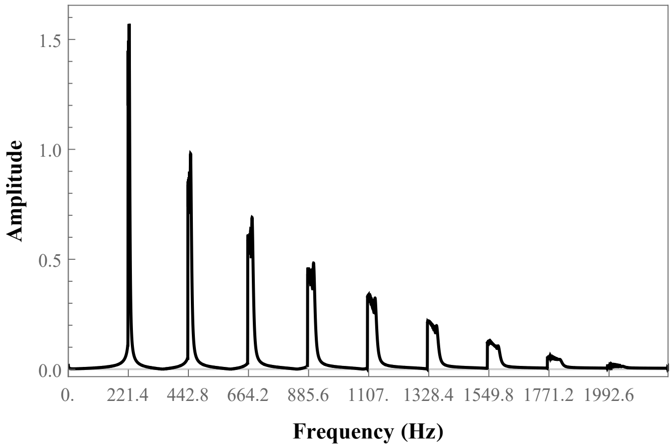

(A) Excitation 1

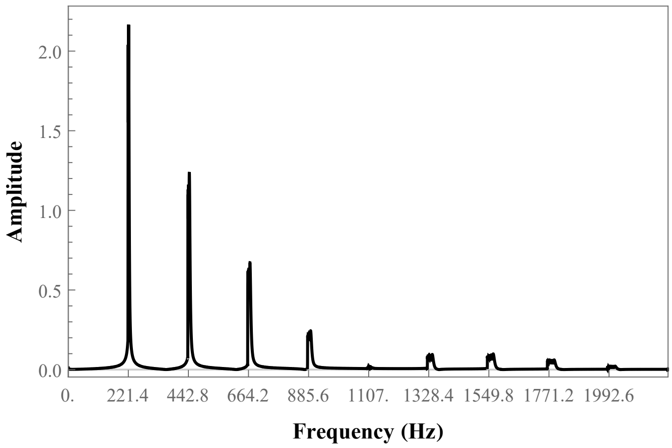

(B) Excitation 2

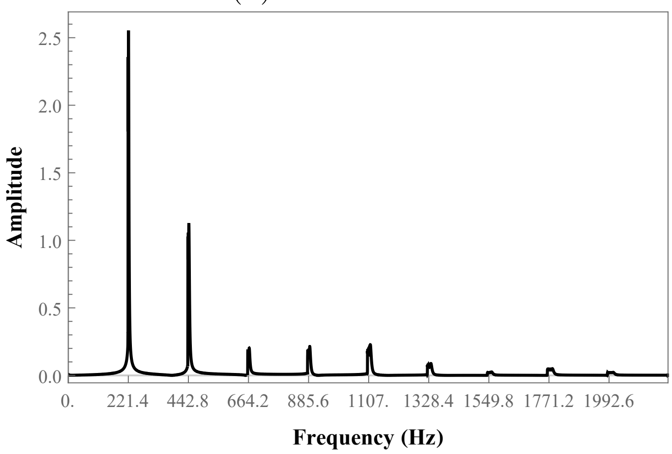

(C) Excitation 3

FIGURE 5.27: The Fourier analysis of the Finite Difference scheme at first observation positions where the model is excited by an initial displacement.

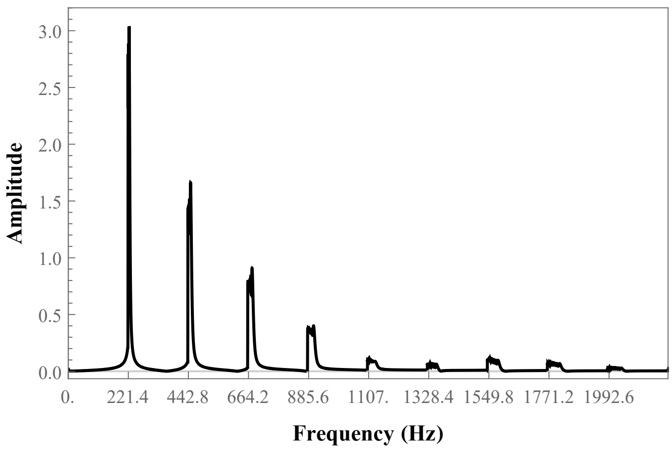

(A) Excitation 1

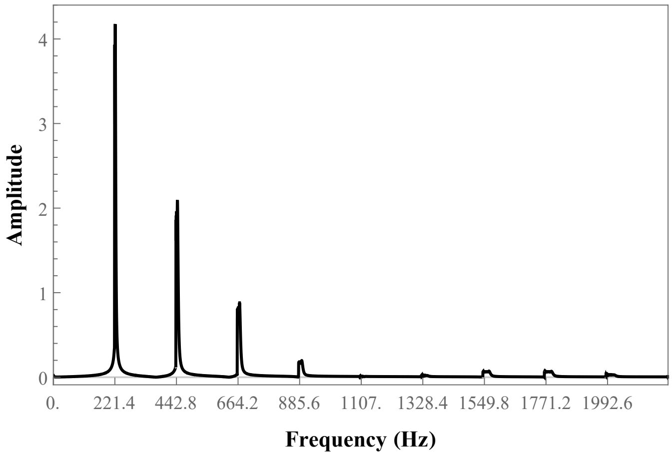

(B) Excitation 2

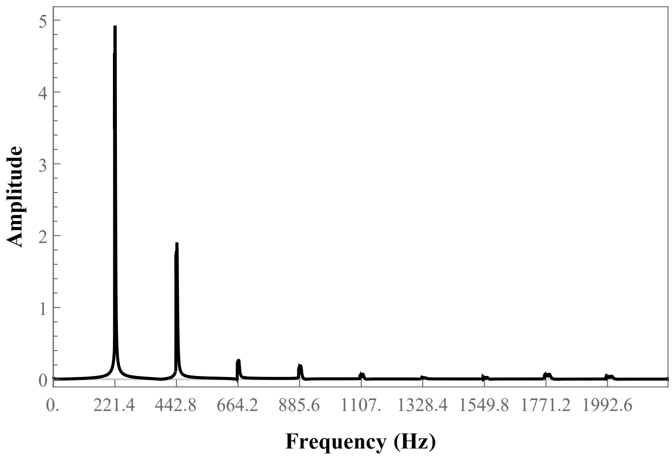

(C) Excitation 3

FIGURE 5.28: The Fourier analysis of the Finite Difference scheme at second observation positions where the model is excited by an initial displacement.

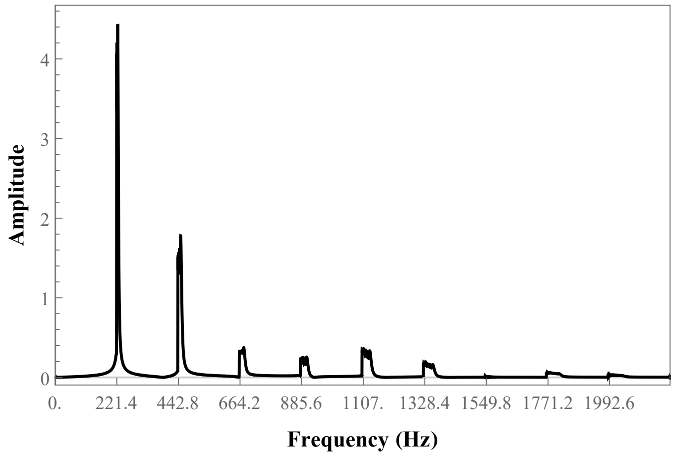

(A) Excitation 1

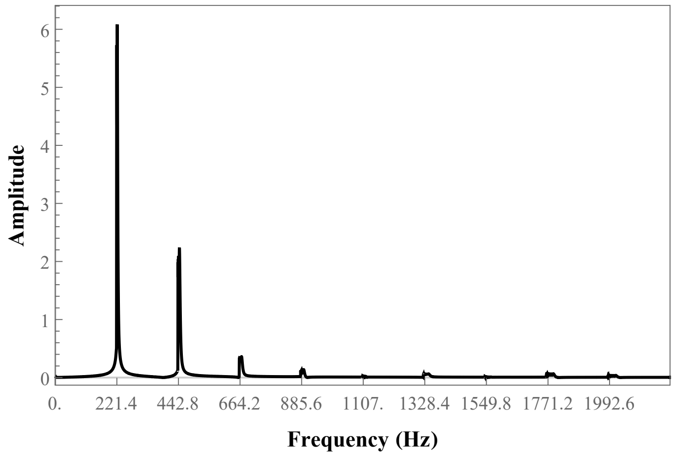

(B) Excitation 2

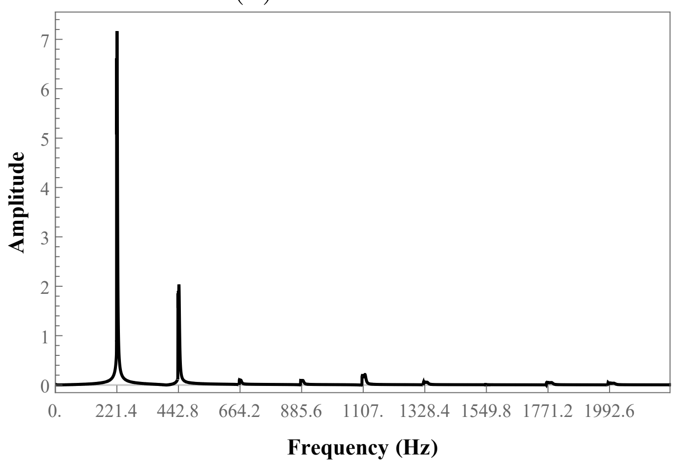

(C) Excitation 3

FIGURE 5.29: The Fourier analysis of the Finite Difference scheme at third observation positions where the model is excited by an initial displacement.

5.6.2 Fourier of the nonlinear model with an Initial Velocity

The figures below are the resulting Fourier analysis graphs of the nonlinear PDE, Equation (4.3), with an initial velocity applied to the string. The initial velocity is defined in Section 3.4 and is given as

$$\begin{aligned} &u(x,0) = 0, \\ &\frac{\partial u}{\partial t}(x,0) = p(x), \\ &f(x_0,x,t) = 0. \end{aligned}$$

The effects of the tension modulation are minimal since the initial velocity creates relatively small displacements and the tension only modulates for large displacements. Thus the results in this section are similar to those in Section 5.3.2, the linear case, and the amplitudes remain relatively small and the nonlinear model has more high frequency detail. The sounds generated by the nonlinear model are similar to the sounds generated by the linear model.

At the first observation position, Figure 5.30, the sounds that are produced are bright sounds since the high frequencies have amplitude levels that have a significant effect on the sound. We see that as the excitation point moves further from the bridge of the guitar the fundamental frequency has more energy. At the first excitation point the harmonic frequencies in the mid range have more energy then the fundamental frequency resulting in a high frequency sound that is bright and thin. At the second observation point, Figure 5.31, the low frequency range has more energy than the high frequency range. The sounds are still found to be bright sounds with low energy. At the third excitation point the high frequencies are at there lowest and the sound produced here will not be as bright as the sounds at the first two excitation points. At the third observation point, Figure 5.32, has the least high frequency detail, this can be seen in the spectrograms provided in Appendix C.3. As observation point moves further away from the bridge of the guitar the sound becomes darker.

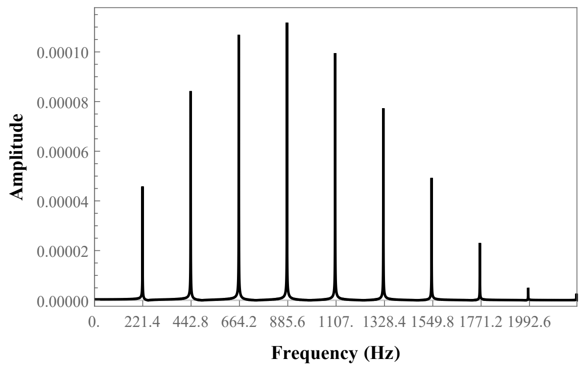

(A) Excitation position 1

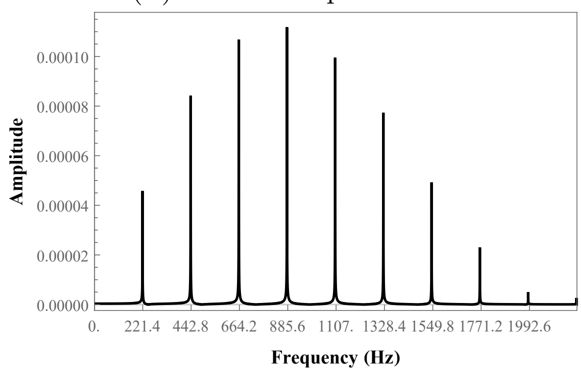

(B) Excitation position 2

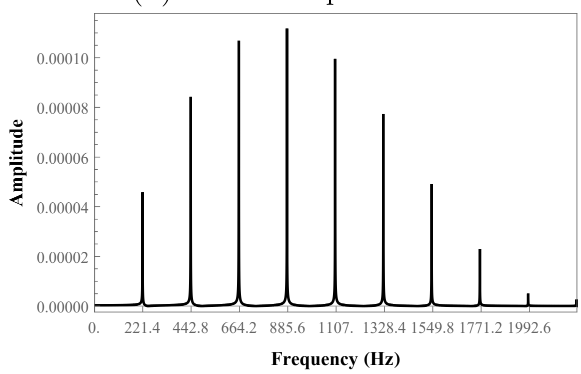

(C) Excitation position 3

FIGURE 5.30: The Fourier analysis of the Finite Difference scheme at the first observation position.

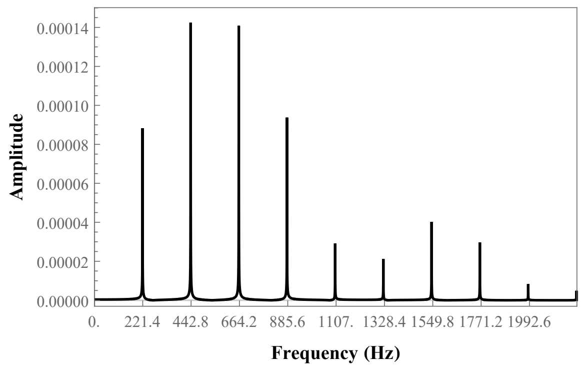

(A) Excitation position 1

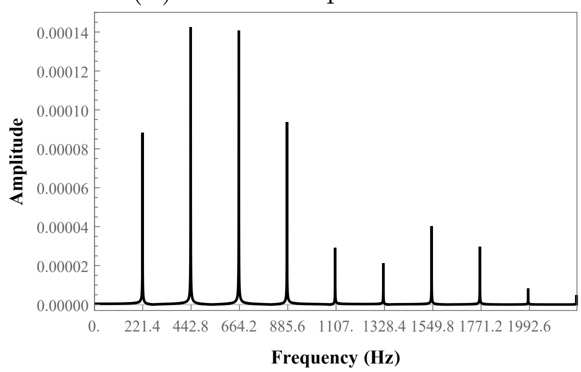

(B) Excitation position 2

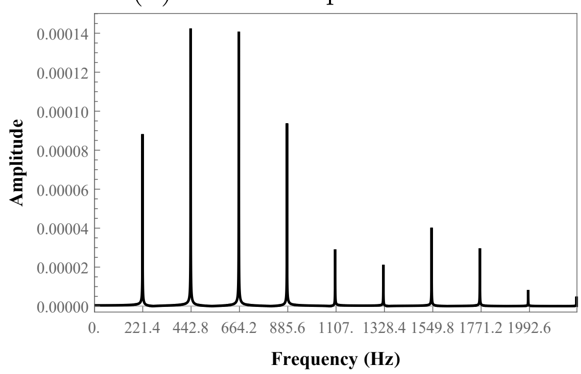

(C) Excitation position 3

FIGURE 5.31: The Fourier analysis of the Finite Difference scheme at the second observation position.

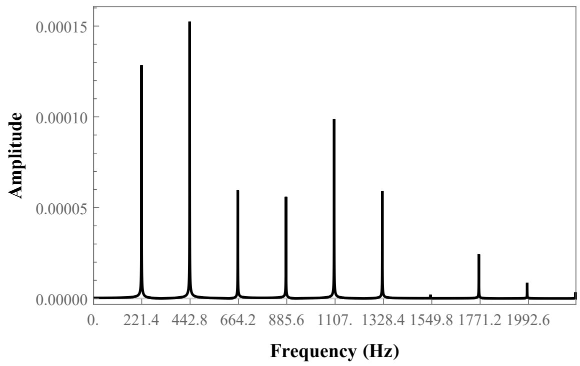

(A) Excitation position 1

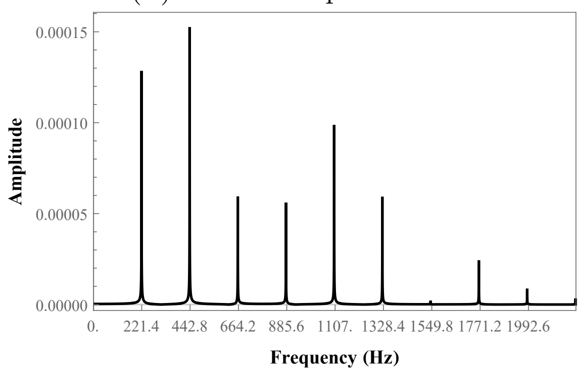

(B) Excitation position 2

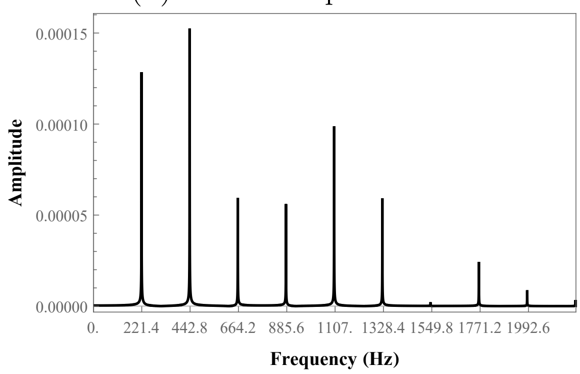

(C) Excitation position 3

FIGURE 5.32: The Fourier analysis of the Finite Difference scheme at the third observation position.

5.6.3 Fourier of the nonlinear model with an Initial Displacement and Initial Velocity

The figures below are the resulting Fourier analysis graphs of the nonlinear PDE, Equation (4.3), with an initial displacement and an initial velocity applied to the string. The initial condition is defined in Section 3.4 and is given as

$$\begin{aligned} &u(x,0) = h(x), \\ &\frac{\partial u}{\partial t}(x,0) = p(x), \\ &f(x_0, x, t) = 0. \end{aligned}$$

The results generated by the initial displacement and initial velocity are similar to the results generated by the initial displacement. The amplitudes generated by the initial velocity are relatively small in comparison to the initial displacement thus the initial displacement dominates the sound. This is seen in the spectrograms and in the linear results. The sound that is generated is predominately constructed by the string being plucked rather than the string being struck. In Figure 5.33a the tension modulation causes a change in frequency. The fundamental frequency is the same as the linear case. The harmonic frequencies shift and the amplitudes decrease as the frequency increases. The tension modulation is prominent in the high frequency range and will effect the high frequency detail in the sound. In Figure 5.33b the amplitudes of the high frequency range are small and the change in frequency is still visible. The fundamental frequency has a higher amplitude resulting in a darker sound since the high frequencies are weak. In Figure 5.33c the fundamental frequency amplitude has increased and the sound has less high frequency detail. The second observation point, Figure 5.34, the high frequencies have relatively small amplitudes and the sound at this observation point have strong fundamental frequency with low amplitude in the high frequencies. The sound at the first excitation point, Figure 5.34a, has a visible change in frequency in the harmonic frequencies but as the excitation point moves away from the bridge of the guitar the effects of the tension modulation are less. At the third observation position, Figure 5.35, the fundamental frequency are at the highest and the high frequency. It can be seen that the nonlinear model has lower energy in the high frequencies. The tension modulation has the effect of reducing the energy in the high frequencies and shifting the harmonic frequencies.

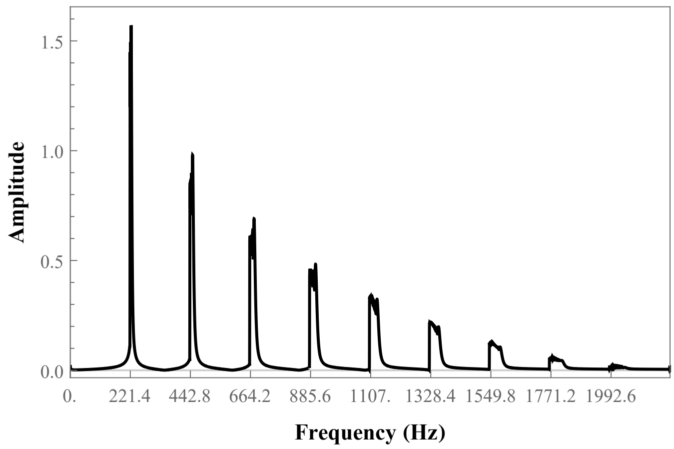

(A) Excitation 1

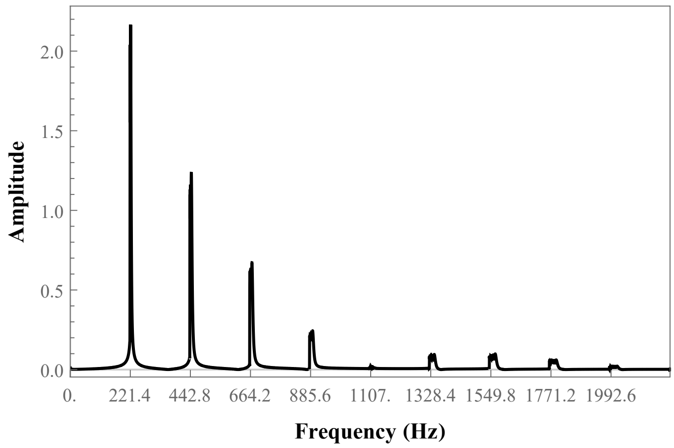

(B) Excitation 2

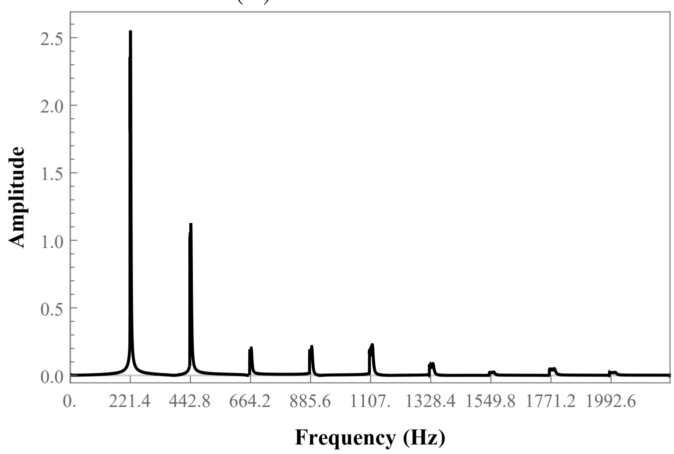

(C) Excitation 3

FIGURE 5.33: The Fourier analysis of the Finite Difference scheme at first observation positions where the model is excited by an initial displacement and an initial velocity.

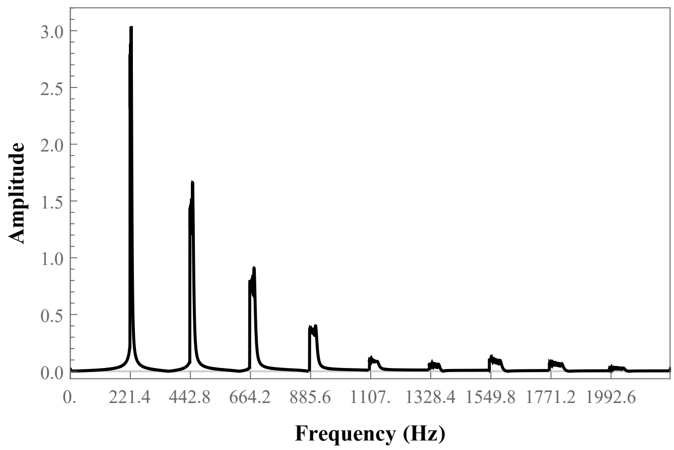

(A) Excitation 1

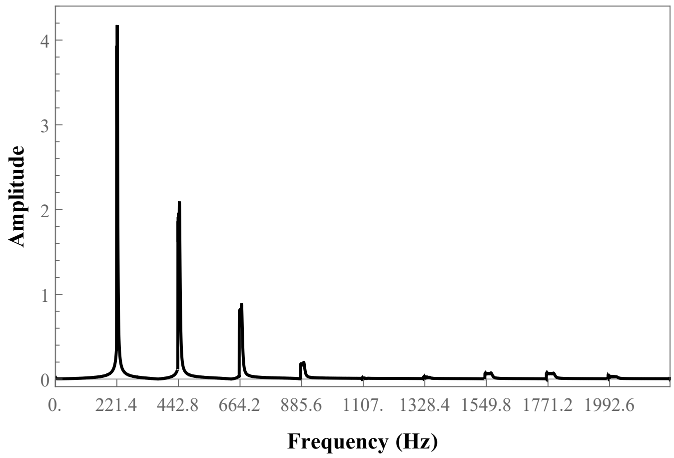

(B) Excitation 2

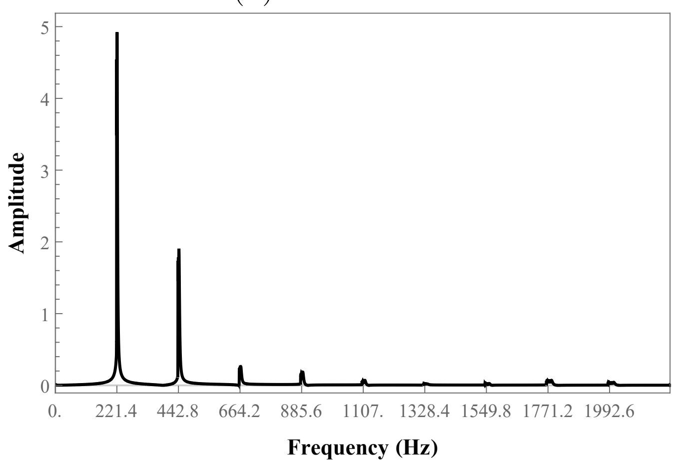

(C) Excitation 3

FIGURE 5.34: The Fourier analysis of the Finite Difference scheme at second observation positions where the model is excited by an initial displacement and an initial velocity.

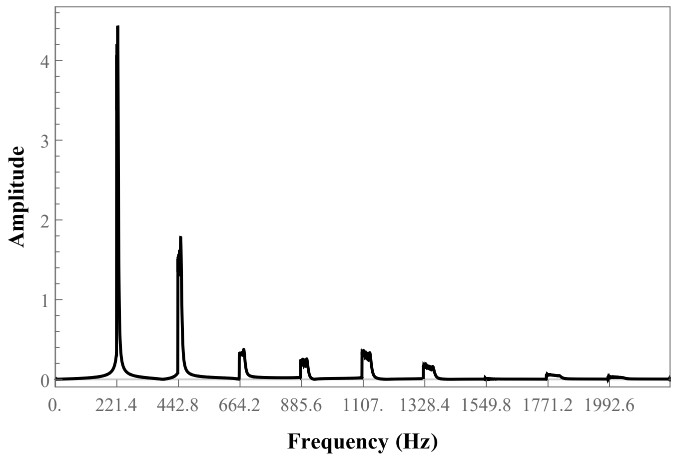

(A) Excitation 1

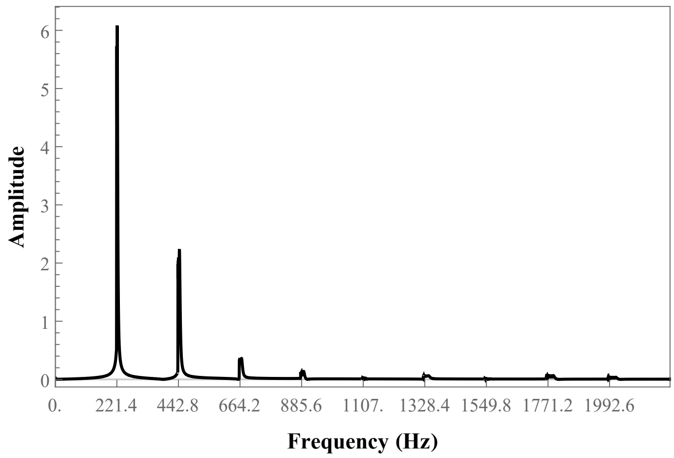

(B) Excitation 2

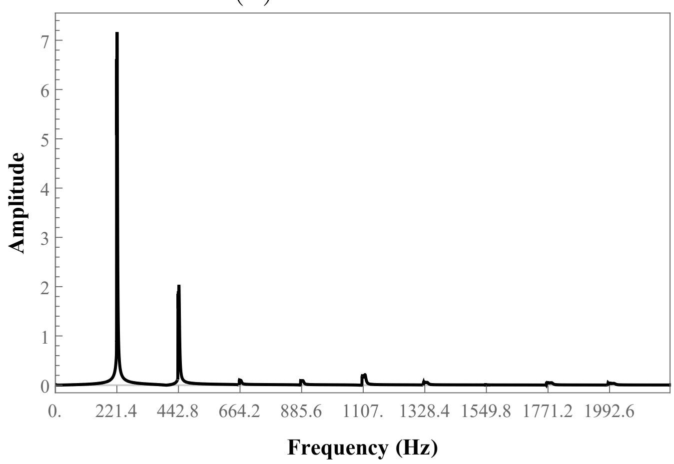

(C) Excitation 3

FIGURE 5.35: The Fourier analysis of the Finite Difference scheme at third observation positions where the model is excited by an initial displacement and an initial velocity.

5.6.4 Fourier of the nonlinear model with an Force Density

The figures below are the resulting Fourier analysis graphs of the nonlinear PDE, Equation (4.3), with a Force Density applied to the string. The initial velocity is defined in Section 3.4 and is given as

$$\begin{aligned} &u(x,0) = 0, \\ &\frac{\partial u}{\partial t}(x,0) = 0, \\ &f(x_0,x,t) = F(t)g(x_0,x). \end{aligned}$$

As the string is excited further away from the bridge of the guitar the energies of the low frequencies increase. At the second excitation position has two envelopes where the first, the envelope over the low frequencies, has the highest energies and the second, the envelope over the high frequencies, has low energies. The third excitation position has the highest energies in the low frequencies and thus will be the darkest sound. The high frequencies have low energies and the sounds are beginning to become full and lose high frequency detail. While tension modulation can still be heard in the sound by creating a change in pitch, the shift in frequency is not as large as the shift seen in Section 5.6.1. When comparing these results to those found in Section 5.3.2, the linear model, the shift in frequency, while small is still present. The high harmonic frequencies have the largest change in frequency. At all the excitation points the most effects of the tension modulation are present in the high harmonic frequencies. As the observation point moves further from the bridge of the guitar the fundamental frequencies are stronger. In Figure 5.38c, the sound is dominated by the fundamental frequency, generating a sound that is dark and with the shift in frequency in the harmonic frequencies.

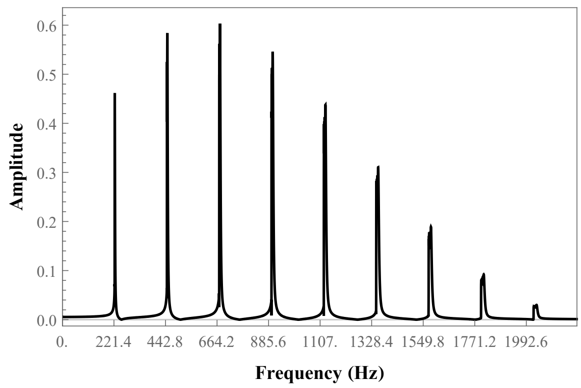

(A) Excitation position 1

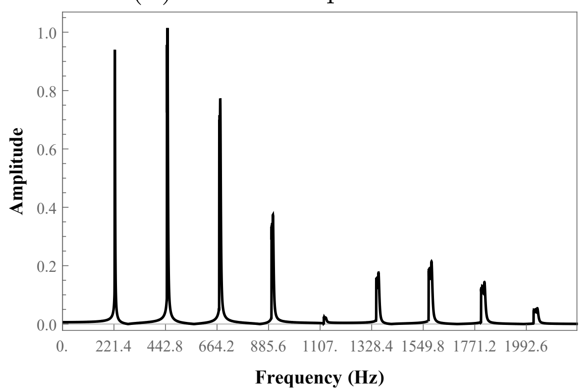

(B) Excitation position 2

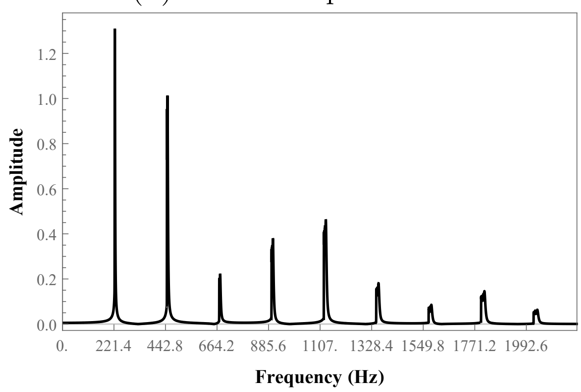

(C) Excitation position 3

FIGURE 5.36: The Fourier analysis of the Finite Difference scheme observed at pick up position 1.

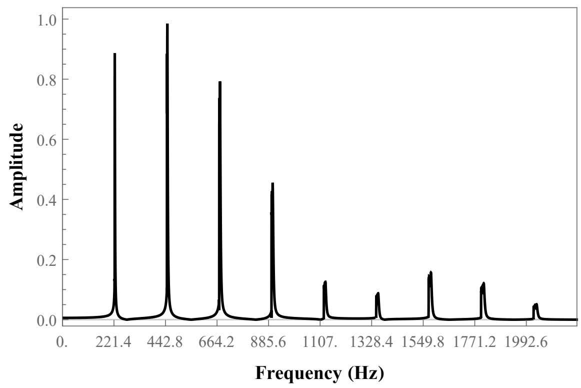

(A) excitation position 1

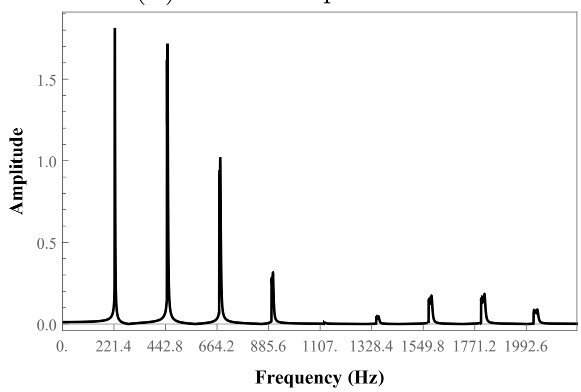

(B) Excitation position 2

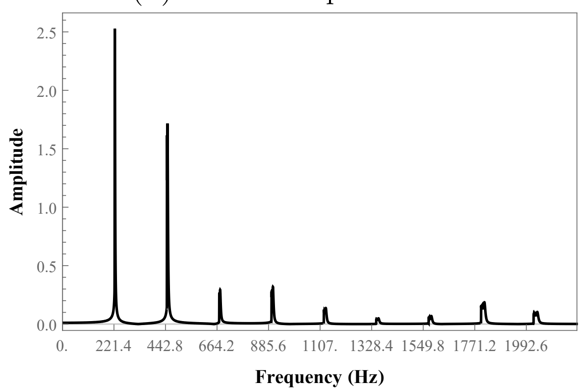

(C) Excitation position 3

FIGURE 5.37: The Fourier analysis of the Finite Difference scheme observed at pick up position 2.

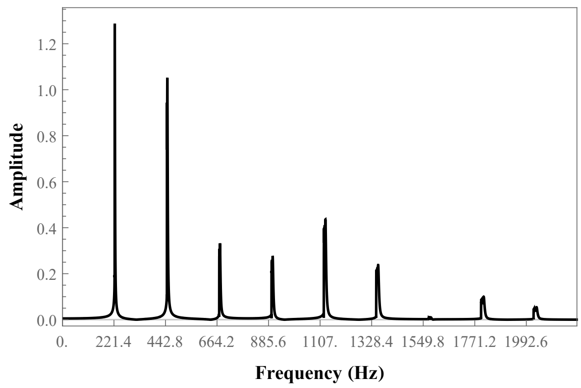

(A) Excitation position 1

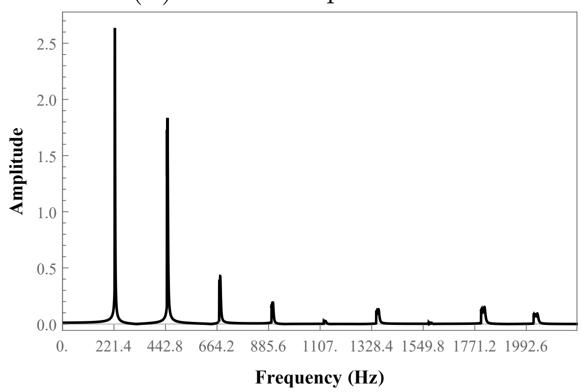

(B) Excitation position 2

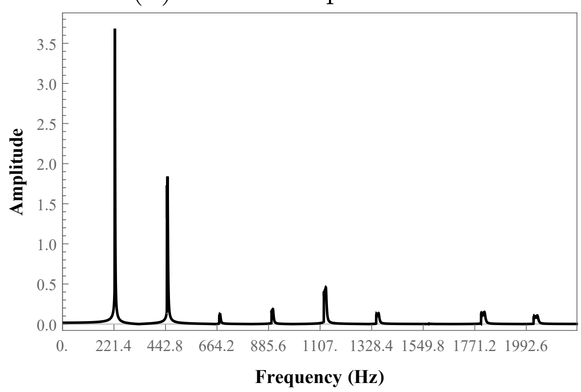

(C) Excitation position 3

FIGURE 5.38: The Fourier analysis of the Finite Difference scheme observed at pick up position 3.

5.7 Discussion on Nonlinear model

As the observation point moves further from the bridge of the guitar the sound becomes darker and rounder since the low frequencies increase in energy, making the high frequencies less significant in the sound. The tension modulation is seen to have the effect of decrease the amplitude at the harmonic frequencies and shifting the harmonic frequencies. The fundamental frequencies are seen to have larger energy in the nonlinear model than in the linear model. As the excitation point moves away from the bridge the fundamental frequency becomes stronger and the harmonic frequencies become weaker due to the tension modulation. The energy disperses as the frequency changes. As seen in the linear model the harmonic frequencies have relatively low amplitudes as compared to the nonlinear model where the change in frequency at any given harmonic frequency effects the amplitude. In Section 5.5 the spectrograms show the spectra behaviour over time. The change in pitch of each sound can be seen, where as in the linear model the change in sounds is only seen as the points of observation and excitation change. The nonlinear model has the change in pitch and sound as the excitation points change, the observation points changes and as the tension varies. The tension variation has the effect of changing the pitch over time.

The tension modulation is not visible on the initial velocity spectrogram and in the Fourier analysis there is no visible change in frequency. The results generated are similar to those generated by the linear model, since the initial velocity creates relatively small displacements. The initial displacement frequencies analysis is similar to the initial displacement and initial velocity. This behaviour is seen in the spectrogram analysis and the Fourier analysis further confirms that the initial displacement takes preference over the initial velocity since it is seen to have an infinitesimal effect on the results. The relatively low amplitudes produced by the initial velocity are insignificant in comparison to the amplitudes produced by the initial displacement. In Aprendix C the spectrograms at all the observation points are provided. The tension modulation is seen at all the points and the model behaviour is present at all the points. The initial velocity spectrograms are seen not to be effected by the tension modulation but the model behaviour is preserved.

The frequency analysis of the force density results have a similar behaviour to those of the initial velocity but the tension modulation effects are visible. This is because the force density generates a larger displacement than the initial velocity. The amplitudes seen are larger than those seen in the initial velocity results but they are smaller than those seen in the initial displacement results. This implies that plucking a guitar string provides the larger displacement generating the more energy than the other initial conditions. The plucked string will see the largest tension modulation and hear the largest pitch glide.

Chapter 6

Conclusion

A linear and a Nonlinear partial differential equation are investigated to describe a phenomenological model that synthesises the vibration of a string. The PDEs are considered under four different initial conditions namely; initial velocity, an initial displacement, a combination of an initial velocity and displacement and a force density. The string is observed by placing pick up positions at certain points along the string, in this case the pick up points are placed at three different positions near the bridge of the guitar. The string is then excited at the three different positions of the string.

In Section 3 a description of the linear model is numerically simulated using the finite difference method, CSCT used by [13], the method is derived in Section 3.5. The stability of the CSCT method, is driven by Δt, which has to be significantly small and the frequency dependent damping term which is selected experimentally. The linear model has further been implemented using the Functional Transformation Method, where the Laplace transformation is used to transform the temporal domain and the Finite Sine transformation is used to transform the spacial domain. The inverse transformations were then applied to the resultant. This method provided an exact solution to the linear PDE, the derivation of the method is provided in Section 3.6. The method is implemented in work done by Trautmann and Rabenstein [10, 16] where the authors use the Strum-Liuoville transformation to transform the spatial domain. The Finite Sine transformation was used since kernel in the method is $\sin(\frac{n\pi x}{L})$ and this configuration satisfies the boundary conditions. The exact solution is determined by implementing the method for infinite nodes but this is computationally intractable. Thus the FTM was adapted to created a method that is computationally efficient to derive the exact solution. This method is then used to verify the approximation method and was found that the CSCT method provides a suitable approximation to the solution of the PDE.

The results are found to correlate with the expected behaviour of the model. The Fourier analysis of the adapted FTM are provided in Appendix B and these results correlate with those produced by the FDM. The presence of the damping variables can bee seen as the frequencies dampen over time, first in the high frequency range and then in the low frequency range. The frequency independent damping term is seen in the way the string displacement dampens over time. The Fourier analysis in the work provided information on the amplitudes at the harmonic frequencies. The sounds produced by applying an initial displacement and the combination of the initial displacement and initial velocity produced sounds that are loud and dark. The highest energies resonated in the low frequencies. The high frequencies in the audible range where seen to have the lower amplitudes. It was also observed that as the observation position moved further from the bridge of the guitar the amplitudes are seen to have an increase range. The amplitudes in the low frequencies are much larger than those in the high frequencies. This is true of all the observation point but the effect increases as you move further form the bridge of the guitar. The initial velocity has amplitudes lower then those observed in the previous initial conditions. The amplitudes are still higher in the low frequencies and low in the high frequencies. The amplitudes do not decay steadily as the frequencies increase but has peaks at low amplitudes and higher frequencies. Applying a force density also produces a spectrogram similar to that of a struck string. The amplitudes of the frequency and the displacements of the string are larger than those produced by the initial velocity. Thus, the force density is a more accurate way to describe the initial condition of a string. When a string is strum on a guitar the action is a combination of plucking and striking since the string is displaced and a velocity is applied to the string.

To describe the tension modulation in the nonlinear model the Kichhoff-Carrier equation was applied. The equation relates the tension modulation to the total variation of the displacement [4, 18]. Hence the tension only modulates for large displacements. From the results we can see that the initial velocity does not generate large displacement therefore the tension modulation is infinitesimal. The tension modulation is illustrated when an initial displacement and a force density is applied, where the largest tension modulation is generated by the initial displacement since plucking a string creates larger displacements then strumming the string. The tension modulation does not cause the model to lose any expected behaviour. The general behaviour of the model provided by the linear model is preserved and the string dampens over time and the frequency dependent decay terms effect is still seen. The tension modulation changes the pitch of the sound over time. Which generates the pitch glide that is present in musical instruments [4]. The nonlinear model was simulated using the CTCS finite difference approximation since the linear model validated the method and the FTM is not applicable for a nonlinear model, since the method is constructed by linear operators.

From the analysis we see that a plucked string has the largest displacements and the largest amplitudes. The tension modulation of the nonlinear plucked model sees the most effect of the tension modulation since tension modulation is dependent on the displacement of the string. The tension modulation decreases as the string dampens and the tension modulation is heard as a change in pitch in the sound. A string that is excited with an initial velocity has small displacement and this results in the sound having low amplitudes and a fast decay of the sound compared to the dampening over time of the string excited with an initial displacement. Seen in both the linear and nonlinear model, when the string is excited by an initial displacement and initial velocity the analysis shows that the initial displacement takes preference over the initial velocity. Thus the tension modulation behaves similarly to the tension modulation of the plucked string.

Appendix A

Linear model Spectrogram

Recall the model is considered with three initial conditions and at varying observation positions. The provided spectrograms are of the linear model and it is excited at three different excitation points and the vibrations are observed at three different observation positions.

A.1 Initial Displacement and Initial Velocity

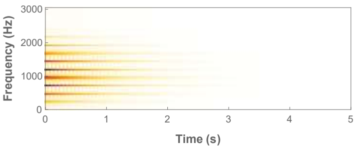

(A) Excited at positon 1 and Observed at position 1

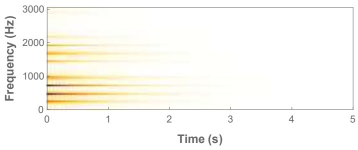

(B) Excited at positon 1 and Observed at position 2

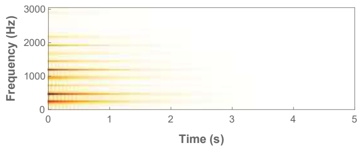

(C) Excited at positon 1 and Observed at position 3

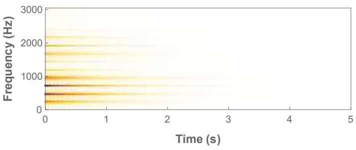

(D) Excited at positon 2 and Observed at position 1

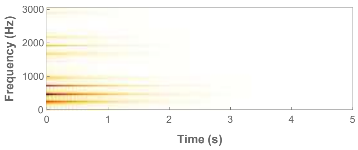

(E) Excited at positon 2 and Observed at position 2

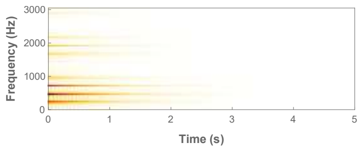

(F) Excited at positon 2 and Observed at position 3

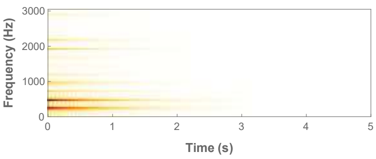

(G) Excited at positon 3 and Observed at position 1

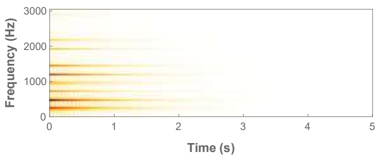

(H) Excited at positon 3 and Observed at position 2

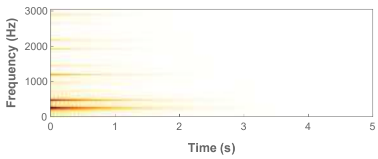

(I) Excited at positon 3 and Observed at position 3

FIGURE A.1: Spectrogram of the Finite Difference scheme with an initial displacement and initial velocity.

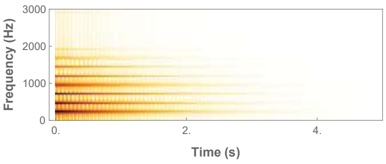

(A) Excited at positon 1 and Observed at position 1

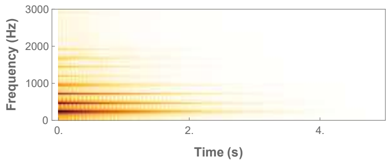

(B) Excited at positon 1 and Observed at position 2

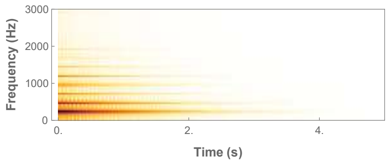

(C) Excited at positon 1 and Observed at position 3

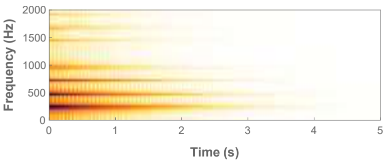

(D) Excited at positon 2 and Observed at position 1

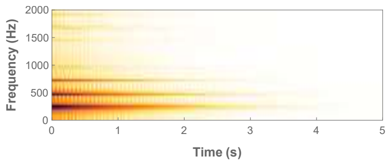

(E) Excited at positon 2 and Observed at position 2

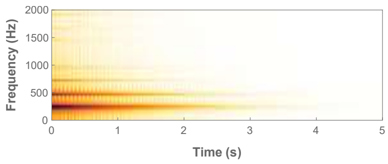

(F) Excited at positon 2 and Observed at position 3

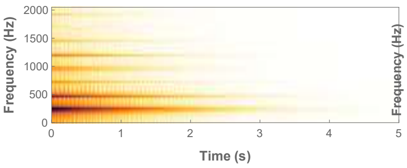

(G) Excited at positon 3 and Observed at position 1

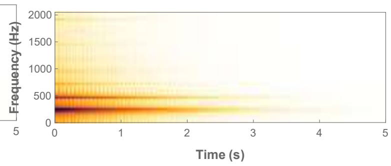

(H) Excited at positon 3 and Observed at position 2

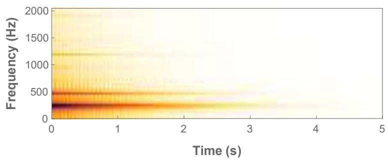

(I) Excited at positon 3 and Observed at position 3

FIGURE A.2: Spectrogram of the adapted functional transformation method with initial displacement and initial velocity.

A.2 Initial Displacement

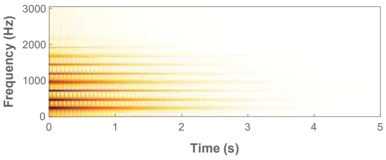

(A) Excited at position 1 and Observed at position 1

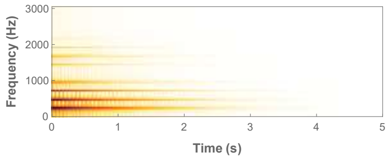

(B) Excited at position 1 and Observed at position 2

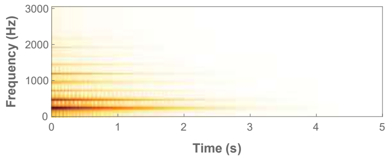

(C) Excited at position 1 and Observed at position 3

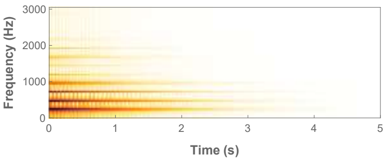

(D) Excited at position 2 and Observed at position 1

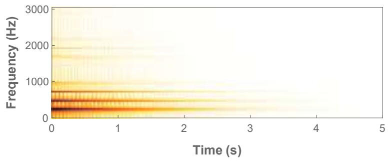

(E) Excited at position 2 and Observed at position 2

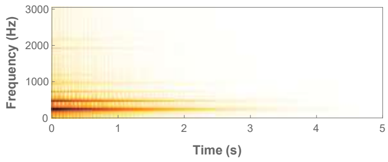

(F) Excited at position 2 and Observed at position 3

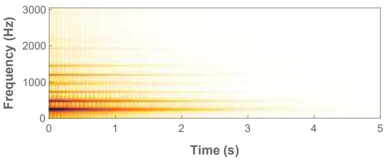

(G) Excited at position 3 and Observed at position 1

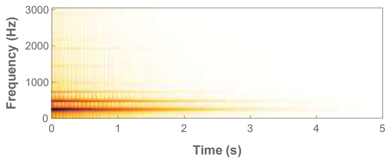

(H) Excited at position 3 and Observed at position 2

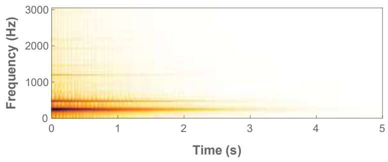

(I) Excited at position 3 and Observed at position 3

FIGURE A.3: Spectrogram of the Finite Difference method with initial displacement.

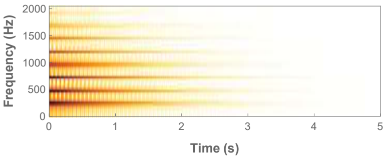

(A) Excited at positon 1 and Observed at position 1

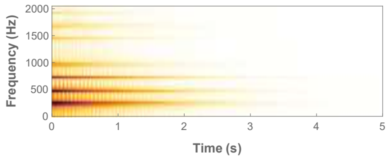

(B) Excited at positon 1 and Observed at position 2

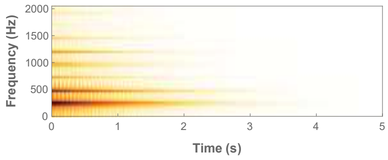

(C) Excited at positon 1 and Observed at position 3

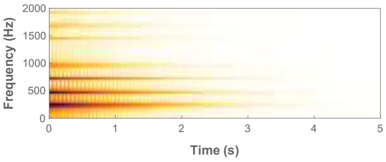

(D) Excited at positon 2 and Observed at position 1

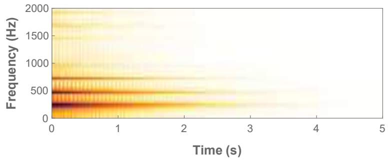

(E) Excited at positon 2 and Observed at position 2

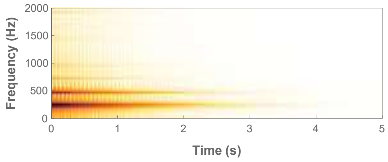

(F) Excited at positon 2 and Observed at position 3

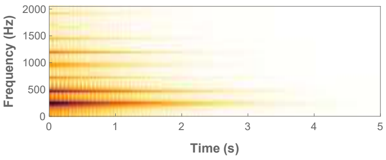

(G) Excited at positon 3 and Observed at position 1

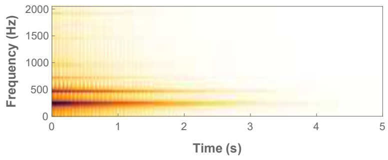

(H) Excited at positon 3 and Observed at position 2

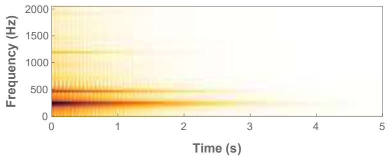

(I) Excited at positon 3 and Observed at position 3

FIGURE A.4: Spectrogram of the adapted functional transformation method with initial displacement.

A.3 Initial Velocity

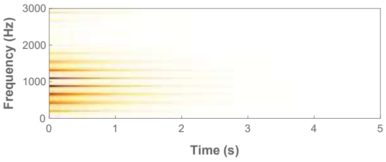

(A) Excited at position 1 and Observed at position 1

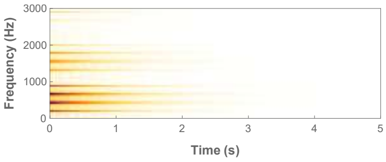

(B) Excited at position 1 and Observed at position 2

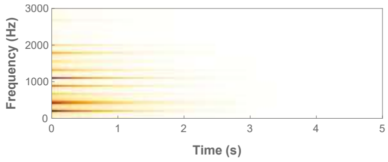

(C) Excited at position 1 and Observed at position 3

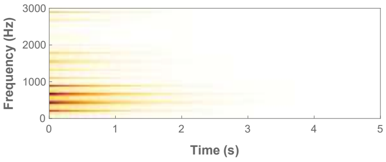

(D) Excited at position 2 and Observed at position 1

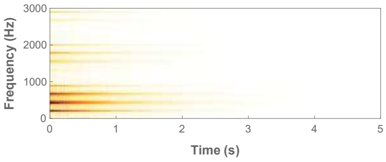

(E) Excited at position 2 and Observed at position 2

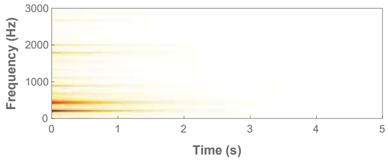

(F) Excited at position 2 and Observed at position 3

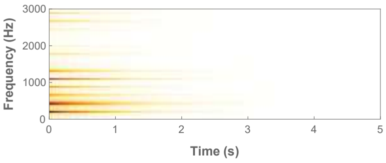

(G) Excited at position 3 and Observed at position 1

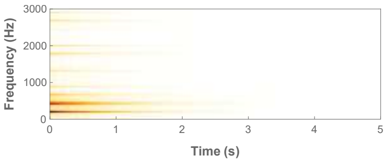

(H) Excited at position 3 and Observed at position 2

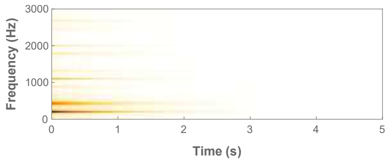

(I) Excited at position 3 and Observed at position 3

FIGURE A.5: Spectrogram of the Finite Difference method with initial velocity.

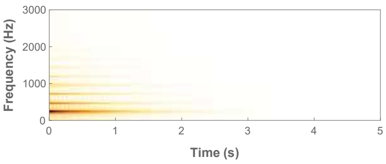

(A) Excited at position 1 and Observed at position 1

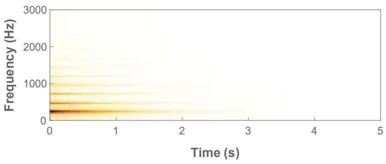

(B) Excited at position 1 and Observed at position 2

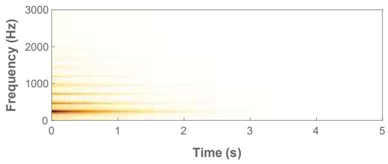

(C) Excited at position 1 and Observed at position 3

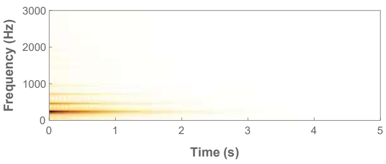

(D) Excited at position 2 and Observed at position 1

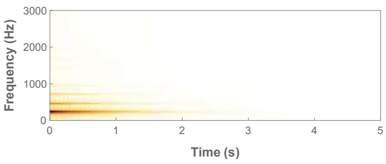

(E) Excited at position 2 and Observed at position 2

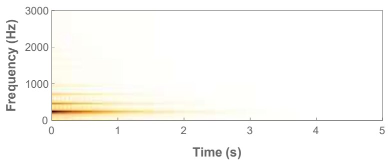

(F) Excited at position 2 and Observed at position 3

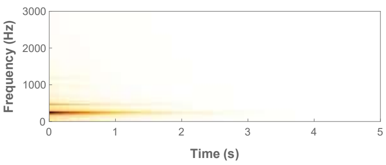

(G) Excited at position 3 and Observed at position 1

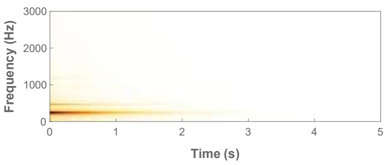

(H) Excited at position 3 and Observed at position 2

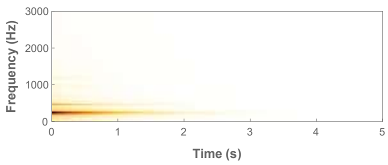

(I) Excited at position 3 and Observed at position 3

FIGURE A.6: Spectrogram of the adapted functional transformation method with initial velocity.

A.4 Force Density

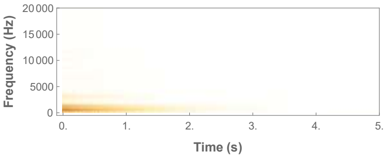

(A) Excited at position 1 and Observed at position 1

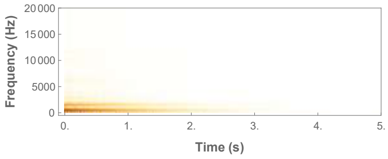

(B) Excited at position 1 and Observed at position 2

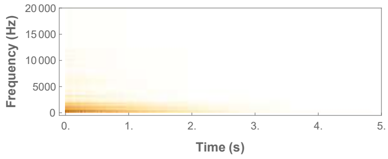

(C) Excited at position 1 and Observed at position 3

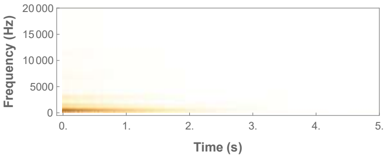

(D) Excited at position 2 and Observed at position 1

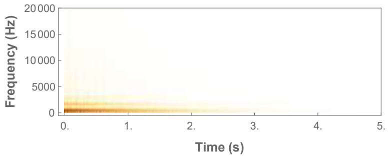

(E) Excited at position 2 and Observed at position 2

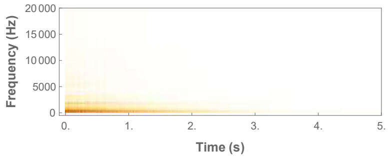

(F) Excited at position 2 and Observed at position 3

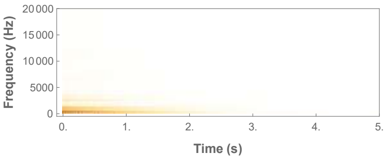

(G) Excited at position 3 and Observed at position 1

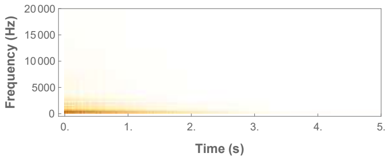

(H) Excited at position 3 and Observed at position 2

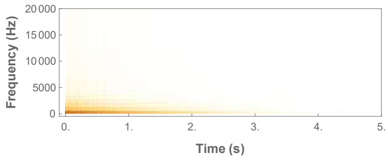

(I) Excited at position 3 and Observed at position 3

FIGURE A.7: Spectrogram of the Finite Difference method with a force density.

Appendix B

Fourier Anaylsis

Recall the model is considered with three initial conditions and at varying observation positions. The provided figures are of the linear model and it is excited at three different excitation points and the vibrations are observed at three different observation positions. The model has been solved using the adapted functional transformation method.

B.1 Initial Displacement

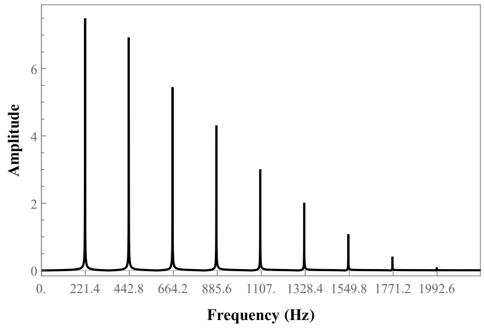

(A) Excitation 1

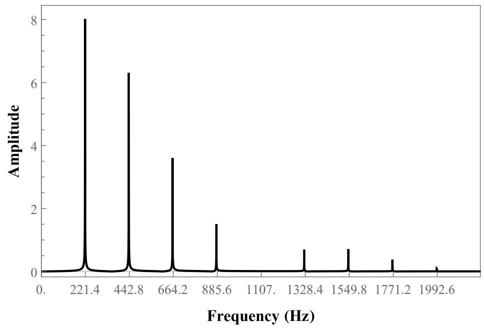

(B) Excitation 2

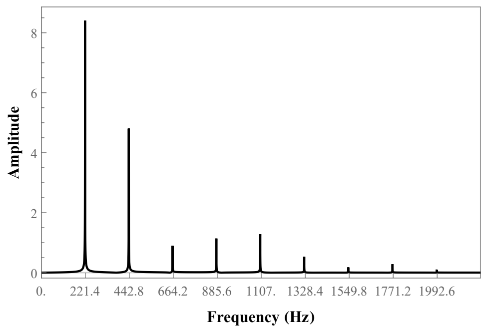

(C) Excitation 3

FIGURE B.1: The Fourier analysis of the adapted functional transformation method at first observation positions where the model is excited by an initial displacement.

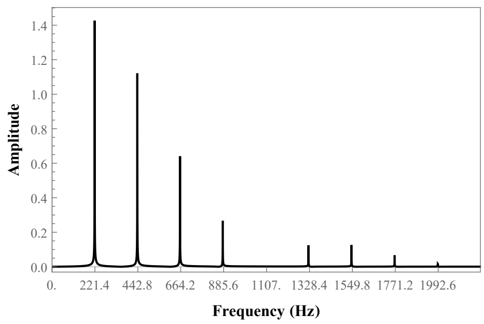

(A) Excitation 1

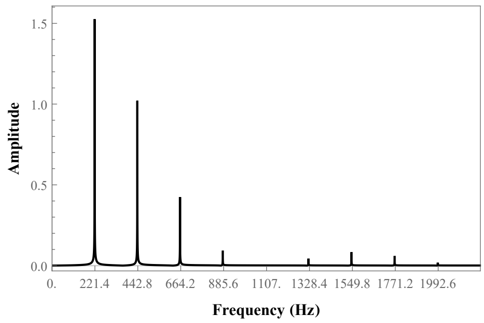

(B) Excitation 2

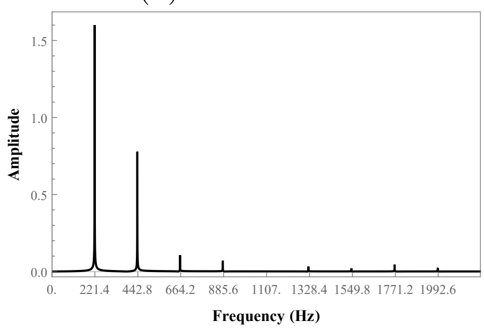

(C) Excitation 3

FIGURE B.2: The Fourier analysis of the adapted functional transformation method at second observation positions where the model is excited by an initial displacement.

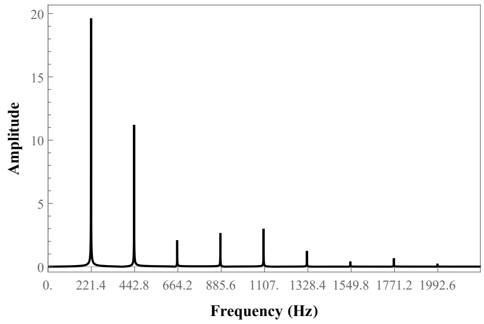

(A) Excitation 1

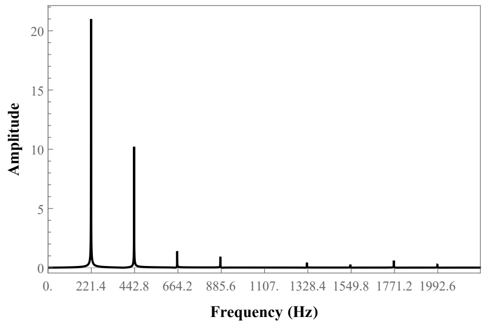

(B) Excitation 2

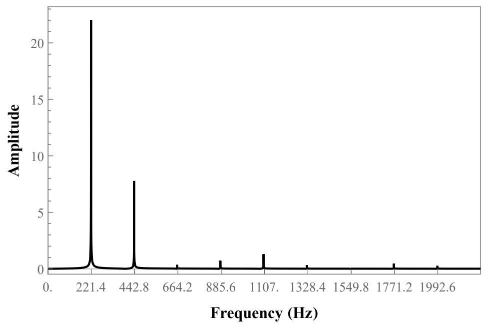

(C) Excitation 3

FIGURE B.3: The Fourier analysis of the functional transformation method at third observation positions where the model is excited by an initial displacement.

B.2 Initial velocity

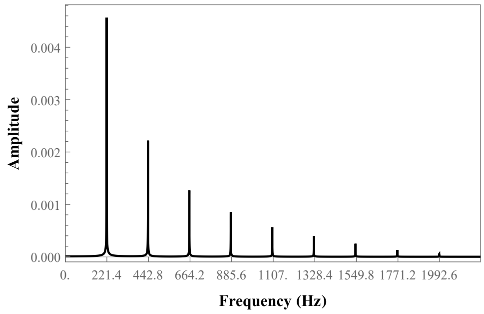

(A) Excitation 1

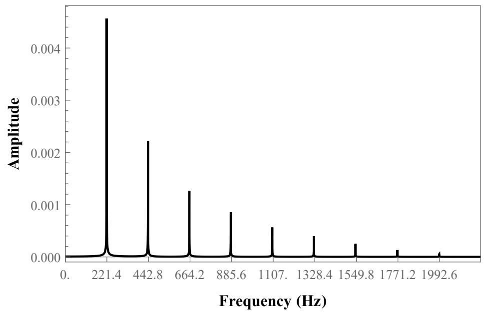

(B) Excitation 2

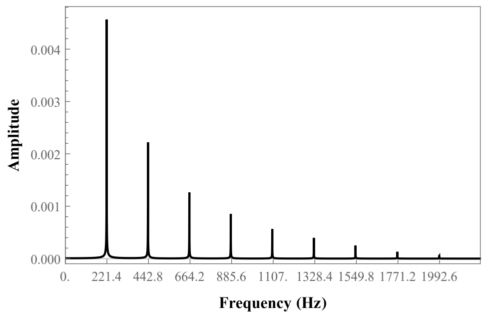

(C) Excitation 3

FIGURE B.4: The Fourier analysis of the adapted functional transformation method at first observation positions where the model is excited by an initial displacement.

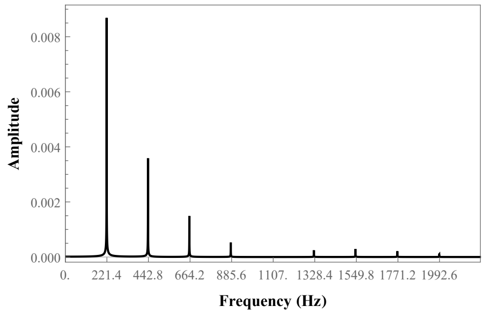

(A) Excitation 1

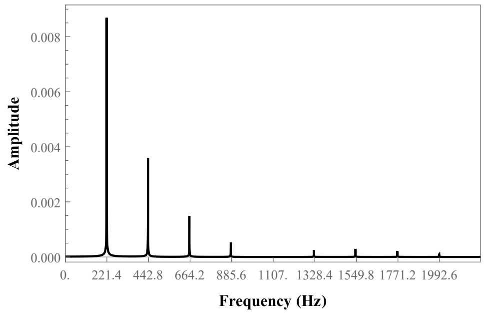

(B) Excitation 2

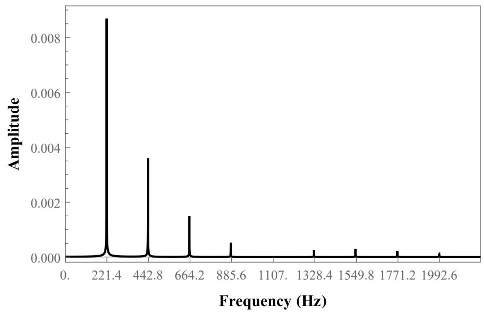

(C) Excitation 3

FIGURE B.5: The Fourier analysis of the adapted functional transformation method at second observation positions where the model is excited by an initial displacement.

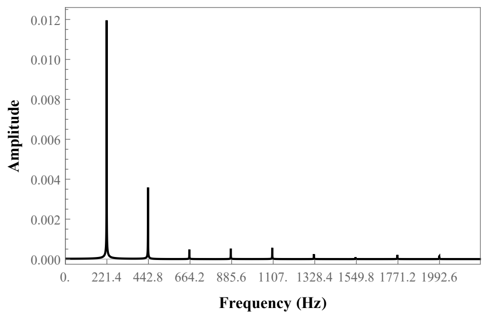

(A) Excitation 1

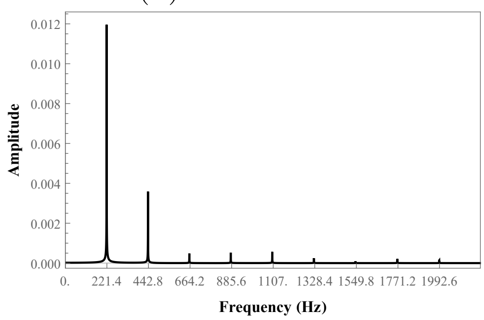

(B) Excitation 2

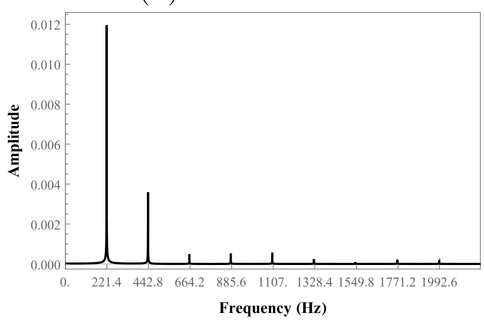

(C) Excitation 3

FIGURE B.6: The Fourier analysis of the functional transformation method at third observation positions where the model is excited by an initial displacement.

B.3 Initial displacement and Initial velocity

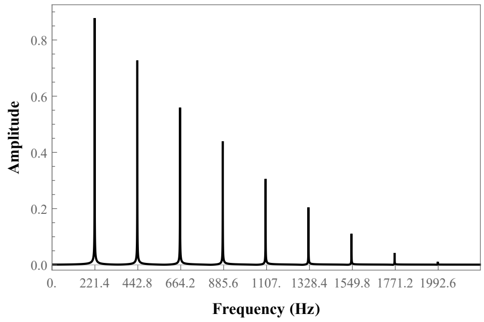

(A) Excitation 1

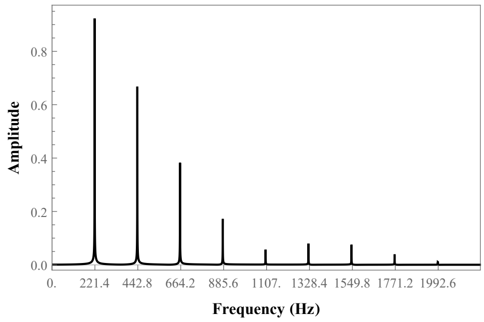

(B) Excitation 2

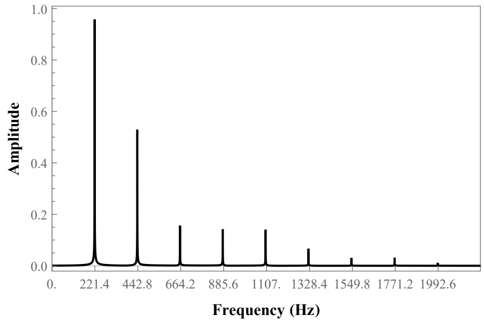

(C) Excitation 3

FIGURE B.7: The Fourier analysis of the adapted functional transformation method at first observation positions where the model is excited by an initial displacement.

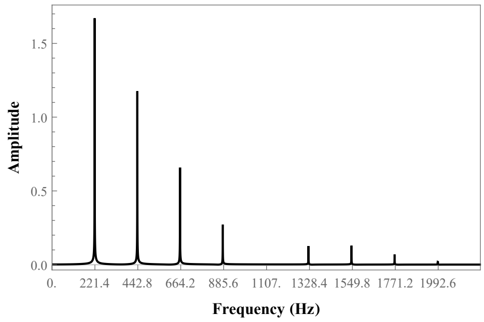

(A) Excitation 1

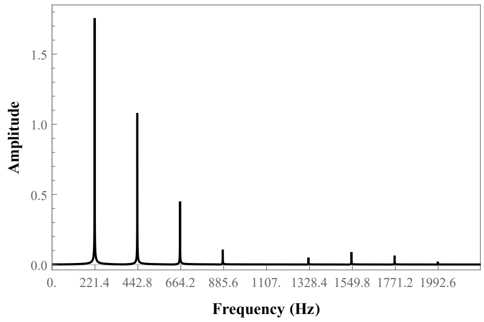

(B) Excitation 2

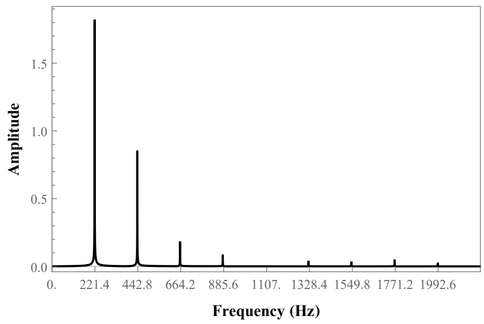

(C) Excitation 3

FIGURE B.8: The Fourier analysis of the adapted functional transformation method at second observation positions where the model is excited by an initial displacement.

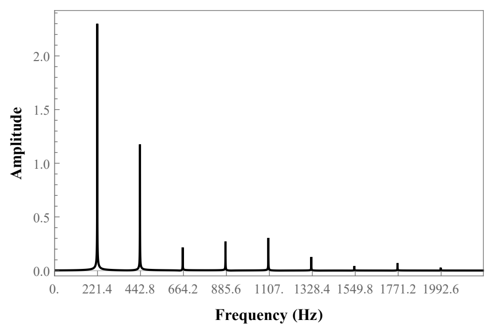

(A) Excitation 1

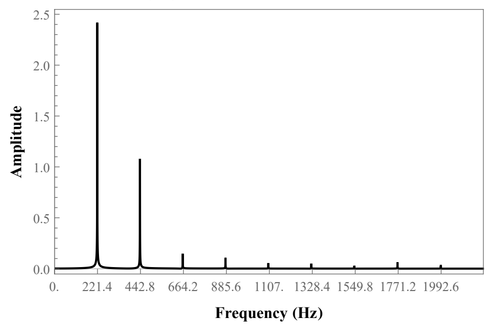

(B) Excitation 2

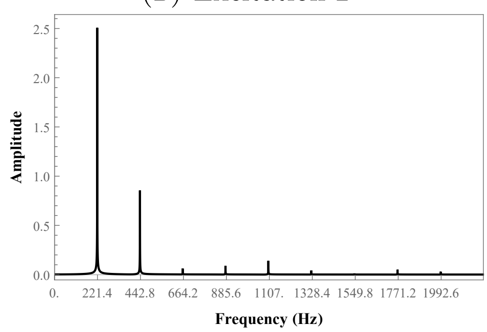

(C) Excitation 3

FIGURE B.9: The Fourier analysis of the functional transformation method at third observation positions where the model is excited by an initial displacement.

Appendix C

Non-linear model Spectrogram

The model is considered with three initial conditions and at varying obseravtion positions. The provided spectrograms are of the nonlinear model and is excited at three different excitation points and the vibrations are observed at three different positions.

C.1 Initial Displacement

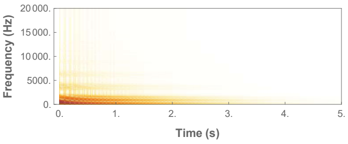

(A) Excited at position 1 and Observed at position 1

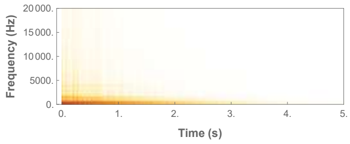

(B) Excited at position 1 and Observed at position 2

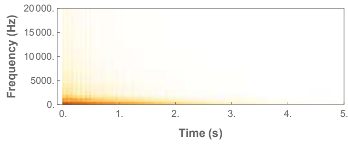

(C) Excited at position 1 and Observed at position 3

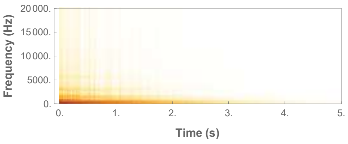

(D) Excited at position 2 and Observed at position 1

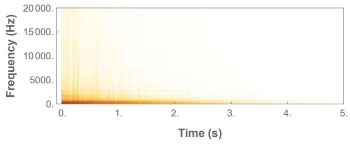

(E) Excited at position 2 and Observed at position 2

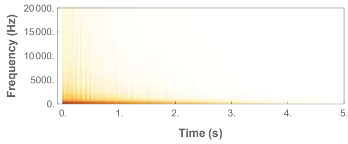

(F) Excited at position 2 and Observed at position 3

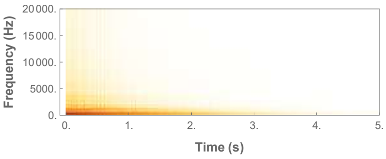

(G) Excited at position 3 and Observed at position 1

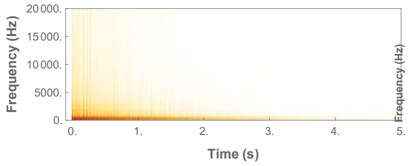

(H) Excited at position 3 and Observed at position2

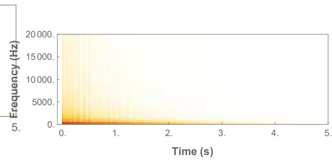

(I) Excited at position 3 and Observed at position3

FIGURE C.1: Spectrogram of the Finite Difference method with initial displacement.

C.2 Initial Displacement and Initial Velocity

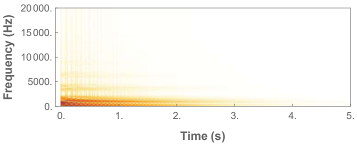

(A) Excited at positon 1 and Observed at position 1

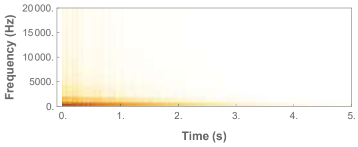

(B) Excited at position 1 and Observed at position 2

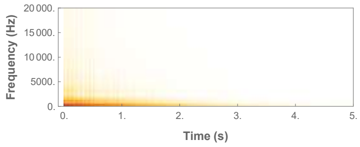

(C) Excited at position 1 and Observed at position 3

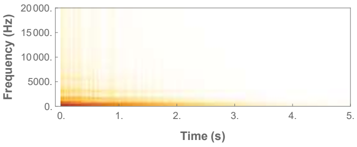

(D) Excited at position 2 and Observed at position 1

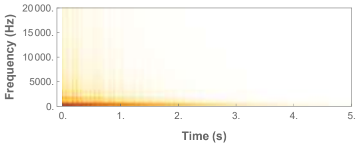

(E) Excited at position 2 and Observed at position 2

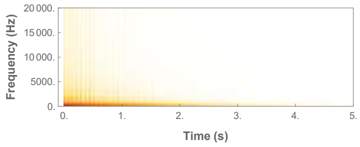

(F) Excited at position 2 and Observed at position 3

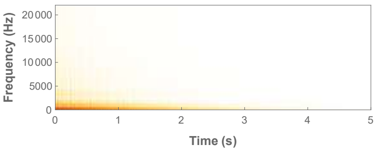

(G) Excited at positon 3 and Observed at position 1

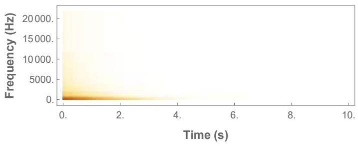

(H) Excited at positon 3 and Observed at position 2

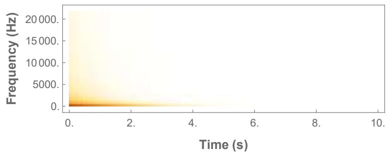

(I) Excited at positon 3 and Observed at position 3

FIGURE C.2: Spectrogram of the Finite Difference scheme with an initial displacement and initial velocity.

C.3 Initial Velocity

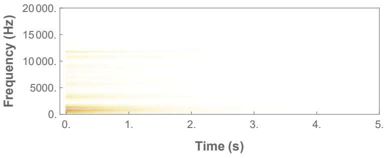

(A) Excited at position 1 and Observed at position 1

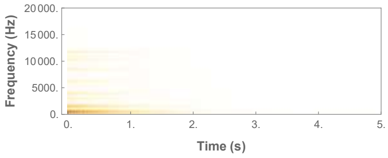

(B) Excited at position 1 and Observed at position 2

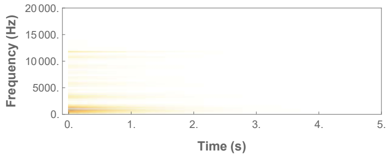

(C) Excited at position 1 and Observed at position 3

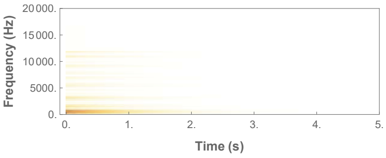

(D) Excited at position 2 and Observed at position 1

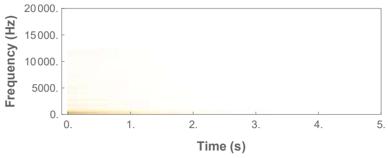

(E) Excited at position 2 and Observed at position 2

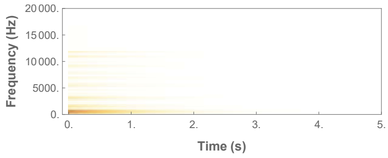

(F) Excited at position 2 and Observed at position 3

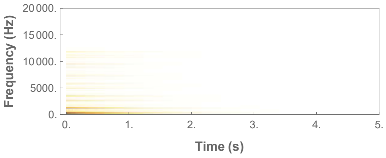

(G) Excited at position 3 and Observed at position 1

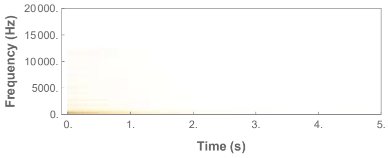

(H) Excited at position 3 and Observed at position 2

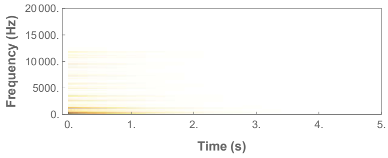

(I) Excited at position 3 and Observed at position 3

FIGURE C.3: Spectrogram of the Finite Difference method with initial velocity.

C.4 Force Density

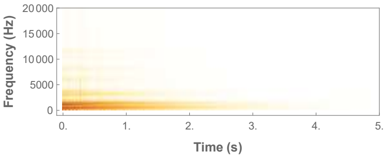

(A) Excited at position 1 and Observed at position 1

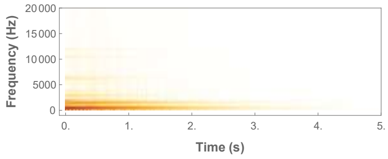

(B) Excited at position 1 and Observed at position 2

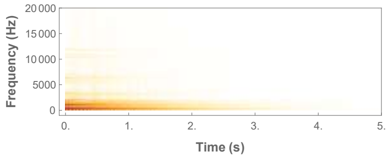

(C) Excited at position 1 and Observed at position 3

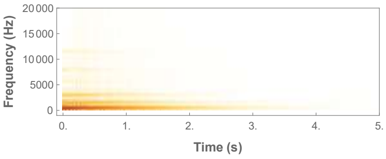

(D) Excited at position 2 and Observed at position 1

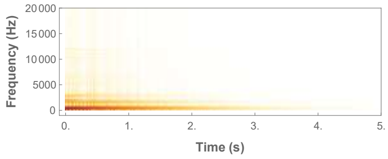

(E) Excited at position 2 and Observed at position 2

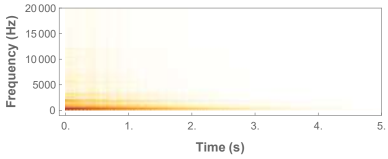

(F) Excited at position 2 and Observed at position 3

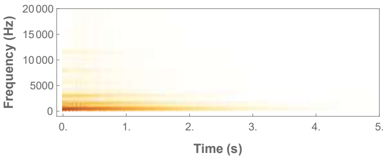

(G) Excited at position 3 and Observed at position 1

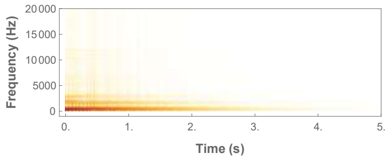

(H) Excited at position 3 and Observed at position 2

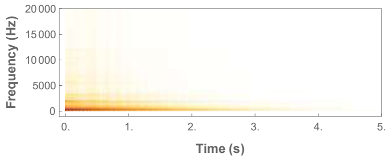

(I) Excited at position 3 and Observed at position 3

FIGURE C.4: Spectrogram of the Finite Difference method with a force density.

Bibliography

[1] Stefanakis, N., Abel, M. and Bergner, A., 2015. Sound synthesis based on ordinary differential equations. Computer Music Journal, 39(3), pp.46-58.

[2] Torin, A., Hamilton, B. and Bilbao, S., 2014. An Energy Conserving Finite Difference Scheme for the Simulation of Collisions in Snare Drums. In DAFx (pp. 145-152)

[3] Slater, D., 1998. Chaotic sound synthesis. Computer Music Journal, 22(2), pp.12-19.

[4] Avanzini, F., Marogna, R. and Bank, B., 2012. Efficient synthesis of tension modulation in strings and membranes based on energy estimation. The Journal of the Acoustical Society of America, 131(1), pp.897-906.

[5] Erkut, C. and Karjalainen, M., 2002. Finite difference method vs. digital waveguide method in string instrument modeling and synthesis. choice, 10(1), p.4.

[6] Smith III, J.O., 2004. On the equivalence of the digital waveguide and finite difference time domain schemes. arXiv preprint physics/0407032.

[7] Chowning, J.M., 1973. The synthesis of complex audio spectra by means of frequency modulation. Journal of the audio engineering society, 21(7), pp.526-534.

[8] Aramaki, M., Kronland-Martinet, R., Voinier, T. and Ystad, S., 2006. A percussive sound synthesizer based on physical and perceptual attributes. Computer Music Journal, 30(2), pp.32-41.

[9] Rabenstein, R. and Trautmann, L., 2001. Digital sound synthesis by physical modelling. In Image and Signal Processing and Analysis, 2001. ISPA 2001. Proceedings of the 2nd International Symposium on (pp. 12-23). IEEE.

[10] Trautmann, L., Petrausch, S. and Rabenstein, R., 2001. Physical modeling of drums by transfer function methods. In Acoustics, Speech, and Signal Processing, 2001. Proceedings.(ICASSP'01). 2001 IEEE International Conference on (Vol. 5, pp. 3385-3388). IEEE.

[11] Mohamad, Z., Dixon, S. and Harte, C., ESTIMATING PICKUP AND PLUCKING POSITIONS OF GUITAR TONES AND CHORDS WITH AUDIO EFFECTS.

[12] Mohamad, Z., Dixon, S. and Harte, C., 2017, March. Pickup position and plucking point estimation on an electric guitar. In Acoustics, Speech and Signal Processing (ICASSP), 2017 IEEE International Conference on (pp. 651-655). IEEE.

[13] Chaigne, A. and Askenfelt, A., 1994. Numerical simulations of piano strings. I. A physical model for a struck string using finite difference methods. The Journal of the Acoustical Society of America, 95(2), pp.1112-1118.

[14] Trautmann, L. and Rabenstein, R., 2002, May. Stable systems for nonlinear discrete sound synthesis with the functional transformation method. In Acoustics, Speech, and Signal Processing (ICASSP), 2002 IEEE International Conference on (Vol. 2, pp. II-1861). IEEE.

[15] Evangelista, G., 2006, September. Fractal modulation effects. In Proc. of the Int. Conf. on Digital Audio Effects (DAFx-06), Montreal, Quebec, Canada (pp. 101-106).

[16] Trautmann, L. and Rabenstein, R., 2012. Digital sound synthesis by physical modeling using the functional transformation method. Springer Science & Business Media.

[17] Smith, J.O., 1992. Physical modeling using digital waveguides. Computer music journal, 16(4), pp.74-91.

[18] Bilbao, S., 2009. Numerical sound synthesis: finite difference schemes and simulation in musical acoustics. John Wiley & Sons.

[19] Avanzini, F., Marogna, R. and Bank, B., 2012. Efficient synthesis of tension modulation in strings and membranes based on energy estimation. The Journal of the Acoustical Society of America, 131(1), pp.897-906.

[20] Karjalainen, M. and Erkut, C., 2004. Digital waveguides versus finite difference structures: Equivalence and mixed modeling. EURASIP Journal on Applied Signal Processing, 2004, pp.978-989.

[21] Rabenstein, R. and Trautmann, L., 2003. Digital sound synthesis of string instruments with the functional transformation method. Signal Processing, 83(8), pp.1673-1688.

[22] Desvages, C. and Bilbao, S., 2015, December. Two-polarisation finite difference model of bowed strings with nonlinear contact and friction forces. In Int. Conference on Digital Audio Effects (DAFx-15).

[23] Petrausch, S. and Rabenstein, R., 2003, September. Sound synthesis by physical modeling using the functional transformation method: Efficient implementations with polyphase-filterbanks. In Proc. International Conference on Digital Audio Effects.

[24] Eckerholm, F. and Evangelista, G., 2008, September. The PluckSynth touch string. In Proc. of Digital Audio Effects Conf.(DAFx '08), Helsinki, Finland (pp. 213-220).

[25] Elaydi, S., 2005. An introduction to difference equations. Springer Science & Business Media.

[26] Hall, D.E., 1992. Piano string excitation. VI: Nonlinear modeling. The Journal of the Acoustical Society of America, 92(1), pp.95-105.

[27] Hodgkin, A.L. and Huxley, A.F., 1952. A quantitative description of membrane current and its application to conduction and excitation in nerve. The Journal of physiology, 117(4), p.500.

[28] D. Terman and D. Wang, "Global competition and local cooperation in a network of neural oscillators," PhysicaD:NonlinearPhenomena,vol.81,no.1-2,pp. 148–176, 1995.

[29] J. Nagumo, S. Arimoto, and S. Yoshizawa, "An active pulse transmission line simulating nerve axon," Proceedings of the IRE, vol. 50, no. 10, pp. 2061–2070, 1962.

[30] Thomas, J.W., 2013. Numerical partial differnetial equatioins: finite difference methods (Vol. 22). Springer SCience & Business Media.

[31] FitzHugh, R., 1955. Mathematical models of threshold phenomena in the nerve membrane. Bulletin of Mathematical Biology, 17(4), pp.257-278.

[32] Smith III, J.O., 2004. On the equivalence of the digital waveguide and finite difference time domain schemes. arXiv preprint physics/0407032.

[33] Chaigne, A., Askenfelt, A. and Jansson, E.V., 1990. Temporal synthesis of string instrument tones. Quarterly Progress and Status Report, 4(81-100), p.167.

[34] Feng, Z., Chen, G. and Hsu, S.B., 2006. A qualitative study of the damped Duffing equation and applications. DISCRETE AND CONTINUOUS DYNAMICAL SYSTEMS SERIES B, 6(5), p.1097.

[35] Jacobs .B, 2016 A Differential Equation Based Approach to Sound Synthesis and Sequencing

[36] Wang, D., 1999. Relaxation Oscillators and Networks. Wiley Encyclopedia of Electrical and Electronics Engineering, Wiley & Sons, vol. 18 ,P.396-405

[37] Burden, R.L. and Faires, J.D., 2001. Numerical analysis (7th). Prindle Weber and Schmidt, Boston.